Advances in Colloid and Interface Science 206 (2014) 17–45

Contents lists available at ScienceDirect

Advances in Colloid and Interface Science

journal homepage: www.elsevier.com/locate/cis

Micelle–monomer equilibria in solutions of ionic surfactants and in ionic–nonionic mixtures: A generalized phase separation model

Krassimir D. Danov [a], Peter A. Kralchevsky [a,*], Kavssery P. Ananthapadmanabhan [b]

[a] Department of Chemical Engineering, Faculty of Chemistry and Pharmacy, Sofia University, Sofia 1164, Bulgaria
[b] Unilever Research & Development, 40 Merritt Blvd., Trumbull, CT 06611, USA

ARTICLE INFO

Available online 13 March 2013

Keywords:
Micelles of ionic surfactants
Counterion binding
Degree of micelle ionization
Critical micellization concentration
Micelle aggregation number
Conductivity of micellar solutions
Mixed surfactant micelles

ABSTRACT

On the basis of a detailed physicochemical model, a complete system of equations is formulated that describes the equilibrium between micelles and monomers in solutions of ionic surfactants and their mixtures with nonionic surfactants. The equations of the system express mass balances, chemical and mechanical equilibria. Each nonionic surfactant is characterized by a single thermodynamic parameter — its micellization constant. Each ionic surfactant is characterized by three parameters, including the Stern constant that quantifies the counterion binding. In the case of mixed micelles, each pair of surfactants is characterized with an interaction parameter, β, in terms of the regular solution theory. The comparison of the model with experimental data for surfactant binary mixtures shows that β is constant — independent of the micelle composition and electrolyte concentration. The solution of the system of equations gives the concentrations of all monomeric species, the micelle composition, ionization degree, surface potential and mean area per head group. Upon additional assumptions for the micelle shape, the mean aggregation number can be also estimated. The model gives quantitative theoretical interpretation of the dependence of the critical micellization concentration (CMC) of ionic surfactants on the ionic strength; of the CMC of mixed surfactant solutions, and of the electrolytic conductivity of micellar solutions. It turns out, that in the absence of added salt the conductivity is completely dominated by the contribution of the small ions: monomers and counterions. The theoretical predictions are in good agreement with experimental data.

Contents

1. Introduction . . . 18
2. The phase separation model for nonionic surfactants . . . 19
   2.1. Mass balances and micelle–monomer chemical equilibrium . . . 19
   2.2. Application of the regular solution theory to binary mixtures . . . 20
3. Ionic surfactants: the effect of counterion binding . . . 20
   3.1. The Stern isotherm and the association–dissociation equilibrium . . . 20
   3.2. Adsorption equations for ionized and non-ionized surfactant molecules . . . 21
   3.3. Equations describing the micelle–monomer equilibrium . . . 22
4. Physicochemical model for micellar solutions of an ionic surfactant . . . 22
   4.1. Chemical equilibria and mass balances . . . 22
   4.2. The jellium model . . . 23
   4.3. Gouy closure . . . 23
   4.4. Mitchell–Ninham (MN) closure . . . 24
   4.5. Determination of the parameters of the model . . . 24
   4.6. The Corrin–Harkins plot . . . 25
   4.7. Computational procedure for concentrations above the CMC . . . 26
   4.8. Electrolytic conductivity of micellar solutions . . . 26

* Corresponding author. Tel.: +359 2 962 5310; fax: +359 2 962 5643.
E-mail address: pk@lcpe.uni-sofia.bg (P.A. Kralchevsky).

0001-8686/$ – see front matter © 2013 Elsevier B.V. All rights reserved.
http://dx.doi.org/10.1016/j.cis.2013.02.001

5. Application of the model to various ionic surfactants . . . 27
5.1. Dodecyltrimethylammonium bromide (DTAB) . . . 27
5.2. Tetradecyltrimethylammonium bromide (TTAB) . . . 28
5.3. Cetyltrimethylammonium bromide (CTAB) . . . 29
5.4. Cetylpyridinium chloride (CPC) . . . 31
5.5. Sodium dodecyl sulfate (SDS) . . . 32
5.6. Discussion on the conductivity of micellar solutions . . . 33
6. Generalization of the model for mixtures of ionic and nonionic surfactants . . . 35
6.1. Completing the system of equations and generalization of the MN closure . . . 35
6.2. CMC of mixed ionic–nonionic surfactant solutions . . . 36
6.3. Effect of electrolyte on the CMC of mixed solutions . . . 36
6.4. Mixed solutions of anionic and zwitterionic surfactants . . . 37
6.5. Mixed solutions of C_nTAB and $C_{12}E_m$ . . . 37
7. Generalization to one ionic surfactant with several different counterions . . . 38
7.1. Stern isotherm and adsorption equations . . . 38
7.2. System of equations describing the micelle–monomer equilibrium . . . 40
8. Conclusions . . . 41
Acknowledgments . . . 42
Appendix A. Micelle surface charge, potential and electrostatic surface pressure . . . 42
Appendix B. Expression for the slope of the Corrin–Harkins plot . . . 43
References . . . 43

1. Introduction

The existence of surfactant micelles was established in the beginning of the twentieth century by W. B. Hardy, J. W. McBain and coworkers in their studies on electrolytic conductivity of carboxylate solutions [1]. They found that the solutions of sodium laurate and myristate contain both *electrolytic* and *colloidal* constituents (dissociated surfactant monomers and surfactant aggregates) [1]. The term "micelle" became widely accepted about twenty years later [2]. Since then, the micelles and micellar solutions have been a subject of intensive studies stimulated by their great scientific and practical importance.

Firstly, some empirical dependencies have been established. In the case of *ionic* surfactants, Corrin and Harkins [3] found that the critical micellization concentration (CMC) depends linearly on the ionic strength of solution (varied by the addition of salt) when plotted in double log scale. The slope of this plot has been interpreted as degree of binding of counterions to the micelle [4], although this interpretation is uncertain and is considered again in the present article (Section 4.6). In the case of *nonionic* surfactants, it has been found that CMC obeys the empirical Klevens equation [5]:

$$\log(\mathrm{CMC}) = \hat{A} - \hat{B}n \tag{1.1}$$

where n is the number of C atoms in the alkyl chain; $\hat{A}$ and $\hat{B}$ are empirical coefficients tabulated for some homologous series [6]. For linear alkyl ethoxylates, C_nE_m, Eq. (1.1) has been generalized in Refs. [7,8].

Various experimental methods have been applied to study the properties of the micelles: viscosimetry [9,10]; conductometry [11–13]; calorimetry [14,15]; fluorescence quenching [16–19]; stratifying foam films [20–22]; static and dynamic light scattering [10,23,24]; small-angle X-ray scattering (SAXS) [25,26] and neutron scattering (SANS) [27,28]; electron paramagnetic resonance (EPR) [27,29]; nuclear magnetic resonance (NMR) [30–32], and various methods to study the dynamics of micellization [33,34].

In the theoretical aspect, four main approaches to the modeling of micelles and micellar solutions have been developed:

The *mass action model* describes the micellization as a chemical reaction [10,35–38]. This model gives a detailed description of the micelles as polydisperse aggregates and allows modeling of the growth of non-spherical micelles and other self-assembled structures [39–44]. Generalizations to ionic micelles are also available [45–50].

The *phase separation model* is focused on the equilibrium between micelles and monomers with respect to the exchange of each component in a multi-component surfactant mixture [51–56]; reviews can be found in [37,38] and Section 2 of the present article. In this model, the micelle polydispersity is usually neglected; average aggregation numbers and charges per micelle are used, and the micelles are treated as a pseudophase that is equilibrated with the monomers. The regular solution theory has been applied to both binary [53] and multi-component surfactant mixtures [57–59]. In the case of ionic surfactants, various models of the effect of electric double layer and counterion binding on micellization have been proposed [60–67].

Molecular thermodynamic models of the micelles have been developed and extended to surfactant mixtures [68,69]. They consider the detailed surfactant molecular structures and give theoretical description of the micellization process based on various free-energy contributions, including those from the hydrophilic heads and hydrophobic tail configurations [70–76].

The computational methodology based on the *quantitative structure–property relationship* approach (QSPR) has been applied also to micelles. First Huibers et al. [77,78] developed this method to predict the CMC of surfactants using a large database of molecular descriptors. So far, the QSPR method has been applied to predict the CMC values of many of nonionic and ionic surfactants [79–83].

The focus of the present article is on models that describe the micelle–monomer equilibria, with applications for characterizing micelles of ionic surfactants and their mixtures by charge and aggregation number; for a deeper understanding of conductivity of micellar solutions; for interpreting the dependence of CMC on the mole fractions of mixed surfactants and on the electrolyte concentration; for analyzing the precipitation and pH variation in micellar carboxylate solutions; for determining the solubility limits of fatty acids and alcohols in micelles of conventional surfactants, etc. For this goal, the most appropriate is the phase separation model, which is based on chemical equilibrium relationships, supplemented by mechanical and mass balance equations. As demonstrated below, the key issue is how to close the system of equations in order to obtain a physically adequate model.

With the final goal to construct a physically transparent, quantitative and easy for application model of micellar solutions, three main approaches are extended and combined here:

(1) The general thermodynamic approach from Ref. [84] for planar ionic-surfactant adsorption layers is extended to ionic-surfactant micelles. In this approach, the key point is the thermodynamically correct incorporation of the *counterion binding*

(charge regulation) effect and of the electrostatic energy contribution in the theoretical model.

(2) The concept by Mitchell and Ninham [85] for *micelle interfacial tension* is extended to the case of counterion binding and for *ionic–nonionic mixtures*. Physically, this concept states that the *repulsive* electrostatic double-layer component of interfacial tension is exactly counterbalanced by the *attractive* non-double-layer component of interfacial tension. The balance of these attractive and repulsive components implies that at equilibrium the micelle is in *tension free state*, like the phospholipid bilayers [86].

(3) The *jellium model* originally developed for suspensions of charged particles [87,88] is adapted and incorporated into the theory in order to calculate the micelle charge, potential and the double-layer component of micelle surface tension, as well as to interpret the *electrolytic conductivity* of micellar solutions.

In Section 2, we briefly review the phase separation model for mixtures of nonionic surfactants. Section 3 is dedicated to the effect of counterion binding in the case of ionic surfactants. In Section 4, all equations of the physicochemical model are assembled to form a complete system of equations. The model is applied to interpret experimental data for ionic surfactants in Section 5, and for ionic–nonionic mixtures — in Section 6. Finally, in Section 7, the model is extended to solutions containing one ionic surfactant, but several kinds of counterions with different binding energies.

2. The phase separation model for nonionic surfactants

2.1. Mass balances and micelle–monomer chemical equilibrium

In view of subsequent generalization, let us first consider a mixed micellar solution of several nonionic surfactants. Three different kinds of mole fractions can be distinguished in mixed micellar solutions [37]: x_i — mole fraction of component i dissolved in monomeric form; y_i — mole fraction of component i in the micelles (in the micellar pseudophase), and z_i — the input mole fraction of component i, which has been fixed by the experimentalist upon the solution preparation. By definition, all these molar fractions refer to the mixture of amphiphilic molecules (the water is not included). Experimentally, only the mole fraction z_i is known. The other two mole fractions, x_i and y_i, can be calculated from the conditions for equilibrium between micelles and monomers. The surfactant mass balance yields [37]:

$$z_i C_T = (C_T - \mathrm{CMC_M}) y_i + x_i \mathrm{CMC_M} \tag{2.1}$$

$i = 1, 2,..., N$, where N is the number of amphiphilic components; C_T is the total surfactant concentration (of all kinds); $\mathrm{CMC_M}$ is the critical micellization concentration of the *mixed* surfactant solution. The two limiting cases of Eq. (2.1) are as follows: (A) At $C_T = \mathrm{CMC_M}$, we have $x_i = z_i$, but y_i is unknown. (B) At $C_T \gg \mathrm{CMC_M}$, we have $y_i = z_i$, but x_i is unknown.

The chemical equilibrium between micelles and monomers with respect to the exchange of surfactant of kind i yields [37]:

$$\mu_i^{(w,0)} + kT \ln(x_i \mathrm{CMC_M}) = \mu_i^{(mic,0)} + kT \ln(f_i y_i). \tag{2.2}$$

Here, $\mu_i^{(w,0)}$ and $\mu_i^{(mic,0)}$ are the standard chemical potentials of a molecule from component i, respectively, as a monomer in the water phase, and incorporated in a micelle; f_i is the activity coefficient of component i in the micelles; k is the Boltzmann constant and T is the absolute temperature. The micellization constant $K_i^{(mic)}$ is related to the work for transferring of a monomer of component i from the solution into a micelle:

$$kT \ln K_i^{(mic)} \equiv \mu_i^{(mic,0)} - \mu_i^{(w,0)}. \tag{2.3}$$

Substituting Eq. (2.3) into Eq. (2.2) and taking inverse logarithm, we obtain [37]:

$$f_i y_i K_i^{(mic)} = x_i \mathrm{CMC_M} \tag{2.4}$$

$i = 1, 2,..., N$. Eq. (2.4) has several corollaries. First, having in mind that the concentration of surfactant monomers is $c_i = x_i \mathrm{CMC_M}$, we obtain:

$$\frac{c_i}{K_i^{(mic)}} = f_i y_i. \tag{2.5}$$

This can be considered as a generalized form of the Raoult's law stating that the concentration of component i in monomeric form is proportional to the activity, $f_i\, y_i$, of this component in the micelles (Fig. 1) — an analogy with the vapor pressure of a drop from a mixture of two liquids. The Raoult's law, itself, corresponds to $f_i = 1$. i.e., to an ideal solution.

Second, summing up in Eq. (2.4) for all amphiphilic components, and using $\sum_i x_i = 1$, we obtain [37]:

$$\mathrm{CMC_M} = \sum_i f_i y_i K_i^{(mic)}. \tag{2.6}$$

Eq. (2.6) has been applied for calculating the phase diagrams of carboxylates in mixture with synthetic surfactants [89].

Third, we present Eq. (2.4) in the form $y_i / \mathrm{CMC_M} = x_i / (f_i K_i^{(mic)})$, sum up for all amphiphilic components, and use $\sum_i y_i = 1$:

$$\frac{1}{\mathrm{CMC_M}} = \sum_i \frac{x_i}{f_i K_i^{(mic)}}. \tag{2.7}$$

If the working temperature is above the Krafft temperature for the component i, i.e., this surfactant forms micelles (rather than crystals), the equilibrium between micelles and monomers for solutions of the *pure* surfactant leads to:

$$\mu_i^{(w,0)} + kT \ln \mathrm{CMC}_i \equiv \mu_i^{(mic,0)} \tag{2.8}$$

where CMC_i is the critical micelle concentration for the pure component i. The comparison of Eqs. (2.3) and (2.8) implies:

$$K_i^{(mic)} = \mathrm{CMC}_i \quad \text{for} \quad T > T_{\mathrm{Krafft}}. \tag{2.9}$$

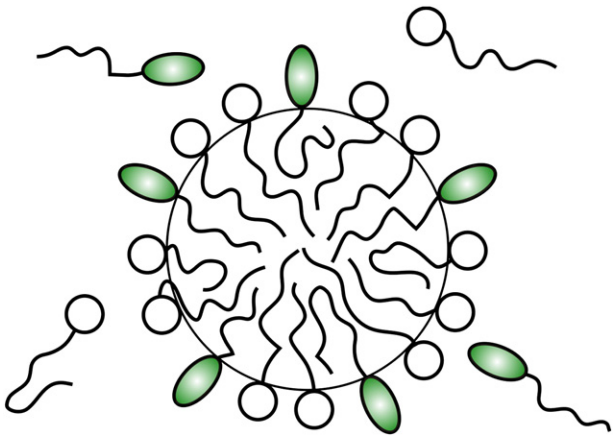

Fig. 1. Sketch of a mixed micelle composed of two nonionic surfactants, which exist in equilibrium with the free monomers of these surfactants in the surrounding aqueous phase.

If $T > T_{\text{Krafft}}$ for all surfactants, then Eq. (2.7) becomes the popular relation between the critical micelle concentrations of the pure components and of the mixture [37]:

$$\frac{1}{\text{CMC}_\text{M}} = \sum_i \frac{x_i}{f_i \text{CMC}_i}. \tag{2.10}$$

At the working temperature, some of the surfactants in the mixture could form crystallites rather than micelles. Then, the more general Eq. (2.7) has to be used, where Eq. (2.9) applies only to the components that are above the Krafft point; see e.g., Ref. [89].

Eqs. (2.1), (2.4) and the identities $\Sigma_i x_i = 1$ and $\Sigma_i y_i = 1$ represent a system of $2N + 1$ equations for determining $2N + 1$ variables: $x_1, \ldots, x_N$; $y_1, \ldots, y_N$, and CMC_M, supposedly C_T, z_i and $K_i^{(\text{mic})}$, $i = 1, \ldots, N$, are known, and expressions for f_i are available; see e.g., Eq. (2.11). [Eq. (2.1) contains $N - 1$ independent relations. Indeed, the summation of all equations in Eq. (2.1) yields an identity.] Our goal in the present article is to generalize this approach for ionic surfactants and their mixtures.

2.2. Application of the regular solution theory to binary mixtures

Let us consider a mixture of two amphiphilic components, A and B. In the theory of regular solutions, the activity coefficients are expressed in the form [90]:

$$f_i = \exp\left[\beta(1-y_i)^2\right], \qquad \beta \equiv -\frac{cw}{2kT}, \qquad i = \text{A, B}. \tag{2.11}$$

β is an interaction parameter; c is the average number of closest neighbors of a given molecule in a micelle;

$$w = w_{\text{AA}} + w_{\text{BB}} - 2w_{\text{AB}} \tag{2.12}$$

where w_{ij} is the energy of interactions of two closest neighbors of type i and j. As a rule, w_{ij} is negative (attraction between two neighboring molecules) [90]. However, w can be eider negative, positive or zero. If $w = 0$, the micelle represents an ideal mixture of the constituent components. For $\beta < 0$ (or $\beta > 0$), we are dealing with negative (positive) deviations from the Raoult's law, Eq. (2.5), i.e., with synergism (antagonism) of the two surfactants in the mixed micelles.

Substituting f_i from Eq. (2.11) into Eq. (2.4), and taking logarithm, we obtain the Rubingh [54] expression for the interaction parameter, β:

$$\beta = \frac{1}{(1-y_i)^2} \ln\left(\frac{x_i \text{CMC}_\text{M}}{y_i K_i^{(\text{mic})}}\right), \quad i = \text{A, B}. \tag{2.13}$$

The elimination of β between the two expressions, for $i = \text{A}$ and B in Eq. (2.13), yields [54]:

$$\frac{1}{(1-y_\text{A})^2} \ln\left(\frac{x_\text{A} \text{CMC}_\text{M}}{y_\text{A} K_\text{A}^{(\text{mic})}}\right) = \frac{1}{(1-y_\text{B})^2} \ln\left(\frac{x_\text{B} \text{CMC}_\text{M}}{y_\text{B} K_\text{B}^{(\text{mic})}}\right) \tag{2.14}$$

where $y_\text{A} + y_\text{B} = 1$. At the critical micellization concentration, the mole fractions $x_i = z_i$ are known. If $K_\text{A}^{(\text{mic})}$ and $K_\text{B}^{(\text{mic})}$ are also known, and CMC_M is measured, then y_A can be determined from Eq. (2.14). Afterwards, β can be found from Eq. (2.13). The generalization of this approach to binary mixtures of ionic and nonionic surfactants is considered in Section 6.

3. Ionic surfactants: the effect of counterion binding

3.1. The Stern isotherm and the association–dissociation equilibrium

Here, we consider a solution that contains a surfactant (e.g., sodium dodecyl sulfate, SDS) and an electrolyte (e.g., NaCl). For simplicity, we assume that the surfactant and salt are 1:1 electrolytes and that the counterion (e.g., Na^+) is the same for the surfactant and the salt. Component 1 is the surfactant ion; component 2 is the counterion and component 3 is the coion due to the salt (e.g., Cl^-).

In the bulk solution, we have association–dissociation equilibrium of the surfactant and the counterion, which is described by the equation:

$$c_1 c_2 = Q_{12} c_{12} \tag{3.1}$$

c_1 and c_2 are the concentrations of the respective components; c_{12} denotes the concentration of non-ionized surfactant molecules or ion pairs; Q_{12} is the equilibrium constant of the reaction described by Eq. (3.1). In the case of carboxylates, $Q_{12} = 1.995 \times 10^{-5}$ M for H^+ counterions, whereas $Q_{12} = 2.84$ M for Na^+ counterions [91]. The latter value is of the order of magnitude of this constant for surfactants like SDS, which are good electrolytes (see below). For SDS and Na carboxylates, Q_{12} describes the association–dissociation equilibrium in a loose solvent-shared (hydrated) ion pair of cation and anion [92]. However, in the case of protonation of carboxylates, H^+ is connected with a chemical bond to the carboxylate anion, and for this reason Q_{12} is much smaller (see above).

Let us first consider the binding of counterions to the headgroups of the surfactant molecules in a *flat* adsorption layer. The concentrations of the reagents in a surface layer of thickness δ are (Fig. 2a):

$$c_2 = c_{2\text{s}}; \quad c_1 = \frac{1}{\delta}(\Gamma_1 - \Gamma_2); \quad c_{12} = \frac{\Gamma_2}{\delta}. \tag{3.2}$$

Here, $c_{2\text{s}}$ is the subsurface concentration of the counterions of kind i; Γ_1 is the total surface concentration of component 1 (the surfactant in both ionized and non-ionized form) in the adsorption layer; Γ_2 is the surface concentration of bound counterions. The substitution of Eq. (3.2) into Eq. (3.1) yields [93]:

$$\frac{c_{2\text{s}}}{Q_{12}} = \frac{\Gamma_2}{\Gamma_1 - \Gamma_2}. \tag{3.3}$$

Note that the thickness δ was canceled, so that Eq. (3.3) is insensitive to its exact choice. We used also the circumstance that in a closed system, the final equilibrium state of the system is independent of the reaction path [94]. From this viewpoint, the equilibrium state of the system should be independent of whether non-ionized surfactant molecules of bulk concentration c_{12} adsorb at the interface, or ionized surfactant molecules first adsorb at the interface, and then counterions bind to their headgroups. Eq. (3.3) can be presented in the equivalent form [84,93]:

$$\frac{\Gamma_2}{\Gamma_1} = \frac{K_{\text{St}} c_{2\text{s}}}{1 + K_{\text{St}} c_{2\text{s}}} \tag{3.4}$$

where K_{St} is the Stern constant that is related to the energy of counterion binding and

$$K_{\text{St}} = \frac{1}{Q_{12}}. \tag{3.5}$$

Eqs. (3.3) and (3.4) are two forms of the Stern isotherm [93]. Eq. (3.5) is expected to hold irrespective of whether the bond between the cation and anion is strong (chemical) or a loose, solvent-shared ion pair is formed; see above. In both cases, the bond is expected to be the same in the bulk and at the surface. The constants K_{St} and Q_{12} are related to the respective bond energy [84,95].

For brevity, here and hereafter we are using the term "non-ionized" surfactant molecules for both non-dissociated molecules (such as protonated fatty acids) and solvent-shared ion pairs of surfactant and counterion.

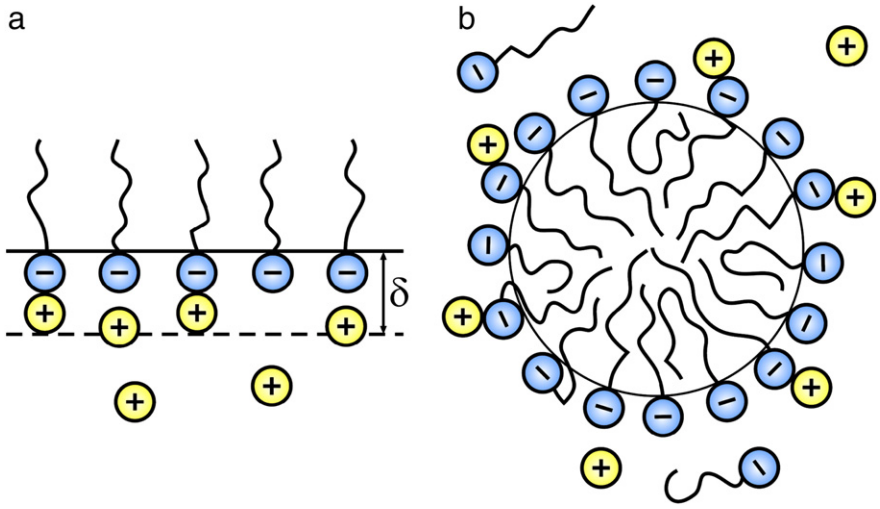

Fig. 2. (a) Sketch of a flat adsorption layer from an ionic surfactant with bound and free counterions. (b) Sketch of a micelle from an ionic surfactant with bound counterions, which exists in dynamic equilibrium with the surfactant monomers and free counterions in the surrounding water phase.

Eq. (3.5) can be rather useful. Indeed, for carboxylates the reaction constant Q_{12} is known, and then from Eq. (3.5) one can determine the respective Stern constant K_{St}. Conversely, for surfactants that are strong electrolytes the Stern constant K_{St} is known (e.g., from a fit of surface-tension data), and then one can determine the reaction constant of the formation of ion pair. For example, for SDS the Stern constant is $K_{St} = 0.6529\ M^{-1}$ [96], and then one estimates $Q_{12} = (K_{St})^{-1} = 1.53$ M, which is of the same order of magnitude as the respective constant for sodium myristate [91]; see above.

3.2. Adsorption equations for ionized and non-ionized surfactant molecules

The effect of counterion binding on the properties of surfactant adsorption monolayers has been first addressed in Refs. [84,97,98]. The adsorption isotherm of the considered ionic surfactant can be expressed in the form [84,99]:

$$K_1(1 + K_{St}c_{2s})c_{1s} = \frac{\Gamma_1}{\Gamma_\infty} f(\Gamma_1). \tag{3.6}$$

Here, K_1 is the surfactant adsorption constant; Γ_∞ is the maximal possible adsorption at dense packing of the surfactant molecules; c_{1s} is the surfactant subsurface concentration; the quantity $f(\Gamma_1)$ accounts for the interaction between the adsorbed surfactant molecules (Fig. 2a) and has the meaning of activity coefficient. Expressions for $f(\Gamma_1)$ corresponding to different adsorption models are given in Table 1. Note that for $\Gamma_1 \to 0$, all expressions in Table 1 give $f(\Gamma_1) \to 1$.

In view of Eq. (3.5), the substitution of $K_{St}c_{2s}$ from Eq. (3.3) into Eq. (3.6) yields:

$$K_1 c_{1s} = \frac{\hat{\Gamma}_1}{\Gamma_\infty} f(\Gamma_1) \tag{3.7}$$

Table 1
Expressions for $f(\Gamma_1)$ corresponding to different adsorption models from [84].

Adsorption model	$f(\Gamma_1)$
Henry	1
Langmuir	$\frac{\Gamma_\infty}{\Gamma_\infty - \Gamma_1}$
Volmer	$\frac{\Gamma_\infty}{\Gamma_\infty - \Gamma_1} \exp\left(\frac{\Gamma_1}{\Gamma_\infty - \Gamma_1}\right)$
Frumkin	$\frac{\Gamma_\infty}{\Gamma_\infty - \Gamma_1} \exp\left(-\frac{2\beta\Gamma_1}{kT}\right)$
van der Waals	$\frac{\Gamma_\infty}{\Gamma_\infty - \Gamma_1} \exp\left(\frac{\Gamma_1}{\Gamma_\infty - \Gamma_1} - \frac{2\beta\Gamma_1}{kT}\right)$

where by definition

$$\hat{\Gamma}_1 \equiv \Gamma_1 - \Gamma_2 \tag{3.8}$$

is the surface concentration (adsorption) of ionized surfactant molecules. A multiplication of Eqs. (3.3) and (3.7), in view of Eqs. (3.5) and (3.8), yields:

$$K_1 K_{St} c_{1s} c_{2s} \equiv \frac{\Gamma_2}{\Gamma_\infty} f(\Gamma_1). \tag{3.9}$$

The surface concentrations c_{1s} and c_{2s} are related to the respective bulk concentrations, c_1 and c_2 by means of the Boltzmann equation:

$$c_{1s} = c_1 \exp(-\Phi_s), \quad c_{2s} = c_2 \exp(\Phi_s) \tag{3.10}$$

where

$$\Phi_s = \frac{e|\psi_s|}{kT} \tag{3.11}$$

is the dimensionless surface electric potential, with ψ_s being the respective dimensional potential and e — the elementary electric charge. Using Eqs. (3.1), (3.5) and (3.10), we can bring Eq. (3.9) in the form:

$$K_1 c_{12} \equiv \frac{\Gamma_2}{\Gamma_\infty} f(\Gamma_1). \tag{3.12}$$

Eq. (3.12), which is similar by form to Eq. (3.7), can be considered as an adsorption isotherm for the non-ionized surfactant molecules. As mentioned above, the equilibrium properties of the solution are independent of whether a non-ionized molecule adsorbs at the interface, or first an ionized molecule adsorbs and then a counterion binds to its head group. This circumstance is reflected in the fact that the system of Eqs. (3.7) and (3.12) is mathematically equivalent to the system of the Stern isotherm, Eq. (3.4), and the surfactant adsorption isotherm, Eq. (3.6).

Finally, we should note that in the case of not-too-low ionic strengths, all concentrations of ionic species, c_i, should be replaced by the respective activities $a_i = c_i\gamma_\pm$, where $\gamma_\pm$ is the activity coefficient.

3.3. Equations describing the micelle–monomer equilibrium

A micelle can be considered as a gas bubble in the limiting case of infinitely small volume of the gas in the bubble. From this viewpoint, the basic chemical–equilibrium relations describing the surfactant adsorption at the bubble surface can be used also in the limiting case of a micelle. The micellar curvature effects that are due to interactions between the surfactant molecules can be considered as being incorporated in the micellization constant $K_1^{(\mathrm{mic})}$.

Thus, we will use Eqs. (3.7) and (3.12) to describe the equilibrium between the surfactant molecules incorporated in the micelle and the surfactant monomers in the bulk; see Fig. 2b. In the case of micelles, it is convenient to make the following replacements:

$$1/K_1 \to K_1^{(\mathrm{mic})}; \quad f(\Gamma_1) \to f_1; \quad \frac{\hat{\Gamma}_1}{\Gamma_\infty} \to y_1; \quad \frac{\Gamma_2}{\Gamma_\infty} \to y_2. \tag{3.13}$$

Here, $K_1^{(\mathrm{mic})}$ is micellization constant; f_1 is activity coefficient for the surfactant molecules in the micelle; y_1 is the molar fraction of ionized surfactant molecules in the micelle; y_2 is the mole fraction of non-ionized surfactant molecules in the micelle (the molar fraction of the bound counterions). In view of Eqs. (3.10) and (3.13), we can bring Eqs. (3.7) and (3.12) (after taking logarithm) in the form:

$$\ln c_1\gamma_\pm = \ln K_1^{(\mathrm{mic})} + \ln(f_1 y_1) + \Phi_s \tag{3.14}$$

$$\ln c_{12} = \ln K_1^{(\mathrm{mic})} + \ln(f_1 y_2) \tag{3.15}$$

where Φ_s is the dimensionless surface electric potential of the micelle; see Eq. (3.11); the bulk concentration of the ionic surfactant monomers, c_1, is replaced by the respective activity $c_1\gamma_\pm$. For a single ionic surfactant, one can set $f_1 = 1$.

Eqs. (3.14) and (3.15) can be obtained also by setting equal the (electro)chemical potentials of the respective molecules in the micelles and in the bulk, and $\ln K_1^{(\mathrm{mic})}$ is expressed through the standard chemical potentials by Eq. (2.3). Eqs. (3.14) and (3.15) represent a nontrivial generalization of Eq. (2.2) to the case of an ionic surfactant because of the following three reasons:

(i) The right-hand side of Eq. (3.14) contains only the fraction y_1 of the *ionized* surfactant molecules in the micelle. The chemical equilibrium of surfactant molecules with bound counterions is expressed by Eq. (3.15).

(ii) The micellization constant $K_1^{(\mathrm{mic})}$ is *the same* in Eqs. (3.14) and (3.15), which describe, respectively, the ionized and non-ionized surfactants. Thus, the number of parameters in the model is reduced, which considerably simplifies the theoretical description of micellization. [The specificity of the counterion is taken into account by Eq. (3.1), which has to be included in the complete system of equations; see below.]

(iii) The electrostatic energy of an ionized surfactant molecule incorporated in the charged micelle is taken into account by the term Φ_s in Eq. (3.14) (or $e\psi_s$ in dimensional form). The form of Eq. (3.14) is in agreement with the general theory of the electric-double-layer energy by Overbeek [100]; see Eq. (12) therein.

4. Physicochemical model for micellar solutions of an ionic surfactant

4.1. Chemical equilibria and mass balances

For reader's convenience, here we summarize the equations of the complete system that describes the chemical equilibria and mass balances in the solutions of an ionic surfactant:

$$\ln(c_1\gamma_\pm) = \ln K_1^{(\mathrm{mic})} + \ln y_1 + \Phi_s \tag{4.1}$$

$$\ln c_{12} = \ln K_1^{(\mathrm{mic})} + \ln y_2 \tag{4.2}$$

$$c_{12} = K_{\mathrm{St}} c_1 c_2 \gamma_\pm^2 \tag{4.3}$$

$$y_1 + y_2 = 1 \tag{4.4}$$

$$c_1 + c_{12} + c_{\mathrm{mic}} = C_1 \tag{4.5}$$

$$c_2 + c_{12} + y_2 c_{\mathrm{mic}} = C_1 + C_{\mathrm{salt}} \tag{4.6}$$

$$\log\gamma_\pm = -\frac{A\sqrt{I}}{1 + Bd_i\sqrt{I}} + bI \tag{4.7}$$

$$I = \frac{1}{2}(c_1 + c_2 + C_{\mathrm{salt}}). \tag{4.8}$$

Eqs. (4.1) and (4.2) (derived above) express the equilibrium between monomers and micelles with respect to the exchange of ionized and non-ionized surfactant molecules, respectively. The presence of non-ionized surfactant molecules in the micelle is equivalent to the effect of counterion binding; see the comment after Eq. (3.12).

Eq. (4.3) is the combination of Eqs. (3.1) and (3.5), where K_{St} is the Stern constant; c_1, and c_{12} are the bulk concentrations of ionized and non-ionized surfactant monomers and c_2 is the bulk concentration of free counterions; the effect of the bulk activity coefficient $\gamma_\pm$ is taken into account. Eq. (4.4) is the standard relation between the molar fractions, y_1 and y_2, of the ionized and non-ionized surfactant molecules in the micelle. Note that the degree of micelle ionization, α, coincides with y_1.

Eq. (4.5) expresses the mass balance of surfactant, where C_1 is the total input surfactant concentration, and c_{mic} is the number of surfactant molecules that are incorporated in micelles per unit volume of the solution. Eq. (4.6) represents the mass balance of counterions. (In the case of SDS + NaCl, these are the Na^+ ions.) In particular, $y_2 c_{\mathrm{mic}}$ accounts for the counterions bound to the micelles, whereas C_{salt} is the total concentration of non-amphiphilic salt in the solution.

Eq. (4.8) expresses the ionic strength I, which is determined solely by the contributions of the small ions in the framework of the jellium model; see Section 4.2 for details. As before, for simplicity we have assumed that both the ionic surfactant and salt are 1:1 electrolytes, and that the counterion due to the surfactant and salt is the same. Thus, Eq. (4.8) includes contributions from the surfactant monomers, c_1, from the counterions, c_2, and from the coions of the salt, C_{salt}. (In the case of SDS + NaCl, the latter are the Cl^- ions.) Generalization to the case of different kinds of counterions is given in Section 7.

Eq. (4.7) is an often used semiempirical expression for the activity coefficient $\gamma_\pm$ originating from the Debye–Hückel theory; the logarithm is decimal; A, Bd_i and b are parameters. Their values at 25 °C, obtained by fitting data for $\gamma_\pm$ of NaCl and NaBr from [101] by Eq. (4.7), are $A = 0.5115\ \mathrm{M}^{-1/2}$, $Bd_i = 1.316\ \mathrm{M}^{-1/2}$ and $b = 0.055\ \mathrm{M}^{-1}$. These values can be used also for solutions of other alkali metal halides.

Eqs. (4.1)–(4.8) represent a system of 8 equations that contains 9 unknown variables: c_1, c_{12}, c_2, c_{mic}, y_1, y_2, $\gamma_\pm$, I, and Φ_s. Hence, we need an additional equation to close the system. This equation should allow us to determine the dimensionless surface electric potential Φ_s in the frame of the electric double layer theory. Two alternative closures are considered in Sections 4.3 and 4.4.

A *reduced* form of the considered system of equations can be obtained if Eq. (4.1) is subtracted from Eq. (4.2) and c_{12} is eliminated from Eq. (4.3):

$$\frac{y_2}{y_1} = K_{\mathrm{St}}\gamma_\pm c_2 \exp(\Phi_s). \tag{4.2a}$$

Eq. (4.2a) expresses the Stern isotherm of counterion binding to the surfactant headgroups at the micelle surface; compare Eqs. (3.3)

and (3.13). Furthermore, in the system of Eqs. (4.1)–(4.8), Eq. (4.2) can be replaced by Eq. (4.2a); Eq. (4.3) can be omitted, and the bulk concentration of non-dissociated surfactant molecules, c_{12}, can be neglected in Eqs. (4.5) and (4.6). Thus, the number of unknown variables and the number of equations are reduced by one. This reduced system is appropriate for ionic surfactants that are good electrolytes, so that the bulk concentration of non-dissociated surfactant molecules, c_{12}, can be neglected. The application of the full system of Eqs. (4.1)–(4.8) to such surfactants gives practically the same numerical results, but yields also the concentration c_{12}, which takes very low values for these surfactants.

4.2. The jellium model

Let us consider the electric double layer formed around a given micelle in the solution. The electric potential ψ obeys the Poisson equation:

$$\frac{1}{r^j}\frac{\mathrm{d}}{\mathrm{d}r}\left(r^j\frac{\mathrm{d}\psi}{\mathrm{d}r}\right) = -\frac{1}{\varepsilon_0\varepsilon}\rho_\mathrm{b} \quad \text{for} \quad r \geq R \tag{4.9}$$

$j = 1, 2$ for cylindrical and spherical micelles, respectively; r is the radial coordinate; ρ_b is the bulk charge density; ε_0 is the dielectric permittivity of vacuum; ε is the relative dielectric constant of solvent (water); R is the average radius of the surface where the centers of the counterions in contact with the micelle are located – the so called *surface of charges* [65]. It has been established that for solutions containing charged colloidal particles, including surfactant micelles, the most adequate description is provided by the *jellium model*, which is based on the following expression for the bulk charge density [21,87,88]:

$$\rho_\mathrm{b} = z_1 e\left(c_1\mathrm{e}^{-\Phi} - c_2\mathrm{e}^{\Phi} + C_\mathrm{salt}\mathrm{e}^{-\Phi} + Zc_\mathrm{m}\right). \tag{4.10}$$

Here, $z_1 = \pm 1$ is the valence of the surfactant ion (1:1 electrolytes assumed);

$$\Phi = \frac{z_1 e\psi}{kT} = \frac{e|\psi|}{kT} \tag{4.11}$$

is the dimensionless electrostatic potential; $c_\mathrm{m} = c_\mathrm{mic} / N_\mathrm{agg}$ is the concentration of micelles; Z and N_agg are, respectively, the number of charges and surfactant monomers per micelle (the aggregation number). The first term in the right-hand side of Eq. (4.10) accounts for the contribution from the ionized surfactant monomers; the second term – for the counterions; the third one – for the coions due to the salt, and the last one – for the micelles as macroions of charge Z. In Eq. (4.10), as usual, the small ions obey the Boltzmann law. The essence of the jellium model is that the macroions (the micelles) are *uniformly* distributed with an average concentration c_m [87,88]. Physically, this means that the electrostatic repulsion between the like charged micelles is strong enough, so that the effect of the potential Φ on their distribution is negligible.

Far from the selected micelle, its electric field vanishes, so that $\Phi = 0$ and Eq. (4.10) reduces to

$$\rho_\mathrm{b} = z_1 e(c_1 - c_2 + C_\mathrm{salt} + Zc_\mathrm{m}) = 0 \tag{4.12}$$

which expresses the condition for *electroneutrality* in the bulk solution. All concentrations in Eq. (4.12) refer to the average bulk concentrations of the respective ions. Eq. (4.12) can be obtained by subtracting Eq. (4.6) from Eq. (4.5) and taking into account that $Zc_\mathrm{m} = (1 - y_2)c_\mathrm{mic}$. Consequently, Eq. (4.12) is not an independent equation from the viewpoint of the system considered in Section 4.1.

Historically, the term "jellium" originates from the quantum theory of electron gas in metals (solid state physics) [102] and it was introduced in colloid science (interactions between charged particles in suspensions) by Beresford-Smith et al. [87,88]. In the case of the micellar solutions, the roles of the nuclei of the atoms of metal and the electrons are played, respectively, by the micelles and their dissociated counterions. This analogy can be further extended to the conductivity of micellar solutions — see Section 4.8.

Substituting Eq. (4.10) into Eq. (4.9), after some transformations we obtain:

$$\frac{1}{r^j}\frac{\mathrm{d}}{\mathrm{d}r}\left(r^j\frac{\mathrm{d}\Phi}{\mathrm{d}r}\right) = \kappa^2[\sinh\Phi + \nu(\cosh\Phi - 1)]. \tag{4.13}$$

Here, Φ is defined by Eq. (4.11); c_2 has been substituted from the electroneutrality condition, Eq. (4.12);

$$\kappa^2 \equiv \frac{2e^2 I}{\varepsilon\varepsilon_0 kT}, \quad I = c_1 + C_\mathrm{salt} + \frac{Z}{2}c_\mathrm{m} \tag{4.14}$$

$$\nu \equiv \frac{Zc_\mathrm{m}}{2(c_1 + C_\mathrm{salt}) + Zc_\mathrm{m}} = \frac{y_1 c_\mathrm{mic}}{2I} < 1. \tag{4.15}$$

The relation $Zc_\mathrm{m} = y_1 c_\mathrm{mic}$ has been also used. At the CMC ($c_\mathrm{m} \to 0$) or at high salt concentrations ($C_\mathrm{salt} \to \infty$), we have $\nu \to 0$. Conversely, at surfactant concentrations well above the CMC ($Zc_\mathrm{m} \gg c_1 + C_\mathrm{salt}$) we might have $\nu \to 1$.

The expressions for the ionic strength I in Eqs. (4.8) and (4.14) are equivalent in view of the electroneutrality condition, Eq. (4.12). The expression for the Debye parameter κ, Eq. (4.14), states that the screening of the electric field is due to the background electrolyte, $c_1 + C_\mathrm{salt}$, plus the counterions dissociated from the micelles, $Zc_\mathrm{m} / 2$ [87,88]. Eq. (4.14) is widely used in the literature, see e.g., Refs. [21,103–106], but it is often forgotten that this equation originates from the jellium model.

4.3. Gouy closure

The standard boundary condition relating the derivative of the potential to the surface charge density reads:

$$\left.\frac{\mathrm{d}\psi}{\mathrm{d}r}\right|_{r=R} = -\frac{1}{\varepsilon\varepsilon_0}\frac{eZ}{A_\mathrm{m}}. \tag{4.16}$$

A_m is the micelle surface area at the level of the surface charges. In Appendix A it is proven that the integration of Eq. (4.13) for $R < r < \infty$, along with the boundary condition, Eq. (4.16), yields:

$$\frac{\kappa y_1 N_\mathrm{agg}}{4A_\mathrm{m} I} \approx 2\sinh\left(\frac{\Phi_\mathrm{s}}{2}\right)\left[\frac{G(\Phi_\mathrm{s})}{\cosh\Phi_\mathrm{s} - 1}\right]^{1/2} + \frac{2j}{\kappa R}\left\{\tanh\left(\frac{\Phi_\mathrm{s}}{4}\right) - \frac{\nu\Phi_\mathrm{s}}{G(\Phi_\mathrm{s})}\left[\frac{\Phi_\mathrm{s}}{4} - \tanh\left(\frac{\Phi_\mathrm{s}}{4}\right)\right]\right\}. \tag{4.17}$$

As usual, Φ_s is the dimensionless surface potential, Eq. (3.11); N_agg is the micelle aggregation number, and $G(\Phi_\mathrm{s})$ is defined as follows:

$$G(\Phi_\mathrm{s}) \equiv \cosh\Phi_\mathrm{s} - 1 + \nu(\sinh\Phi_\mathrm{s} - \Phi_\mathrm{s}). \tag{4.18}$$

Eq. (4.17) represents the relation between the micelle surface *charge* and surface *potential*, which generalizes the known Gouy equation for planar interfaces [107,108] to the case of micelles. At the CMC, the micelle concentration is negligible; then $\nu \to 0$ and Eq. (4.17) reduces to the more special expression derived in Refs. [85,109]:

$$\frac{\kappa y_1 N_\mathrm{agg}}{4A_\mathrm{m} I} \approx 2\sinh\left(\frac{\Phi_\mathrm{s}}{2}\right) + \frac{2j}{\kappa R}\tanh\left(\frac{\Phi_\mathrm{s}}{4}\right). \tag{4.17a}$$

Note that the second term $\propto 1 / \kappa R$ in Eqs. (4.17) and (4.17a) is always a small correction. Indeed, we have $1 / \kappa R \ll 1$ at the *higher* surfactant concentrations. In addition, Φ_s is greater at the *lower*

surfactant concentrations, where $\sinh(\Phi_s/2) \gg \tanh(\Phi_s/4)$, so that the first term in the right-hand side of Eq. (4.17a) is predominant again.

Eqs. (4.1)–(4.8) and (4.17) form a complete system, which contains three unknown parameters: $K_1^{(mic)}$, K_{St} and N_{agg}, which can be determined as adjustable parameters from fits of experimental data. N_{agg} obtained in this way represents an average value of the aggregation number for the considered concentration interval.

However, N_{agg} usually increases with the rise of the surfactant concentration, even for spherical micelles [21,22,110]. Indeed, with the rise of surfactant concentration (and of the ionic strength I), the electrostatic repulsion between the headgroups at the micelle surface decreases, which allows the incorporation of new surfactant molecules in the micelle. These effects can be quantitatively taken into account by using another closure, as follows.

4.4. Mitchell–Ninham (MN) closure

Because the micelle exchanges monomers with the surrounding water phase, it represents an open system. The equilibrium state of the latter corresponds to a minimum of the grand thermodynamic potential, Ω. Because of that, the derivative of Ω with respect to the micelle surface area, which equals the micelle interfacial tension γ, should be equal to zero [85]:

$$\gamma = \gamma_0 + \gamma_{el} = \gamma_0 - \pi_{el} = 0. \tag{4.19}$$

Here, γ_{el} and γ_0 are, respectively, the electrostatic and non-electrostatic components of γ, and $\pi_{el} = -\gamma_{el}$ is the micelle electrostatic surface pressure. In other words, Eq. (4.19) means that the micelle is in *tension free state*.

The term "tension free state" was introduced by Evans and Skalak [86] in the mechanics of phospholipid bilayers and biological membranes. Physically, zero tension means that the acting lateral repulsive and attractive forces counterbalance each other. In the case of ionic surfactant micelles, the electrostatic repulsion in the head group region is counterbalanced by a net lateral attractive force due to the cohesion between the surfactant hydrocarbon tails, and to the hydrophobic effect in the contact zone tail/water at the micelle surface.

Different definitions of surface tension of a spherical interface (and micelle) can be given, because of the existence of mechanical and thermodynamic approaches, and because of the dependence of surface tension on the location of the dividing surface [111–113]. Here, we are following and further developing the approach by Mitchell and Ninham [85], so that it is natural to use their definition for micelle interfacial tension. According to Eq. (4.19), at equilibrium $\gamma = 0$, so that the respective state can be termed "tension free state" in analogy with the case of phospholipid membranes [86].

As demonstrated in Appendix A, π_{el} can be calculated from the expression:

$$\pi_{el} = \varepsilon\varepsilon_0 \int_R^\infty \left(\frac{d\psi}{dr}\right)^2 dr + O\left[\frac{1}{(\kappa R)^2}\right]. \tag{4.20}$$

With the help of Eq. (4.13), the integral in Eq. (4.20) can be estimated (see Appendix A):

$$\gamma_0 = \pi_{el} = 8\varepsilon\varepsilon_0\kappa\left(\frac{kT}{e}\right)^2 \left\{ H(\Phi_s)\sinh^2\left(\frac{\Phi_s}{4}\right) - \frac{\nu\Phi_s}{4}\frac{\frac{\Phi_s}{4} - \tanh\left(\frac{\Phi_s}{4}\right)}{H(\Phi_s)\sinh\left(\frac{\Phi_s}{2}\right)} + \frac{j}{\kappa R}\ln\left[\cosh\left(\frac{\Phi_s}{4}\right)\right] \right\} \tag{4.21}$$

where

$$H(\Phi_s) \equiv \left[\frac{G(\Phi_s)}{\cosh(\Phi_s) - 1}\right]^{1/2}. \tag{4.22}$$

$G(\Phi_s)$ is defined by Eq. (4.18). At the CMC, we have $\nu \to 0$ and Eq. (4.21) reduces to the more special expression obtained in Refs. [46,85]:

$$\gamma_0 = \pi_{el} \approx 8\varepsilon\varepsilon_0\kappa\left(\frac{kT}{e}\right)^2 \left\{ \sinh^2\left(\frac{\Phi_s}{4}\right) + \frac{j}{\kappa R}\ln\left[\cosh\left(\frac{\Phi_s}{4}\right)\right] \right\}. \tag{4.21a}$$

The value of γ_0 is determined mostly by the van der Waals and steric interactions between the surfactant hydrocarbon tails inside the micelle. For this reason, γ_0 is expected to be constant, i.e., independent of the solution's ionic strength, and on C_1 and C_{salt}, in particular.

Eqs. (4.1)–(4.8) and (4.21) form a complete system, which contains three unknown constant parameters: $K_1^{(mic)}$, K_{St} and γ_0, which can be determined as adjustable parameters from fits of experimental data (see below). The solution of the problem gives the concentrations of all species in the bulk: c_1, c_{12}, c_2, and c_{mic}; the composition of the micelle: y_1 and y_2, and the micelle surface potential Φ_s. The degree of micelle ionization is $\alpha = y_1$. Next, from Eq. (4.17) one can calculate the number of surfactant headgroups per unit area of the micelle surface:

$$\Gamma_1 = \frac{1}{a_1} = \frac{N_{agg}}{A_m} \tag{4.23}$$

where a_1 is the area per surfactant head group at the micelle surface. Furthermore, from the value of Γ_1 one can calculate N_{agg} only if A_m is determined in the framework of a given model of micelles shape, e.g., spherical, elongated, hairy, etc.

The values of the physical variables, c_1, c_{12}, c_2, c_{mic}, y_1, y_2, Φ_s, Γ_1, and N_{agg}, can be calculated from the system of Eqs. (4.1)–(4.8) and (4.21) for each given surfactant and salt concentrations, C_1 and C_{salt}. To do that, we have to first determine the three constant thermodynamic parameters of the model: $K_1^{(mic)}$, K_{St} and γ_0.

4.5. Determination of the parameters of the model

Eq. (4.1) and the combination of Eqs. (4.2) and (4.3) can be represented in the form:

$$e^{-\Phi_s} c_1 \gamma_\pm = K_1^{(mic)} y_1 \tag{4.24}$$

$$K_{St} c_1 c_2 \gamma_\pm^2 = K_1^{(mic)} y_2. \tag{4.25}$$

Summing up the above two equations and using the identity $y_1 + y_2 = 1$, we obtain a useful expression for Φ_s:

$$\Phi_s = \ln\left(\frac{c_1\gamma_\pm}{K_1^{(mic)} - K_{St} c_1 c_2 \gamma_\pm^2}\right). \tag{4.26}$$

For an ionic surfactant, the Stern constant, K_{St}, is supposed to be determined by fitting data for the solutions' surface tension at different salt concentrations; see e.g., [84,96,99,114–116]. The other two parameters, $K_1^{(mic)}$ and γ_0 can be determined by fitting the experimental dependence of the CMC on the salt concentration. As an example, in Fig. 3a we have shown data from Refs. [96,116–120] for the CMC of solutions of dodecyltrimethylammonium bromide (DTAB) vs. the concentration of added NaBr, C_{salt}. The principles of the computational procedure are as follows.

The input data are the coordinates of the experimental points for CMC vs. C_{salt} (like those in Fig. 3a); the value of the Stern constant

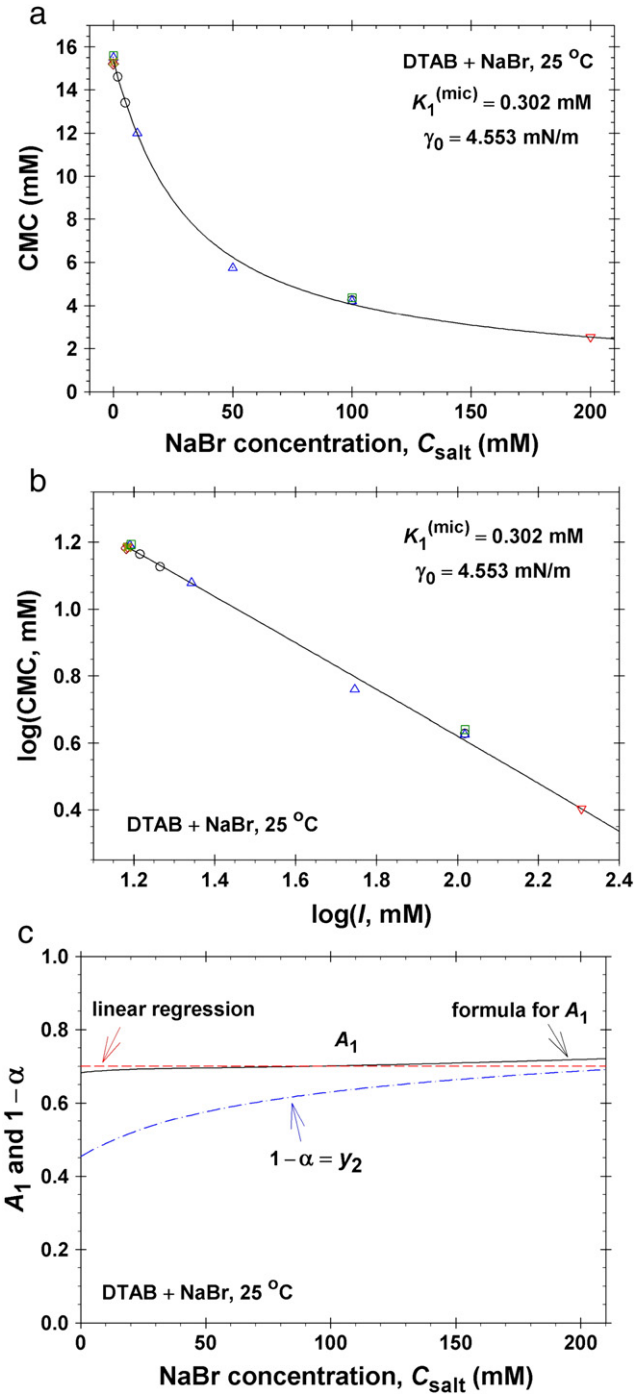

Fig. 3. (a) CMC of DTAB in the presence of NaBr at 25 °C: ○ – Ref. [96]; ▽ – Ref. [116]; Δ – Ref. [117]; ◊ – Ref. [118]; × – Ref. [119]; □ – Ref. [120]; the solid line is the best fit corresponding to $K_1^{(mic)}$ = 0.302 mM and γ_0 = 4.553 mN/m. (b) Corrin–Harkins plot: the points and line in panel a are plotted as log(CMC) vs. log(*I*). (c) Plot of A_1 and of the degree of counterion binging, 1 − α, vs. the NaBr concentration; the solid line is A_1 calculated from Eq. (4.30), whereas the dashed line correspond to the fit of the data in panel b by linear regression.

from a surface tension fit is K_{St} = 0.748 M^{-1} [96]. R = 2.01 nm is estimated as in Ref. [21], and the values of the parameters A, Bd_i, and b in Eq. (4.7) for the activity coefficient are also knows; see above. At the CMC, the concentration of micelles is negligible, so that c_{mic} = 0. Then, from Eqs. (4.5), (4.6) and (4.8) we obtain $c_1 \approx C_1$ = CMC and $c_2 = c_1 + C_{salt} = I$, where c_{12} is neglected for DTAB. Our goal is to calculate the theoretical dependence of c_1 = CMC on C_{salt}, and to compare the calculated curve with the experimental data in Fig. 3a. The steps of the used procedure are:

(1) We assign tentative values of $K_1^{(mic)}$ and γ_0.
(2) To apply the bisection method, we assign lower and upper boundaries for the variation of c_1 in view of the experimental range of CMC.
(3) For a given C_{salt}, an initial value of c_1 is assigned, and then $c_2 = I = c_1 + C_{salt}$.
(4) $\gamma_\pm$ and κ and Φ_s are calculated from Eqs. (4.7), (4.14) and (4.26), respectively.
(5) The obtained κ and Φ_s are substituted in Eq. (4.21a), which is solved numerically to determine c_1 using the bisection method; j = 2 is to be set for spherical micelles.

Thus, we obtain the theoretical dependence CMC = $c_1(C_{salt}, K_1^{(mic)}, \gamma_0)$, which is fitted to the experimental data (see e.g., Fig. 3a) by varying the adjustable parameters $K_1^{(mic)}$ and γ_0 with the help of the least squares method.

For the considered example, the best fit is shown by solid line in Fig. 3a, where the values of $K_1^{(mic)}$ and γ_0 are also shown. It is interesting that the theoretical model excellently fits the data even at the higher salt concentrations (≈200 mM), where the micelles can be elongated, rather than spherical. This is due to the fact that at the higher salt concentrations the last term in Eq. (4.21a), the one $\propto (\kappa R)^{-1}$, becomes negligible, so that the micelle–monomer equilibrium, described by the considered system of Eqs. (4.1)–(4.8) and (4.21), is insensitive to the micelle shape.

4.6. The Corrin–Harkins plot

Corrin and Harkins [3] showed that the dependence of CMC of the ionic surfactants on the solution's ionic strength I becomes linear when plotted in double logarithmic scale:

$$\log \mathrm{CMC} = A_0 - A_1 \log I. \tag{4.27}$$

A_0 and A_1 are constant coefficients. Note that at the CMC the ionic strength coincides with the concentration of counterions: $I = c_2 = c_1 + C_{salt}$. As an illustrative example, Fig. 3b shows the plot of the data for DTAB in accordance with Eq. (4.27).

If CMC_0 is the value of CMC at a given ionic strength I_0, then Eq. (4.27) can be expressed in the equivalent form:

$$\frac{\mathrm{CMC}}{\mathrm{CMC}_0} = \left(\frac{I}{I_0}\right)^{-A_1}. \tag{4.28}$$

Corrin [4] interpreted A_1 as the degree of counterion binding, i.e., as the occupancy of the micellar Stern layer by adsorbed counterions. In our notations, the degree of counterion binding is y_2; see Eq. (4.2). Note that $y_2 = 1 - \alpha$, where α is the ionization degree of the micelles.

In view of Eq. (4.27), A_1 can be presented in the form:

$$A_1 = \frac{\mathrm{d}\ln \mathrm{CMC}}{\mathrm{d}\ln I}. \tag{4.29}$$

Because Eqs. (4.1)–(4.8) and (4.21a) represent a complete system of equations, they allow one to calculate the derivative in Eq. (4.29) analytically, and to check whether really $A_1 = y_2$. This derivative is calculated in Appendix B. The result, substituted in Eq. (4.29), yields the following expression for A_1:

$$A_1 = y_2 + \frac{(1-y_2)\tanh(\Phi_s/4)}{1 + j/[2\kappa R \cosh^2(\Phi_s/4)]} + (1+y_2)\frac{\mathrm{d}\ln \gamma_\pm}{\mathrm{d}\ln I}. \tag{4.30}$$

Eq. (4.30) shows that in general $A_1 \neq y_2$. In Fig. 3c, we compare (i) the constant value of A_1 calculated from the fit of the data in Fig. 3b by

linear regression; (ii) the variable A_1 calculated from Eq. (4.30) and (iii) the degree of counterion binding, y_2, calculated from Eq. (4.25).

In the calculations, we used the dependence $c_1 = c_1(C_{salt}, K_1^{(mic)}, \gamma_0)$ corresponding to the best fit (the solid line) in Fig. 3a. Furthermore, $I = c_2 = c_1 + C_{salt}$; $\gamma_\pm$ is computed from Eq. (4.7), and Φ_s — from Eq. (4.26). The derivative in the last term of Eq. (4.30), calculated from Eq. (4.7), is:

$$\frac{d\ln\gamma_\pm}{d\ln I} = \left[bI - \frac{A\sqrt{I}}{2\left(1+Bd_i\sqrt{I}\right)^2}\right]\ln 10. \tag{4.31}$$

The results shown in Fig. 3c show that A_1 calculated from Eq. (4.30) is almost constant and very close to the slope of the linear-regression fit of the data in Fig. 3b. In contrast, y_2 is markedly smaller than A_1, especially at the lower salt concentrations, and y_2 essentially varies (increases) with the rise of the salt concentration. For example, in the absence of salt $y_2 = 0.45$, whereas $A_1 = 0.68$ as estimated from Eq. (4.30).

In conclusion, the slope of the Corrin–Harkins plot A_1 is different from the degree of counterion binging, y_2. Values of these quantities for various surfactants are compared in Section 5.

4.7. Computational procedure for concentrations above the CMC

Having determined $K_1^{(mic)}$ and γ_0 from fits of experimental data for the CMC (Section 4.5), we can further use the complete system of Eqs. (4.1)–(4.8) and (4.21) to calculate the properties of the system, such as c_1, c_2, c_{mic}, y_1, y_2, Φ_s and $\Gamma_1 = 1/a_1$, at any concentrations of surfactant and salt (C_1 and C_{salt}) above the CMC. For this goal, we solved the system numerically. First, we will derive some auxiliary equations that are used in the numerical procedure.

It is convenient to introduce the parameters

$$\tilde{K}_1^{(mic)} \equiv K_1^{(mic)} e^{\Phi_s} \quad \text{and} \quad \tilde{K}_{St} \equiv K_{St} e^{\Phi_s}. \tag{4.32}$$

Next, from Eqs. (4.24) and (4.25) we can express y_1 and y_2

$$y_1 = \frac{c_1\gamma_\pm}{\tilde{K}_1^{(mic)}}, \qquad y_2 = \frac{\tilde{K}_{St}c_1c_2\gamma_\pm^2}{\tilde{K}_1^{(mic)}}. \tag{4.33}$$

Substituting the above equations in the identity $y_1 + y_2 = 1$, we can express c_2 as a function of c_1:

$$c_2 = \frac{1}{\tilde{K}_{St}\gamma_\pm}\left(\frac{\tilde{K}_{mic}}{c_1\gamma_\pm} - 1\right). \tag{4.34}$$

From the mass balance equations, Eqs. (4.5) and (4.6), we deduce:

$$y_1C_1 + C_{salt} + y_2c_1 - c_2 - y_1c_{12} = 0 \tag{4.35}$$

$$y_1c_{mic} = c_2 - c_1 - C_{salt}. \tag{4.36}$$

The computational procedure, which is non-trivial, is as follows. The input parameters are C_1, C_{salt}, K_{St}, $K_1^{(mic)}$, γ_0, and R; $j = 2$ for spherical micelles. [$j = 2$ can be used also for spheroidal micelles, because the curvature terms $\propto 1/(\kappa R)$ in Eqs. (4.17) and (4.21) represent only small corrections; see above]. All calculations have been performed in double precision.

(1) A tentative value of Φ_s is assigned in a given interval, say $0.1 \le \Phi_s \le 6$.
(2) $\tilde{K}_1^{(mic)}$ and $\tilde{K}_{St}$ are calculated from Eq. (4.32).
(3) As a zero-order approximation for the ionic strength we set $I = C_1 + C_{salt}$.
(4) $\gamma_\pm$ is calculated from Eq. (4.7);
(5) A tentative value of c_1 is assigned in the interval $0 < c_1 < \tilde{K}_{mic}/\gamma_\pm$ — start of a procedure to solve Eq. (4.35) by the bisection method.
(6) c_2 is calculated from Eq. (4.34); y_1 — from Eq. (4.33), and $y_2 = 1 - y_1$.
(7) The results are substituted in Eq. (4.35) (with $c_{12} = 0$ in zero-order approximation). Eq. (4.35) becomes an implicit equation for c_1, which is solved numerically by using the bisection method. The left-hand side of Eq. (4.35) is a monotonic function of c_1. In this way, the values of c_1, as well as of c_2, y_1 and y_2 are determined.
(8) The obtained c_1 and c_2 are substituted in Eq. (4.8) to obtain the next approximation for the ionic strength I and the iteration procedure for I continues from point (4) above. The iterations finish when the relative error in I becomes $<10^{-8}$. Usually, 6 iterations are enough to reach this precision.
(9) κ is calculated from Eq. (4.14) and ν — from Eqs. (4.15) and (4.36).
(10) The results are substituted in Eq. (4.21), which represents an implicit equation for Φ_s that is solved numerically by the bisection method repeating the steps from (2) to (9) for different Φ_s values. [The right-hand side of Eq. (4.21) is a monotonic function of Φ_s].
(11) The procedure yields the values of Φ_s, I, c_1, c_2, y_1, y_2, and $\gamma_\pm$. Finally, c_{mic} is calculated from Eq. (4.36) and Γ_1 — from Eq. (4.23) along with Eq. (4.17). From the value of Γ_1, one can calculate the micelle aggregation number, $N_{agg} = A_m\Gamma_1$, only if the micelle surface area A_m is determined in the framework of a given model of micelle shape (spherical, elongated, hairy, etc.).

For carboxylate solutions, c_{12} can be important. A first approximation for c_{12} can be obtained by substituting the obtained c_1, c_2, and $\gamma_\pm$, in Eq. (4.3). More accurate values of c_{12} can be obtained by further iterations.

Illustrative results for c_1, c_2 and c_{mic} vs. C_1 at $C_{salt} = 0$ are shown in Fig. 4a for DTAB for the values of K_{St}, $K_1^{(mic)}$, γ_0, and R from Section 4.5. As seen in Fig. 4a, the concentration of surfactant in micellar form, c_{mic}, decreases with the decrease of the DTAB concentration and reaches $c_{mic} = 0$ at $C_1 = 15.3$ mM, which is the value of CMC. From a physical viewpoint, this is what should be expected, but from a computational viewpoint this result is quite nontrivial because the system of Eqs. (4.1)–(4.8) and (4.21) automatically predicts the value of CMC, which corresponds to $c_{mic} = 0$.

At $C_1 >$ CMC, the presence of micelles leads to a difference between the concentrations of surfactant ions and counterions, c_1 and c_2. As seen in Fig. 4a, c_1 begins to decrease, whereas c_2 keeps increasing, but with a smaller slope. Physically, the decrease of c_1 can be explained with the reduced repulsion between the surfactant headgroups in the micelle that allows accommodation of more surfactant molecules in the micelle. From the viewpoint of the micelle–monomer equilibrium, the rise of surfactant concentration increases the ionic strength, I, which leads to a lower micelle surface potential, Φ_s, and to a smaller y_1 (greater y_2 because of the counterion binding), which leads to lowering also of c_1 in accordance with Eq. (4.1). The smaller slope of c_2 above the CMC is due to the binding of a part of the counterions to the micelle surfaces.

In our calculations, we estimated the micelle radius at the level of surface charges, R, as the length of the surfactant molecule using molecular size considerations; see e.g., Refs. [21,40,44,115,116,121,122].

4.8. Electrolytic conductivity of micellar solutions

The quantitative description of the variations of c_1 and c_2 above the CMC (see Fig. 4a) is important for the correct interpretation of the electrolytic conductivity, κ_e, of micellar solutions. As an illustration, Fig. 4b

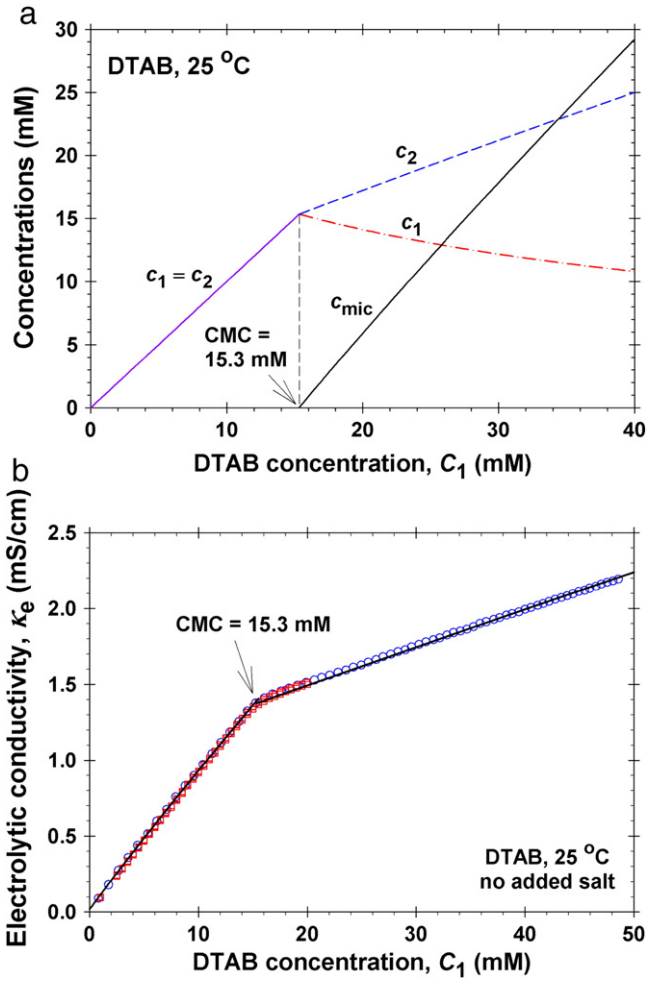

Fig. 4. (a) Plot of the concentrations of surfactant ions c_1, coions c_2, and surfactant in micellar form, c_{mic}, vs. the DTAB concentration, C_1, calculated by the procedure in Section 4.7 with the parameter values determined from the fit in Fig. 3a. (b) Plot of conductivity κ_e vs. C_1; ○ — data from Ref. [123]; □ — data from Ref. [124] obtained at three frequencies: 0.2, 2.1 and 20 MHz. The solid line is the theoretical curve drawn according to Eq. (4.37); details in Section 5.1.

shows a set of experimental data for κ_e for DTAB solutions from Refs. [123,124]. The CMC appears as a kink in the conductivity vs. surfactant concentration plot. The following equation can be used for the quantitative interpretation of this plot: [125,126]:

$$\kappa_e = \kappa_0 + \lambda_1^{(0)} c_1 + \lambda_2^{(0)} c_2 + \lambda_{co}^{(0)} C_{salt} + Z\lambda_m c_m - AI^{3/2} + BI^2. \qquad (4.37)$$

Here, $\lambda_1^{(0)}$, $\lambda_2^{(0)}$ and $\lambda_{co}^{(0)}$ are the limiting (at infinite dilution) molar conductances, respectively, of the surfactant ions, counterions and coions due to the non-amphiphilic salt (if any). Here, it is assumed that all electrolytes (except the micelles) are of 1:1 type. Values of the conductances of various ions can be found in handbooks [127,128]. The term $Z\lambda_m c_m$ accounts for the contribution of the micelles to the conductivity κ_e; λ_m stands for the molar conductance of the micelles; as before, c_m and Z are the micelle concentration and charge. The constant term κ_0 accounts for the presence of a background electrolyte in the water used to prepare the solution. Usually, κ_0 is due to the dissolution of a small amount of CO_2 from the atmosphere; κ_0 is to be determined as an adjustable parameter. In the special case $C_1 <$ CMC, Eq. (4.37) has to be used with $c_m = 0$ and $I = c_2 = c_1 + C_{salt}$.

The last two terms in Eq. (4.37), where A and B are constant parameters, present an empirical correction (the complemented Kohlrausch law) that accounts for long-range interactions between the ions in the aqueous solution. It was experimentally established that A and B are not so sensitive to the type of 1:1 electrolyte [125,126]. As an illustration, Table 2 shows the values of A and B from Ref. [127] for four different 1:1 electrolytes at 25 °C; I is measured in M and κ_e — in mS/cm. In the present study, for all solutions that contain Br^- and Cl^- ions (both below and above the CMC), the values of the parameters A and B in Eq. (4.37) have been taken for NaBr and NaCl, respectively; see Table 2.

In Section 5, Eq. (4.37) is used to interpret data for the conductivity of several ionic surfactants, like those in Fig. 4b. The results are discussed in Section 5.6.

5. Application of the model to various ionic surfactants

Here, we apply the model from Section 4 to five different surfactants: DTAB, TTAB, CTAB, CPC and SDS. The unknown parameters $K_1^{(mic)}$ and γ_0 are determined from fits of the dependence of CMC on the concentration of added salt. Having determined all parameters of the model, we further predict different micellar properties, such as surface electric potential, ψ_s, head group density at the micelle surface, $\Gamma_1 = 1 / a_1$; degree of ionization, α, aggregation number, N_{agg}, and electrolytic conductivity of the micellar solutions, κ_e. All calculations have been carried out using the MN closure; see Eqs. (4.21) and (4.21a). The predictions of the model for α, N_{agg} and κ_e are compared with available literature data.

5.1. Dodecyltrimethylammonium bromide (DTAB)

As seen in Fig. 3a, the theoretical model presented in Section 4 excellently describes the dependence of the CMC on the concentration of added salt. As already mentioned, the model contains only four parameters: $K_1^{(mic)}$, γ_0, K_{St} and R. Two of them, $K_1^{(mic)}$ and γ_0, have been determined from the fit of the data in Fig. 3a. K_{St} has been previously determined [96] from the fit of data for the surface tension of DTAB solutions, and R is set equal to the length of the DTAB molecule estimated by molecular size considerations; see e.g., [21]. In Table 3, the values of these four parameters for DTAB are compared with the respective values for the other surfactants investigated in the present article.

Note that in the paper by Mitchell and Ninham [85], the reported values of γ_0 are greater than those in Table 3 because the effect of counterion binding was not taken into account in this study. As a result, the calculated values of Φ_s and π_{el} become considerably greater, and consequently, a greater γ_0 is necessary to counterbalance π_{el}; see Eq. (4.19).

As mentioned above, having determined the parameters of the model, we can further calculate (predict) all properties of the micellar solution that are related to this model: c_1, c_2, c_{mic}, ψ_s, Γ_1, $\alpha = y_1$, N_{agg}, κ_e, etc. In Section 4.7, we already presented and discussed the dependencies of c_1, c_2 and c_{mic} on the DTAB concentration; see Fig. 4a.

Fig. 5a shows the calculated dependencies of ψ_s and Γ_1 on C_{salt} at the CMC. As expected, the surface electric potential decreases, from 113 to 76 mV with the rise of the NaBr concentration, which leads to a considerable decrease of the electrostatic energy of a surfactant

Table 2
Values of the parameters A and B in Eq. (4.37) from Ref. [127] for different 1:1 electrolytes at 25 °C.

Electrolyte	A [mS cm^{-1} M$^{-3/2}$]	B [mS cm^{-1} M^{-2}]
NaCl	88.6	93.6
NaBr	88.2	63.0
KCl	94.4	95.9
KBr	94.1	94.1

Table 3
Thermodynamic parameters for different ionic surfactants estimated as explained in Section 4.

Surfactant	K_{St} (M^{-1}), reference	$K_1^{(mic)}$ (mM)	$\gamma_0 = \gamma_{0,1}$ (mN/m)	R (nm)
DTAB	0.748 [96]	0.303	4.553	2.01
TTAB	2.40 [116]	0.0576	3.492	2.26
CTAB	7.50 [129]	0.0110	2.994	2.52
CPC	5.93 [21]	0.0132	2.289	2.58
SDS	0.653 [84,114,115]	0.0933	4.352	2.03

ion in the micelle. Correspondingly, the density of surfactant headgroups at the micelle surface, Γ_1, increases about 3 times, which represents a significant rise. The maximal value $\Gamma_1 = 4.5$ μmol/m^2 (Fig. 5a) corresponds to $a_1 = 1 / \Gamma_1 = 36.9$ Å^2 per molecule which is close to the area 36.5 Å^2 per DTAB molecule at close packing [96].

Fig. 5b shows results at concentrations above the CMC, viz. the dependencies of α and N_{agg} on the DTAB concentration, C_1, without added salt. In the calculation of N_{agg} from Eq. (4.17), $A_m = 4\pi R^2$ for a spherical micelle is assumed. The calculated values of α for DTAB in the range of 0.46–0.56 and N_{agg} in the range of 52–70 are very close to those obtained in Ref. [22] for SDS by analysis of the stepwise transitions in the thickness of foam films formed from micellar solutions. Literature data for the aggregation number of DTAB, $N_{agg} = 53$ [130] and 56 [131], belong to the same range.

At $C_1 <$ CMC, the data for conductivity of DTAB solutions in Fig. 4b are fitted by means of Eq. (4.37) with $c_m = 0$ and $I = c_2 = C_1 + C_{salt}$. Two parameters, $\lambda_1^{(0)} = 21.6 \pm 0.1$ cm^2 S/mol and $\kappa_0 = 0.018 \pm 0.002$ mS/cm, have been determined from this fit.

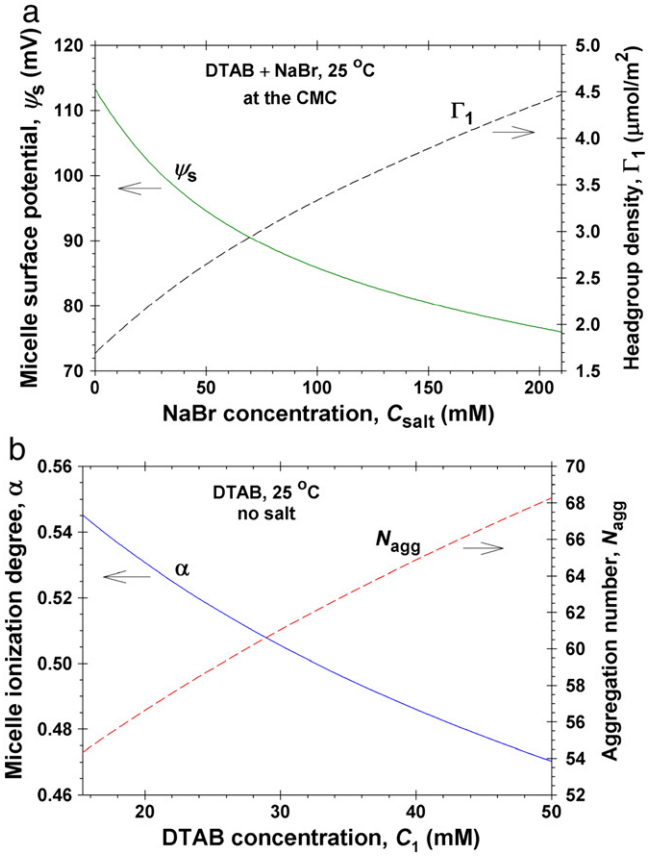

Fig. 5. Numerical results for DTAB micelles. (a) Micelle surface potential, ψ_s, and head group surface density, Γ_1, vs. the concentration of NaBr, calculated at $C_1 =$ CMC = 15.3 mM, using the procedure in Section 4.5. (b) Micelle ionization degree, α, and aggregation number, N_{agg}, vs. the DTAB concentration calculated using the procedure in Section 4.7.

In Table 4, the value of $\lambda_1^{(0)}$ for the DTA$^+$ ion is compared with the respective values for other surfactant ions obtained by us in the same way, by fit of literature data for κ_e at $C_1 <$ CMC with the help of Eq. (4.37); see below. The values of $\lambda_i^{(0)}$ for the Na$^+$, Cl$^-$ and Br$^-$ ions in Table 4 are from Ref. [127].

In Fig. 4b, at $C_1 >$ CMC the theoretical curve is calculated using Eq. (4.37) with $\lambda_m = 0$, and with values of all other parameters taken from Tables 2, 3 and 4 (no adjustable parameters). The amazing agreement between the data and this theoretical curve implies that the micelles give no contribution to the conductivity κ_e as carriers of electric current. In Sections 5.2–5.5, this conclusion is verified for other ionic surfactants and the results are discussed in Section 5.6.

5.2. Tetradecyltrimethylammonium bromide (TTAB)

Fig. 6a shows experimental data from Refs. [132–134] for the dependence of the CMC of TTAB solutions on the concentration of added NaBr. The data are fitted by using the procedure described in Section 4.5, and the values of $K_1^{(mic)}$ and γ_0 have been determined as adjustable parameters using K_{St} and R for TTAB from Table 3. $K_1^{(mic)}$ and γ_0 are given in Fig. 6a and compared with the respective values for other surfactants in Table 3.

In Fig. 6b, the data and line from Fig. 6a are presented as a Corrin–Harkins plot, log(CMC) vs. log$I$. We recall that at the CMC the amounts of micelles and bound counterions are negligible, so that the concentration of free counterions is $c_2 = I = C_1 + C_{salt}$. The theoretical line in Fig. 6b is slightly curved, which is better visible in Fig. 6c, where the solid line represents the running slope, A_1, of the line in Fig. 6b. The degree of counterion binding, $y_2 = 1 - \alpha$, is markedly lower than A_1 at the lower salt concentrations (Fig. 6c). Thus, at $C_{salt} = 0$ we have $y_2 = 0.49$, whereas $A_1 = 0.69$ for the running slope and 0.74 for the mean slope (the horizontal dashed line).

Fig. 7a shows the calculated dependencies of ψ_s and Γ_1 on C_{salt} for TTAB micelles at the CMC. As expected, the surface electric potential decreases, from 122 to 78 mV with the rise of the NaBr concentration, which leads to a decrease of the electrostatic energy of a surfactant ion in the micelle. Correspondingly, the density of surfactant headgroups at the micelle surface, Γ_1, increases. In Fig. 7a, the values $\Gamma_1 > 4.55$ μmol/m^2 at $C_{salt} > 80$ mM are non-realistic because they correspond to $a_1 = 1 / \Gamma_1 < 36.5$ Å^2 per molecule which is the area per surfactant molecule at close packing [96]. Hence, one can expect that at $C_{salt} > 80$ mM the formed micelles are non-spherical (elongated).

Fig. 7b shows results at concentrations above the CMC, viz. the dependencies of α and N_{agg} on the TTAB concentration, C_1, without added salt. As before, N_{agg} is calculated from Eq. (4.17) under the assumption that the micelles are spherical with surface area $A_m = 4\pi R^2$. At the CMC, $\alpha = 0.51$ is close to that of DTAB at the CMC, but at higher surfactant concentrations α decreases faster for TTAB, so that at $C_1 = 50$ mM $\alpha = 0.33$ for TTAB vs. 0.47 for DTAB: compare Figs. 5b and 7b. In the range CMC $< C_1 < 50$ mM, the calculated aggregation number of the TTAB micelles increases from 50 to 95 (Fig. 7b). Literature data for this quantity, viz. $N_{agg} = 64$ [135] and 68 [136], belong to the same range.

Table 4
Limiting molar conductances, $\lambda_i^{(0)}$, of ions in water solutions at 25 °C.

Ion	$\lambda_i^{(0)}$ (cm^2 S/mol)
Na$^+$	50.1
Cl$^-$	76.35
Br$^-$	78.1
DTA$^+$ (from DTAB)	21.6
TTA$^+$ (from TTAB)	21.1
CTA$^+$ (from CTAB)	20.6
CP$^+$ (from CPC)	19.5
DS$^-$ (from SDS)	21.5

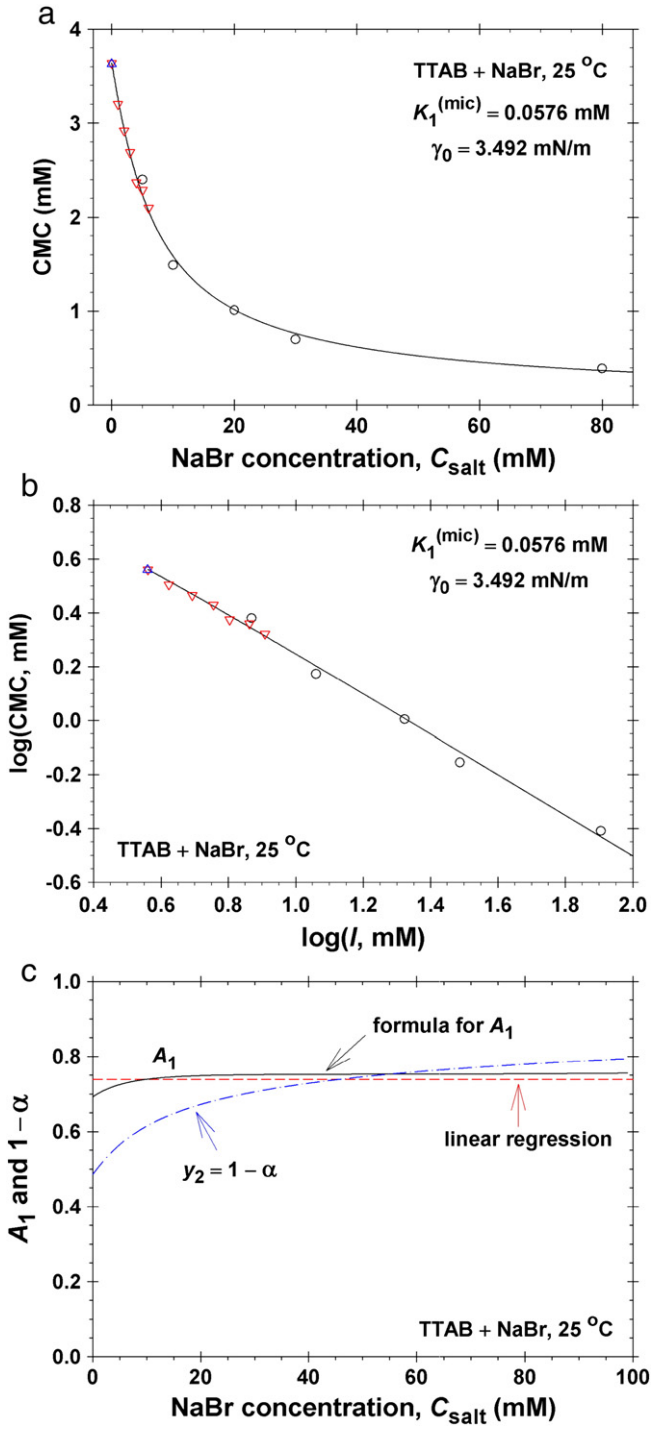

Fig. 6. (a) CMC of TTAB in the presence of NaBr at 25 °C: ○ – Ref. [133]; ▽ – Ref. [134]; Δ – Ref. [132]; the solid line is the best fit corresponding to $K_1^{(mic)} = 0.0576$ mM and $\gamma_0 = 3.492$ mN/m. (b) Corrin–Harkins plot: the points and line in panel a are plotted as log(CMC) vs. log(I). (c) Plot of A_1 and of the degree of counterion binging, $1 - \alpha$, vs. the NaBr concentration; the solid line is A_1 calculated from Eq. (4.30), whereas the dashed line correspond to the fit of the data in panel b by linear regression.

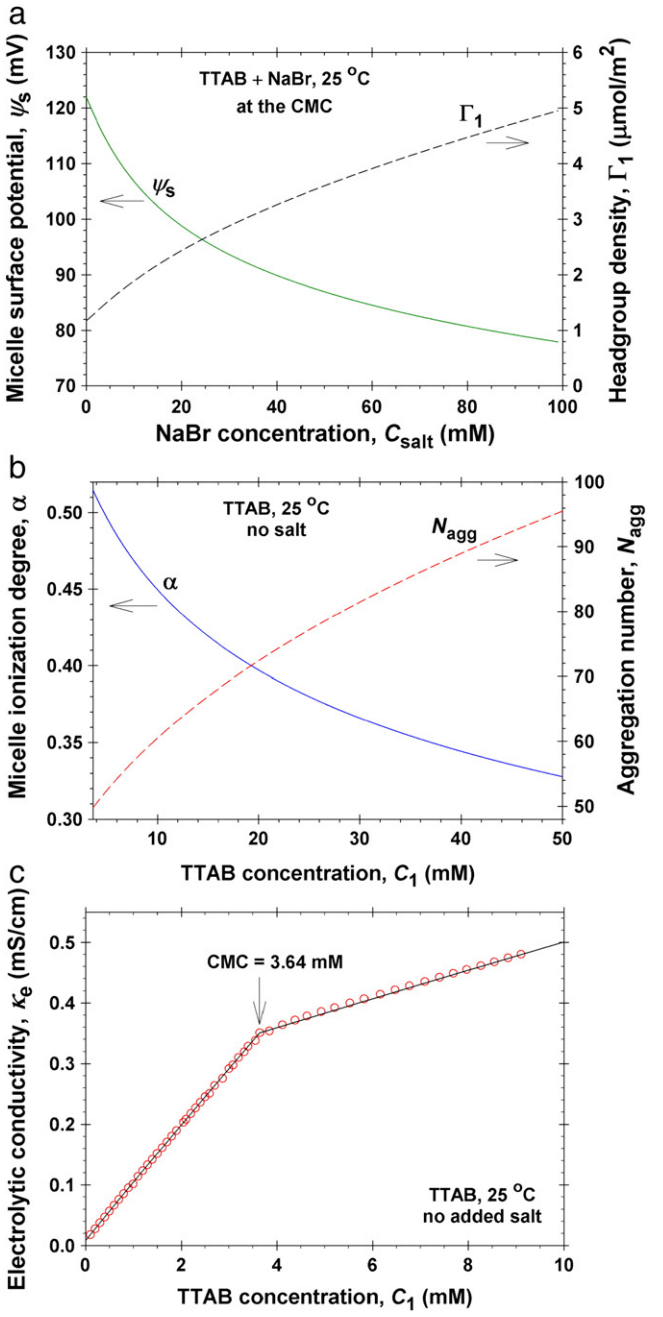

Fig. 7. (a) Surface potential, ψ_s, and head group surface density, Γ_1, of TTAB micelles vs. the concentration of NaBr, calculated at C_1 = CMC = 15.3 mM, using the procedure in Section 4.5. (b) Micelle ionization degree, α, and aggregation number, N_{agg}, vs. the TTAB concentration, C_1, calculated using the procedure in Section 4.7. (c) Conductivity vs. C_1: the experimental points are from Ref. [132]; the solid line is the theoretical curve drawn according to Eq. (4.37); details in Section 5.2.

At C_1 < CMC, the data for conductivity κ_e of TTAB solutions in Fig. 7c are fitted by means of Eq. (4.37) with $c_m = 0$ and $I = c_2 = C_1 + C_{salt}$. Two parameters, $\lambda_1^{(0)} = 21.1 \pm 0.1$ cm^2 S/mol and $\kappa_0 = 0.008 \pm 0.001$ mS/cm, have been determined from this fit. In Table 4, the value of $\lambda_1^{(0)}$ for the TTA^+ ion is compared with the respective values for other surfactant ions obtained by us in a similar way.

In Fig. 7c, at C_1 > CMC the theoretical curve for κ_e of TTAB solutions is calculated using Eq. (4.37) with $\lambda_m = 0$, and with values of all other parameters taken from Tables 2, 3 and 4 (no adjustable parameters). As in the case of DTAB, the calculated line excellently agrees with the experimental data. As already mentioned, this result indicates that the micelles give no contribution to the conductivity κ_e as carriers of electric current. This conclusion is discussed in Section 5.6 on the basis of the results obtained for all investigated surfactants.

5.3. Cetyltrimethylammonium bromide (CTAB)

Fig. 8a shows experimental data from Refs. [129,133] for the dependence of the CMC of CTAB solutions on the concentration of

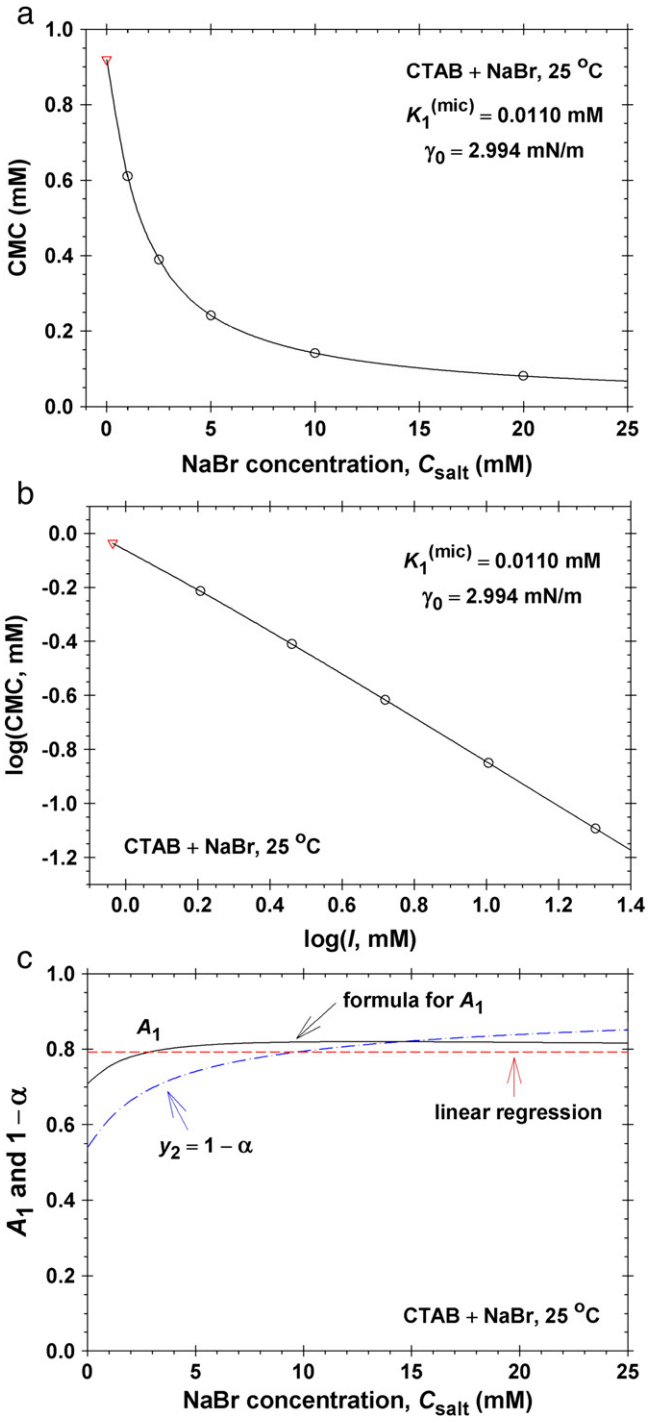

Fig. 8. (a) CMC of CTAB in the presence of NaBr at 25 °C: ○ – Ref. [133]; ▽ – Ref. [129]; the solid line is the best fit corresponding to $K_1^{(mic)} = 0.0110$ mM and $\gamma_0 = 2.994$ mN/m. (b) Corrin–Harkins plot: the points and line in panel a are plotted as log(CMC) vs. log(*I*). (c) Plot of A_1 and of the degree of counterion binging, $1 - \alpha$, vs. the NaBr concentration; the solid line is A_1 calculated from Eq. (4.30), whereas the dashed line correspond to the fit of the data in panel b by linear regression.

added NaBr. The data are fitted by using the procedure described in Section 4.5. $K_1^{(mic)}$ and γ_0 have been determined as adjustable parameters using K_{St} and R for CTAB from Table 3. The values of $K_1^{(mic)}$ and γ_0 are given in Fig. 8a, and are compared with the respective values for other surfactants in Table 3.

In Fig. 8b, the data and line from Fig. 8a are presented as a Corrin–Harkins plot, log(CMC) vs. log*I*. The dependence in Fig. 8b is close to linear, but still has a small curvature that is better visible in Fig. 8c, where the solid line represents the running slope, A_1, of the line in Fig. 8b. The degree of counterion binding, $y_2 = 1 - \alpha$, is markedly lower than A_1 at the lower salt concentrations (Fig. 8c). Thus, at $C_{salt} = 0$ we have $y_2 = 0.54$, whereas $A_1 = 0.71$ for the running slope and 0.79 for the mean slope (the horizontal dashed line).

The solid and dashed lines in Fig. 9a show the calculated dependencies of N_{agg} and α on the CTAB concentration, C_1, without added salt. N_{agg} is calculated from Eq. (4.17) under the assumption that the micelles are spherical with surface area $A_m = 4\pi R^2$. In the concentration range $10 \le C_1 \le 50$ mM CTAB, the calculated N_{agg} increases from 93 to 165, whereas α decreases from 0.30 to 0.19.

The symbols in Fig. 9a show data for N_{agg} and α, which have been determined in Refs. [21,22] by quantitative interpretation of experimental results for the stepwise thinning of foam films formed from

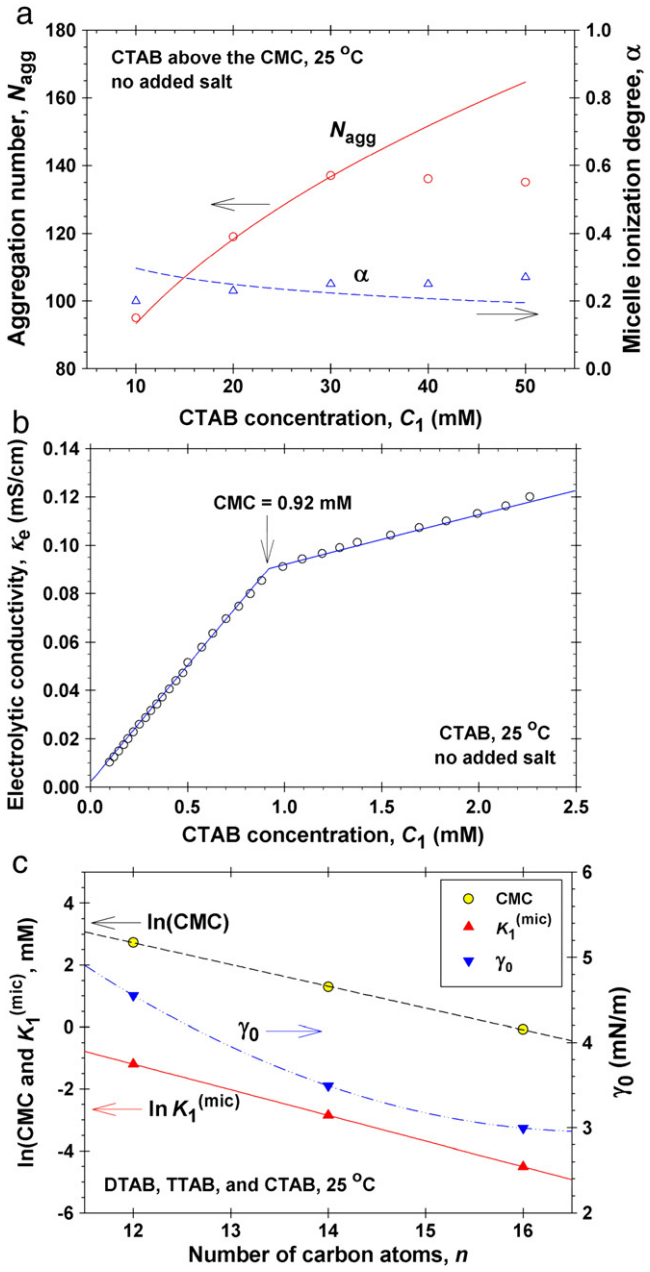

Fig. 9. (a) Micelle aggregation number, N_{agg}, and ionization degree, α, vs. the CTAB concentration C_1: the points are from Ref. [22]; the lines are calculated by the procedure in Section 4.7; no adjustable parameters; (b) conductivity vs. C_1: the experimental points are from Ref. [137]; the solid line is the theoretical curve drawn according to Eq. (4.37); details in Section 5.3. (c) Plot of ln(CMC), ln$K_1^{(mic)}$ and γ_0 vs. *n* for the homologous series C_nTAB, $n = 12$, 14 and 16.

micellar CTAB solutions. Note that the theoretical lines in the same figure are drawn completely independently and do not represent fits of the data points from Refs. [21,22]. The agreement between the curves and the points is good, except at the higher values of N_{agg}, where the difference probably indicates the formation of non-spherical (elongated) CTAB micelles.

At C_1 < CMC, the data for conductivity κ_e of CTAB solutions in Fig. 9b from Ref. [137] are fitted by means of Eq. (4.37) with $c_m = 0$ and $I = c_2 = C_1 + C_{salt}$. Two parameters, $\lambda_1^{(0)} = 20.6 \pm 0.1$ cm^2 S/mol and $\kappa_0 = 0.002 \pm 0.001$ mS/cm, have been determined from this fit. A very close value of the molar conductance of the CTA^+ ions, $\lambda_1^{(0)} = 20$ cm^2 S/mol, is reported in Refs. [138,139].

In Fig. 9b, at C_1 > CMC the theoretical curve for κ_e of CTAB solutions is calculated using Eq. (4.37) with $\lambda_m = 0$, and with values of all other parameters taken from Tables 2, 3 and 4 (no adjustable parameters). As in the case of DTAB and TTAB, the calculated line excellently agrees with the experimental data, indicating that the micelles give a negligible contribution to the conductivity κ_e as carriers of electric current; for discussion see Section 5.6.

Fig. 9c, compares the values of CMC, $K_1^{(mic)}$ and γ_0 for three members of the homologous series, C_nTAB, $n = 12$, 14 and 16. The plot of ln(CMC) vs. n is linear, as expected; see Eq. (1.1). The plot of $\ln K_1^{(mic)}$ vs. n is also linear — it is an analog of the Traube's rule [140,141] for micelles. The slope of this plot gives 0.83 kT gain of standard free energy per CH_2 group upon the transfer of the hydrocarbon tail from water into the micelle.

The dependence of the non-electrostatic component of micelle surface tension, γ_0, on the number of C atoms in the surfactant tail turns out to be nonlinear. The three points for γ_0 in Fig. 9c can be interpolated by an empirical exponentially decaying function:

$$\gamma_0 = \gamma_\infty + \Delta\gamma_{12} \exp[-b(n-12)] \tag{5.1}$$

where $\gamma_\infty = 2.5535$ mN/m; $\Delta\gamma_{12} = 1.9995$ mN/m and $b = 0.3782$. Eq. (5.1) can be used for estimating γ_0 at other n values by interpolation or extrapolation. Additional studies, both experimental and theoretical are needed to interpret the dependence of γ_0 on the surfactant chain length.

5.4. Cetylpyridinium chloride (CPC)

Fig. 10a shows experimental data from Refs. [21,142] for the dependence of the CMC of CPC solutions on the concentration of added salt (Na, Li and K chlorides). The data have been fitted by using the procedure described in Section 4.5. $K_1^{(mic)}$ and γ_0 have been determined as adjustable parameters using K_{St} and R for CPC from Table 3. The values of $K_1^{(mic)}$ and γ_0 are given in Fig. 10a and compared with the respective values for other surfactants in Table 3.

In Fig. 10b, the data and line from Fig. 10a are presented as a Corrin–Harkins plot, log(CMC) vs. log$I$. The dependence in Fig. 10b has a noticeable curvature that is better visible in Fig. 10c, where the solid line represents the running slope, A_1, of the line in Fig. 10b. The degree of counterion binding, $y_2 = 1 - \alpha$, is lower than A_1 at the lower salt concentrations (Fig. 10c). Thus, at $C_{salt} = 0$ we have $y_2 = 0.34$, whereas $A_1 = 0.55$. Conversely, at the higher salt concentrations the calculations give $y_2 > A_1$. For example, $C_{salt} = 100$ mM we have $y_2 = 0.85$, whereas $A_1 = 0.77$.

The solid and dashed lines in Fig. 11a show the calculated dependencies of N_{agg} and α on the CPC concentration, C_1, without added salt. As usual, N_{agg} is calculated from Eq. (4.17) under the assumption that the micelles are spherical with surface area $A_m = 4\pi R^2$. In the concentration range $10 \le C_1 \le 50$ mM CPC, the calculated N_{agg} increases from 53 to 99, whereas α decreases from 0.42 to 0.28.

The symbols in Fig. 11a show data for N_{agg} and α, which have been determined in Refs. [21,22] by quantitative interpretation of experimental results for the stepwise thinning of foam films formed from

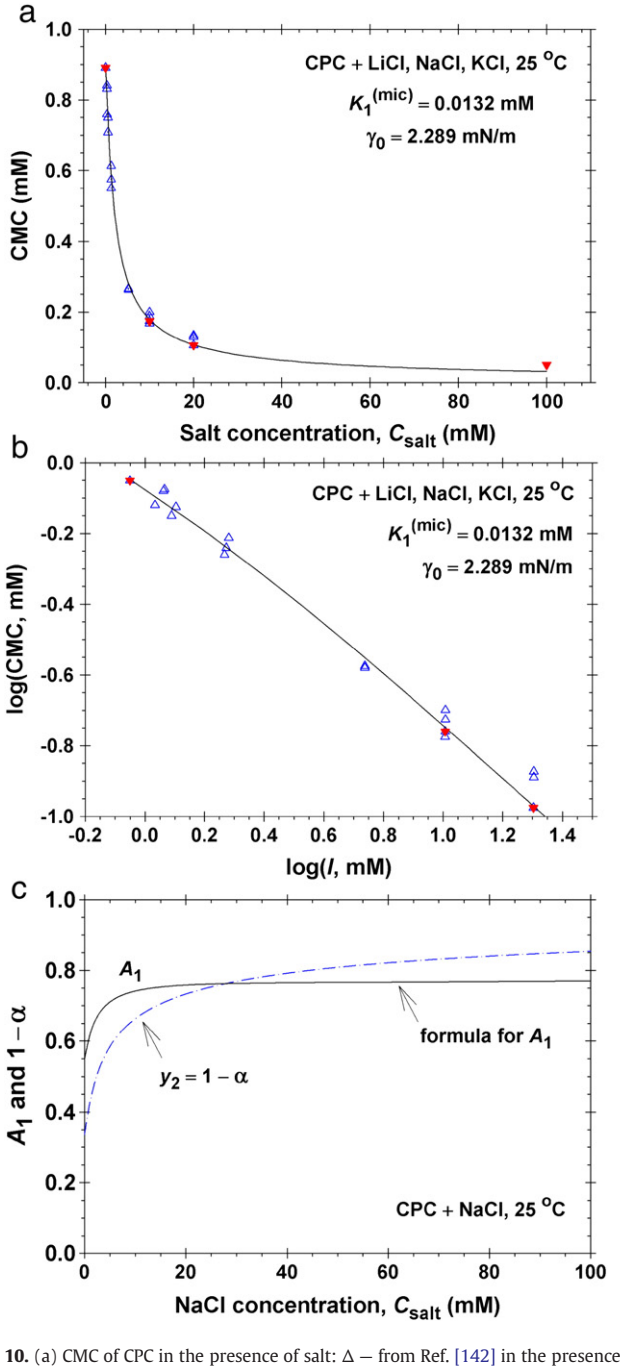

Fig. 10. (a) CMC of CPC in the presence of salt: Δ — from Ref. [142] in the presence of LiCl, NaCl, and KCl; ▽ — from Ref. [21] in the presence of NaCl; the solid line is the best fit corresponding to $K_1^{(mic)} = 0.0132$ mM and $\gamma_0 = 2.289$ mN/m. (b) Corrin–Harkins plot: the points and line in panel a are plotted as log(CMC) vs. log(I). (c) Plot of A_1 and of the degree of counterion binging, $y_2 = 1 - \alpha$, vs. the NaCl concentration; A_1 and y_2 are calculated from Eqs. (4.30) and (4.33), respectively.

micellar CPC solutions. The theoretical lines in the same figure are drawn independently and do not represent fits of the data points from Refs. [21,22]. The good agreement between the curves and the points in Fig. 11a, which have been obtained in quite different ways, supports the adequacy of the physicochemical model from Section 4.

At C_1 < CMC, the data for conductivity κ_e of CPC solutions in Fig. 11b are fitted by means of Eq. (4.37) with $c_m = 0$ and $I = c_2 = C_1 + C_{salt}$. Two parameters, $\lambda_1^{(0)} = 19.5 \pm 0.1$ cm^2 S/mol and $\kappa_0 = 0.002 \pm 0.0002$ mS/cm, have been determined from this fit. The investigated CPC sample contains an admixture of 0.08 mol% NaCl, which has been taken into account in the calculations. The determined limiting molar

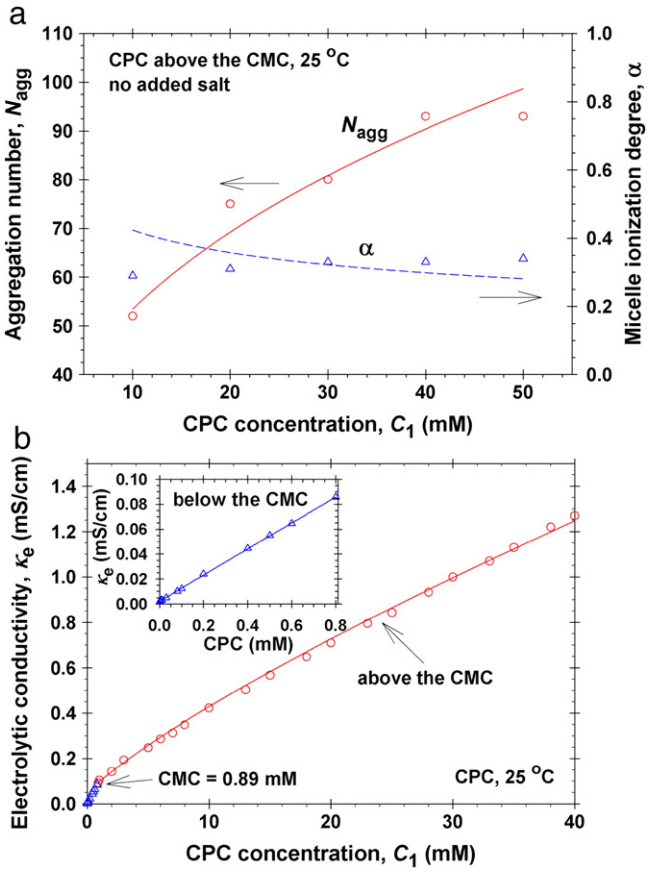

Fig. 11. Comparison of theory and experiment for CPC. (a) Micelle aggregation number, N_{agg}, and ionization degree, α, vs. the CPC concentration C_1: the points are from Ref. [22]; the lines are calculated by the procedure in Section 4.7; no adjustable parameters; (b) conductivity vs. C_1: the experimental points are from Ref. [21]; the inset shows the data at $C_1 <$ CMC in an enlarged scale; the solid line is the theoretical curve drawn according to Eq. (4.37); details in Section 5.4.

conductance, $\lambda_1^{(0)}$, of the CP^+ ion is compared in Table 4 with the conductances of the other investigated surfactant ions.

In Fig. 11b, at $C_1 >$ CMC the theoretical curve for κ_e of CPC solutions is calculated using Eq. (4.37) with $\lambda_m = 0$, and with values of all other parameters taken from Tables 2, 3 and 4 (no adjustable parameters). As in the case of DTAB, TTAB and CTAB the calculated line excellently agrees with the experimental data, indicating that the micelles give no contribution to the conductivity κ_e as carriers of electric current (see Section 5.6 for a discussion of this result).

5.5. Sodium dodecyl sulfate (SDS)

Fig. 12a shows experimental data from Refs. [96,120,143–148] for the dependence of the CMC of SDS solutions on the concentration of added sodium salts. The data are fitted by using the procedure described in Section 4.5. $K_1^{(mic)}$ and γ_0 have been determined as adjustable parameters using K_{St} and R for SDS from Table 3. In this table, the obtained values of $K_1^{(mic)}$ and γ_0 are compared with the respective values for other surfactants.

In Fig. 12b, the data and line from Fig. 12a are presented as a Corrin–Harkins plot, log(CMC) vs. log$I$. The dependence in Fig. 12b is very close to a straight line, which is visualized also in Fig. 12c, where the solid line represents the running slope (A_1) of this line in Fig. 12b. The degree of counterion binding, $y_2 = 1 - \alpha$, is markedly lower than A_1, especially at the lower salt concentrations (Fig. 12c). Thus, at $C_{salt} = 0$ we have $y_2 = 0.34$, whereas $A_1 = 0.64$.

The solid and dashed lines in Fig. 13a show the calculated dependencies of N_{agg} and α on the SDS concentration, C_1, without added

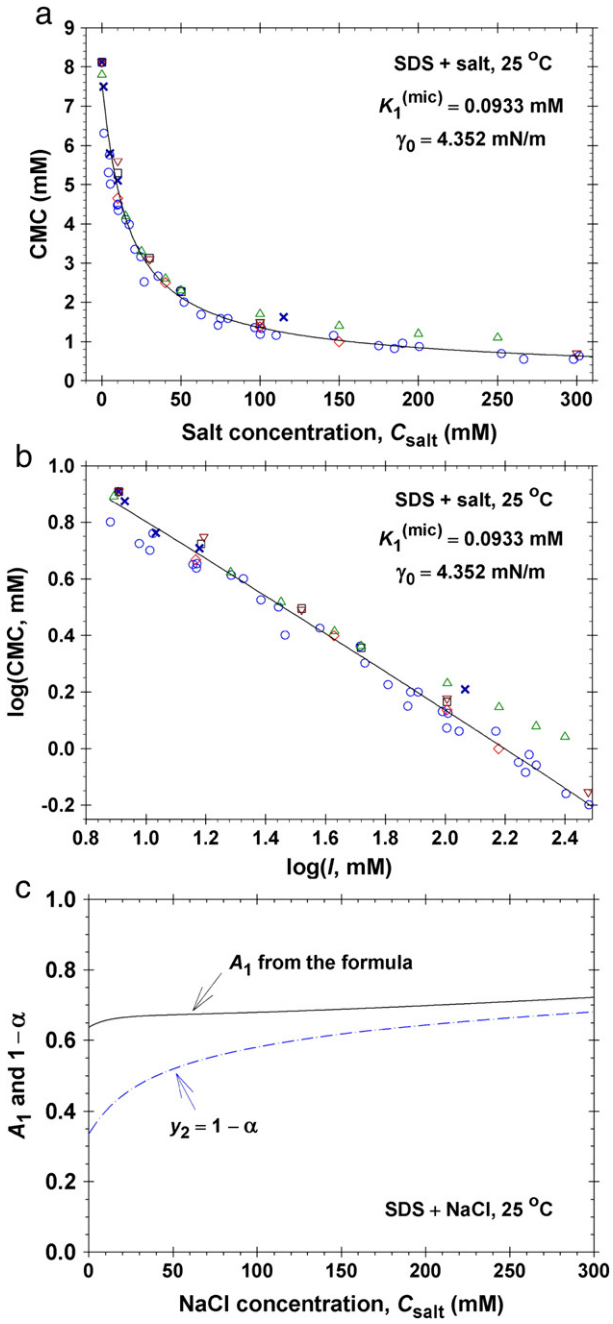

Fig. 12. (a) CMC of SDS in the presence of salt: ○ — with NaCl, NaAc, NaPr, and NaBu from Ref. [143], and with NaCl: ▽ — from Ref. [120]; △ — from Ref. [144]; ◊ from Ref. [96]; × — from Refs. [145–147]; □ — from Ref. [148]; the solid line is the best fit corresponding to $K_1^{(mic)} = 0.0933$ mM and $\gamma_0 = 4.352$ mN/m. (b) Corrin–Harkins plot: the points and line in panel a are plotted as log(CMC) vs. log(I). (c) Plots of A_1 and of the degree of counterion binding y_2 vs. C_{salt} calculated from Eqs. (4.30) and (4.33), respectively.

salt. N_{agg} is calculated from Eq. (4.17) under the assumption that the micelles are spherical with surface area $A_m = 4\pi R^2$. In the concentration range $30 \le C_1 \le 100$ mM SDS, the calculated N_{agg} increases from 53 to 73, whereas α decreases from 0.56 to 0.46.

The symbols in Fig. 13a show data for N_{agg} from Ref. [110] and α from Ref. [22]. The theoretical lines in the same figure are drawn independently and do not represent fits of the data points. The agreement between the curves and the points in Fig. 13a give additional evidence in support of the adequacy of the used physicochemical model (Section 4).

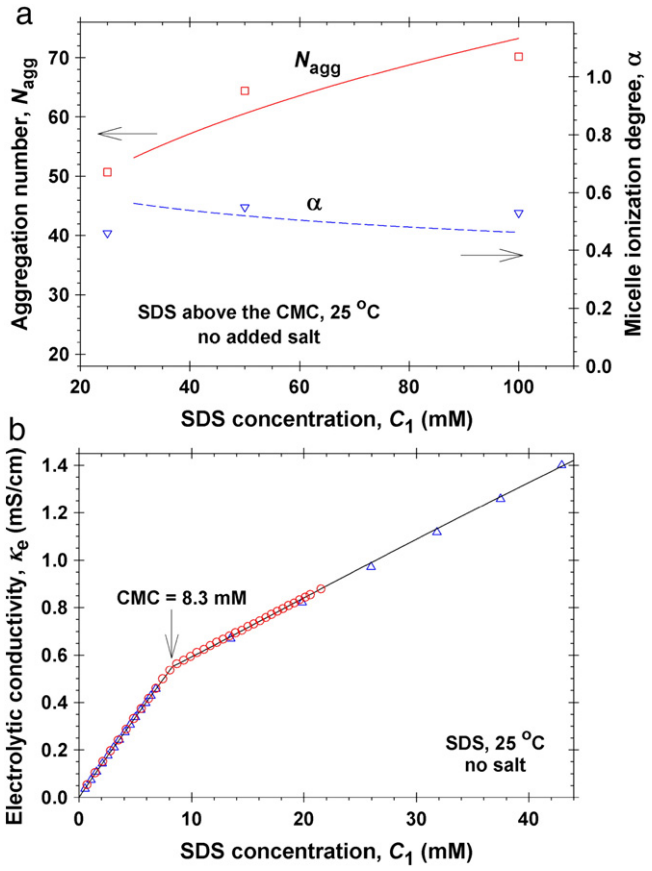

Fig. 13. Comparison of theory and experiment for SDS. (a) Micelle aggregation number, N_{agg}, and ionization degree, α, vs. the SDS concentration C_1: □ — N_{agg} from Ref. [110]; ▽ — α from Ref. [22]; the lines are calculated by the procedure in Section 4.7; no adjustable parameters; (b) conductivity vs. C_1: ○ — data from Ref. [123]; Δ — data from Ref. [149]; the solid line is the theoretical curve drawn according to Eq. (4.37); details in Section 5.5.

At $C_1 <$ CMC, the data for the conductivity κ_e of SDS solutions in Fig. 13b are fitted by means of Eq. (4.37) with $c_m = 0$ and $I = c_2 = C_1 + C_{salt}$. The fit gives $\lambda_1^{(0)} = 21.5$ cm^2 S/mol, which coincides with the value obtained in Ref. [149]. The determined limiting molar conductance, $\lambda_1^{(0)}$, of the DS^- ion is compared in Table 4 with the conductances of the other investigated surfactant ions.

For the data at $C_1 >$ CMC in Fig. 13b, we first applied the same approach, with $\lambda_m = 0$, as for the surfactants in Sections 5.1–5.4. However, this time the calculated curve for κ_e was lying slightly below the experimental points, being parallel to them. Because the molecular parameters, such as N_{agg}, α and R, are close for SDS and DTAB, we can expect that if $\lambda_m \equiv 0$ for DTAB (and for TTAB, CTAB and CPC, as well) we should have $\lambda_m \equiv 0$ also for SDS. For this reason, the theoretical curve at $C_1 >$ CMC in Fig. 13b is drawn with $\lambda_m \equiv 0$, but using the Stern constant, K_{St}, as an adjustable parameter, taking all other parameters from Tables 2, 3 and 4. In this way, from the best fit we obtained an effective "dynamic" value of the Stern constant, $K_{St}^{(dyn)} = 0.380$ M^{-1}, which is somewhat smaller than the "static" Stern constant, $K_{St} = 0.653$ M^{-1}, in Table 3 that has been obtained from the equilibrium surface tension of SDS solutions [84,114,115]. The lower value of $K_{St}^{(dyn)}$ indicates a lower effective binding energy of the Na^+ counterions to the sulfate headgroups at the surface of the SDS micelle under dynamic conditions.

It should be noted that the conductivity measurement is an essentially dynamic experiment. Alternating voltage is used in the conductivity meters at typical frequencies in the range of 1–3 kHz. Higher frequencies, up to 20 MHz, have been used in some experiments [124]. The idea for dynamic Stern layer has been already considered in the literature in another context [150].

In our case, the lower value of $K_{St}^{(dyn)}$ could be interpreted as follows. The diameter of the hydrated Na^+ ion, 0.72 nm [44], is greater than that of the sulfate head group, 0.60 nm [115]. For this reason, the bound Na^+ counterions are protruding from the micelle surface (Fig. 14a) and experience the action of the hydrodynamic viscous drag force, which is due to the directional motion of the free Na^+ counterions during the conductivity measurement. Indeed, the concentration of free Na^+ counterions is the greatest near the surface of the oppositely charged micelle, so that the hydrodynamic drag force resulting from their motion can detach a part of the bound counterions. This would result in a lower effective counterion binding energy, and respectively, in a lower dynamic Stern constant, $K_{St}^{(dyn)}$, in comparison with the static one, K_{St}.

Conversely, in the cases of DTAB, TTAB and CTAB the diameter of the hydrated Br^- ion, 0.66 nm [44], is somewhat smaller than that of the trimethylammonium head group, 0.70 nm [21]. For this reason, the Br^- counterions intercalated between the trimethylammonium head groups (Fig. 14b), are hidden in their "hydrodynamic shadow" and are not detached by the viscous flow accompanying the electric current. In the case of CPC, the protecting effect of the headgroups is even greater, because the pyridinium ring is protruding by additional 0.67 nm above the level of the surface charges; see e.g., Fig. 2 in Ref. [21].

5.6. Discussion on the conductivity of micellar solutions

The fact that the conductivity κ_e of an ionic surfactant solution decreases at the CMC is usually attributed to the lower mobility of the larger micelles [151]. Our quantitative analysis of the conductivity data in Sections 5.1–5.4 unambiguously yields λ_m identically equal to zero in the whole range of investigated surfactant concentrations, i.e., the mobility of the micelles gives no contribution to the conductivity of the micellar solutions. In other words, the conductivity is solely due to the small ions, viz. the free counterions, the surfactant monomers, and the ions of the added salt. The micelles contribute to the conductivity only indirectly, through the counterions dissociated from their surfaces.

There can be at least two hypotheses for explaining the result $\lambda_m = 0$. (1) The effect of the electrophoretic migration of the micelles on conductivity can be negligible if the measurements are performed under such conditions that the micelles cannot release their charges on the electrode, as discussed by Dukhin and Derjaguin [152]. (2) The electric repulsion between a given micelle and its neighbors is so strong that it counterbalances the effect of the applied external electric field, which is unable to bring the micelles into directional motion as carriers of electric current.

Let us verify the latter hypothesis. The system of charged micelles (or other charged particles) can be considered as a suspension of densely packed effective spheres of diameter d_{eff}; see Fig. 14c. A semi-empirical expression for estimating d_{eff} is [22]:

$$d_{eff} = 2R\left\{1 + \frac{3}{(2R)^3}\int_{2R}^{\infty}\left[1 - \exp\left(-\frac{3u_{el}(r)}{kT}\right)\right]r^2 dr\right\}^{1/3} \tag{5.2}$$

where, as usual, R is the micelle radius (without the counterion atmosphere) and $u_{el}(r)$ is the energy of electrostatic interaction between two micelles in the solution; see [21,22] for details. For charged micelles or particles, d_{eff} can be several times greater than the micelle hydrodynamic diameter, $2R$.

It has been found that the thickness of foam films from micellar solutions decreases in a stepwise manner with a height of the step $\Delta h = d_{eff} = c_m^{-1/3}$ [21,22,153,154], where c_m is the micelle (particle) number concentration. Likewise, the surface force measured by the

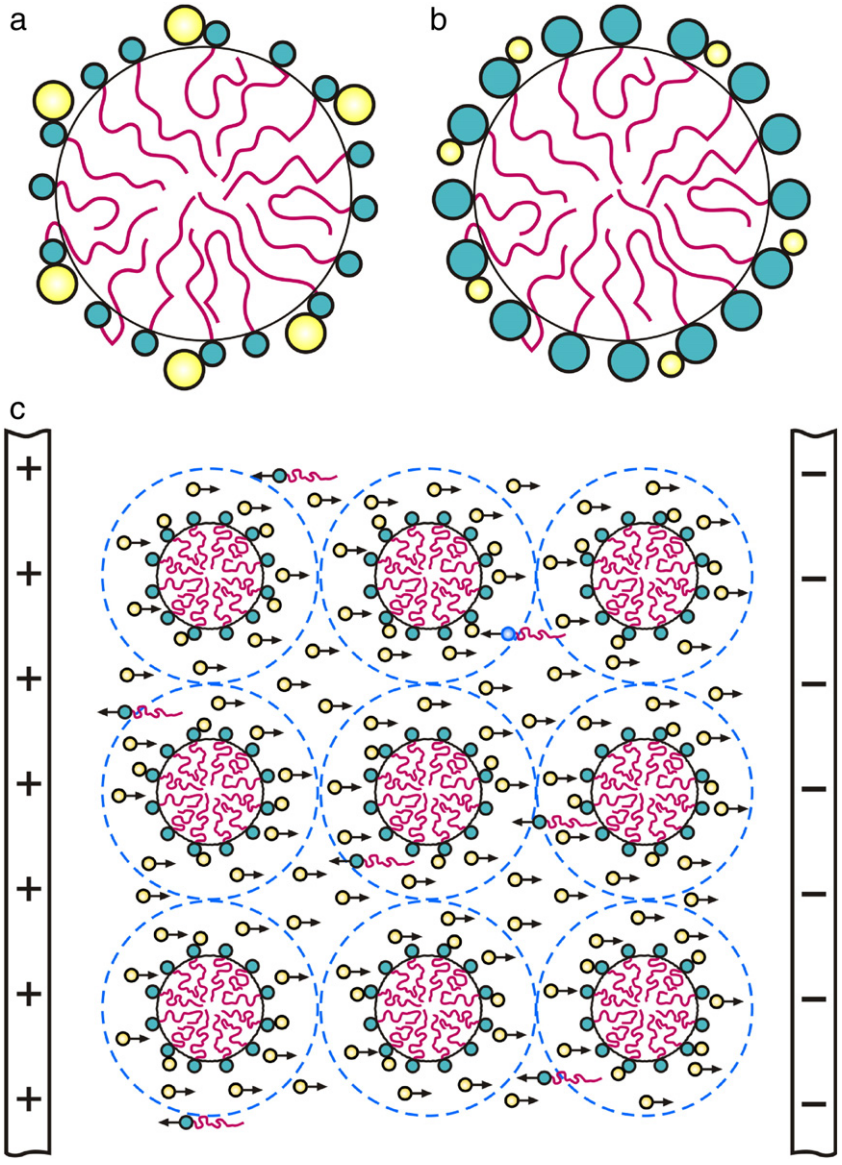

Fig. 14. (a) If the counterions are bigger, they protrude out of the layer of surfactant headgroups and can be detached by the viscous flow during the conductivity measurements. (b) If the counterions are smaller than the headgroups, they are hidden in the "hydrodynamic shadow" of the headgroups and cannot be detached by the viscous flow. (c) Because of the electrostatic repulsion between them, the charged micelles can be considered as effective "hard spheres" of diameter d_{eff} presented by dashed circles. The repulsion between a given micelle with its neighbors can counterbalance the applied external field, and then only the small ions become carriers of the electric current, whereas the micelles do not contribute to the solution's conductivity. In most cases, the micelles in the bulk are disordered (like the molecules of a liquid), with an average distance d_{eff} between the nearest neighbors.

colloidal-probe AFM technique across a suspension of charged particles exhibits oscillations of period $\Delta h = c_m^{-1/3}$ [155,156]. In other words, in these experiments the charged particles (including micelles) behave as effective spheres of diameter $\Delta h = d_{eff} = c_m^{-1/3}$. The inverse cubic root in the latter dependence corresponds to an effective simple cubic close packing of the effective spheres (Fig. 14c). Such a close packing could be the reason for the suppression of micelle mobility under the action of an applied (relatively weak) external field, and for $\lambda_m \equiv 0$ (see above). It is important to note that d_{eff} is not only a theoretical characteristic defined by Eq. (5.2), but it is directly measurable as the height of the steps, Δh, of stratifying foam films containing ionic micelles [21,22].

The stepwise thinning of the films [21] and the oscillations of surface force [157] disappear upon the addition of a sufficient amount of electrolyte. This can be interpreted as $d_{eff} < c_m^{-1/3}$, i.e., the effective diameter d_{eff} has become smaller than the average intermicellar distance, $c_m^{-1/3}$. Indeed, d_{eff} shrinks upon the addition of electrolyte, whereas c_m remains the same; see Fig. 18 in Ref. [21].

In relation to our results for conductivity, in Fig. 15 we check the relation between d_{eff} and $c_m^{-1/3}$ in the other limiting case — that of *low* ionic strengths. The respective calculations have been carried out for CPC without added salt using the procedure from Section 4.7 and the parameter values for CPC from Table 3. The obtained $Z = \alpha N_{agg}$ is substituted in Eq. (4.16), and the latter is used as a boundary condition for the nonlinear Poisson–Boltzmann equation in the frame of the jellium model, which is solved numerically to determine $u_{el}(r)$. Finally d_{eff} is calculated from Eq. (5.2); see Ref. [21] for details. The obtained d_{eff} remains finite when approaching the CMC (Fig. 15). In contrast, in the same limit we have $c_m \to 0$, and then $c_m^{-1/3} \to \infty$. However, the difference between d_{eff} and $c_m^{-1/3}$ is significant (the effective spheres are not pressed against each other and the micelles are mobile) only in the very close vicinity of the CMC (Fig. 15),

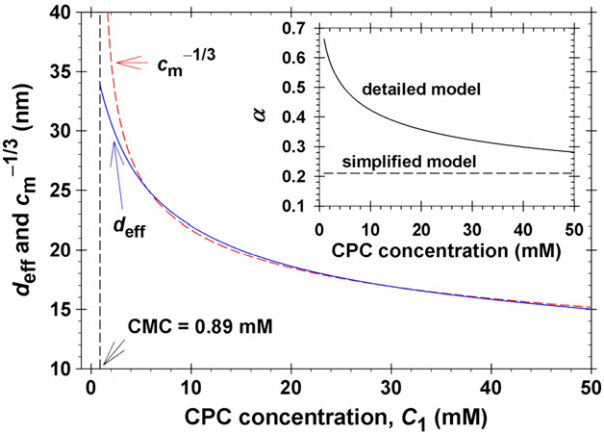

Fig. 15. Effect of surfactant concentration, C_1, on the effective diameter, d_{eff}, of the counterion atmospheres of CPC micelles. Except a narrow vicinity of the CMC, the calculated d_{eff} coincides with the mean distance between the micelles, $c_m^{-1/3}$, and then the micelles form a jellium (Fig. 14c) and do not migrate under the action of an applied external field. The inset compares the values of the ionization degree, α, calculated in the framework of the detailed model (Section 4) and simplified model (see the text).

where the contribution of the micelles to the solution's conductivity can be neglected because of their low concentration. Thus, the micelles give a negligible contribution to conductivity in the whole concentration range above the CMC. We recall that $\lambda_m = 0$ directly follows from the comparison of the prediction of the detailed model with the experimental data for κ_e (see above).

Now, let us compare the detailed model from Section 4 with the simplified model with constant N_{agg}, α and c_1. Such a model is often used to determine the micelle ionization degree by interpretation of conductivity data, κ_e vs. C_1, at concentrations above the CMC; see e.g., Ref. [149]. In the framework of the simplified model, the micellar term in Eq. (4.37) is expressed in the form:

$$Z\lambda_m c_m = \frac{\alpha^2 N_{agg} e^2 N_A}{6\pi\eta R}(C_1 - \mathrm{CMC}) \tag{5.3}$$

where N_A is the Avogadro number; C_1 and CMC are to be substituted in mol/m^3; $1/(6\pi\eta R)$ is the hydrodynamic mobility of the ions according to Stokes [125] with η being the viscosity of water, and the following relations have been also used: $Z = \alpha N_{agg}$ and $c_m = (C_1 - \mathrm{CMC})/N_{agg}$. Further, an average value of N_{agg} is taken from another experiment or from molecular-size estimate, and the dependence of κ_e on C_1 above the CMC (see e.g., Fig. 13b) is fitted with a linear regression, determining α in Eq. (5.3) as an adjustable parameter.

Thus, the simplified model gives a constant value of α for the whole concentration domain above the CMC. This constant $\alpha = 0.21$, calculated with $N_{agg} = 75$ for CPC micelles [21], is shown with the horizontal dashed line in the inset of Fig. 15. It is considerably smaller than α calculated using the detailed model, which varies in the range of 0.28–0.66; see the solid line in the same inset. These results illustrate the fact that the simplified model gives systematically smaller values of α than the detailed model. The origin of this difference is the following.

In the simplified model, it is presumed that λ_m gives a finite contribution, see Eq. (5.3), and a part of the electric current is carried by the micelles. Then, to get the same experimental conductivity, κ_e, it is necessary to have a lower concentration of dissociated counterions. As a result, the fit of the conductivity using Eq. (5.3) leads to a lower degree of micelle ionization α determined as an adjustable parameter.

In the detailed model, $\lambda_m \equiv 0$ was obtained by comparing the calculated concentrations of the ionic species above the CMC with the experimental κ_e; see Sections 5.1–5.4. No expression for λ_m, like Eq. (5.3), has been postulated.

Whatever the explanation of the fact that $\lambda_m \equiv 0$ could be, it should be taken into account when determining the micelle ionization degree α from the conductivity data. This fact can be also important for the interpretation of results from the measurements by micellar electrokinetic chromatography (MEKC) [158], where the micelles play the role of a pseudo-stationary phase [159–162].

In the framework of the jellium model of charged particle suspensions, only the small ions take part in the Debye screening of the electric field of a given particle, whereas the macroions are uniformly distributed; see Section 4.2 and Refs. [87,88]. The model for colloidal suspensions makes an analogy with the jellium model for metals [102]. The results obtained here imply that this physical analogy can be further extended to the electric conductivity. Indeed, in metals the charged atomic nuclei are fixed in a crystal lattice, whereas the whole conductance is due to the transport of electrons in the valence zone. In the case of micellar solutions, the roles of nuclei and electrons are played, respectively, by the micelles and their dissociated counterions; see Fig. 14c.

6. Generalization of the model for mixtures of ionic and nonionic surfactants

6.1. Completing the system of equations and generalization of the MN closure

Here, we extend the model from Section 4 to the case of mixed solutions of ionic and nonionic surfactant, which may contain also added salt. In this case, two additional variables appear: the concentration of nonionic surfactant monomers, c_n, and the molar fraction of this surfactant in the micelles, y_n. To determine these two variables, we have to include two additional equations in the system:

$$\ln c_n = \ln K_n^{(mic)} + \ln(f_n y_n) \tag{6.1}$$

$$c_n + y_n c_{mic} = C_n. \tag{6.2}$$

Eq. (6.1) expresses the chemical equilibrium between the micelles and the surrounding water phase with respect to the exchange of molecules of the nonionic surfactant; Eq. (6.2) expresses the mass balance with respect to this surfactant; C_n is its total (input) concentration; $K_n^{(mic)}$ is its micellization constant — see Eq. (2.3); f_n is the activity coefficient for the nonionic surfactant, which accounts for the fact that the mixing of the two surfactants in the micelle can be non-ideal; c_{mic} is the total number of surfactant molecules in micellar form per unit volume. The presence of nonionic surfactant leads also to modifications in Eqs. (4.1), (4.2), (4.4) and (4.5), which acquire the following form:

$$\ln(c_1\gamma_\pm) = \ln K_1^{(mic)} + \ln f_1 y_1 + \Phi_s \tag{6.3}$$

$$\ln c_{12} = \ln K_1^{(mic)} + \ln f_1 y_2 \tag{6.4}$$

$$y_1 + y_2 + y_n = 1 \tag{6.5}$$

$$c_1 + c_{12} + (y_1 + y_2)c_{mic} = C_1. \tag{6.6}$$

Here, f_1 is the activity coefficient for the ionic surfactant; see Eqs. (3.14) and (3.15).

Further, we need an expression for the non-electrostatic component of surface tension of a mixed micelle, γ_0, which is expected to depend on the micelle composition. We verified the applicability of different models by comparing their predictions with experimental data for the CMC of mixed surfactant solutions. It turned out that the simple linear mixing model (LMM), which has been used to describe the interfacial tension of organic liquid mixtures against water [163], gives perfect agreement with experimental data for

micellar solutions (see below). The expression for γ_0 in the framework of LMM is:

$$\gamma_0 = f_1 y_1 \gamma_{1,0} + f_1 y_2 \gamma_{12,0} + f_n y_n \gamma_{n,0} \tag{6.7}$$

where the activity coefficients are given by the expressions from the regular solution theory [90], viz.

$$f_1 = \exp\left(\beta y_n^2\right), \quad f_n = \exp\left[\beta(1-y_n)^2\right]. \tag{6.8}$$

β is the interaction parameter, see Eqs. (2.11) and (2.12). In Eq. (6.7) $\gamma_{i,0}$ is the non-electrostatic components of surface tension in the cases of pure component '*i*' ($i \to 1$, 12, n). As before, the subscript '12' refers to a surfactant ion with bound counterion. In the case of non-charged micelle, $\pi_{el} = 0$ and consequently $\gamma_{12,0} = \gamma_{n,0} = 0$; see Eq. (4.19). Then, in view of Eq. (6.7), the MN closure acquires a relatively simple form:

$$f_1 y_1 \gamma_{1,0} = \pi_{el}(\Phi_s) \tag{6.9}$$

where the dependence $\pi_{el}(\Phi_s)$ is given by the right-hand side of Eq. (4.21). At the CMC, we have $c_m = 0$ and the function $\pi_{el}(\Phi_s)$ reduces to the simpler expression in Eq. (4.21a). Note that $\gamma_{1,0}$ coincides with γ_0 for the pure ionic surfactant; its values for the investigated surfactants are given in Table 3.

In summary, Eqs. (4.3), (4.6)–(4.8), (6.1)–(6.6) and (6.9) represent a complete system of 11 equations for determining the 11 unknown variables c_1, c_{12}, c_2, c_n, c_{mic}, y_1, y_2, y_n, $\gamma_\pm$, I, and Φ_s. The micellar activity coefficients are given by Eq. (6.8). The micelle radius, R, can be determined by molecular size considerations, e.g.,

$$R = (1-y_n)R_1 + y_n R_n \tag{6.10}$$

where R_1 and R_n can be estimated as the lengths of the molecules of the respective surfactants.

The system contains only 5 thermodynamic parameters: K_{St}, $K_1^{(mic)}$, $\gamma_{1,0}$, $K_n^{(mic)}$ and β. The first three of them have been already determined for several ionic surfactants — see Table 3. $K_n^{(mic)}$ equals the CMC of the pure nonionic surfactant, see Eq. (2.9). Then only the interaction parameter β remains to be determined as a single adjustable parameter by the analysis of data for mixed micellar solutions of ionic and nonionic surfactants (see below).

6.2. CMC of mixed ionic–nonionic surfactant solutions

Expressing y_n, y_1 and y_2 from Eqs. (6.1), (6.3) and (6.4), and substituting the results in Eq. (6.5), we derive:

$$\frac{1}{CMC_M} = \frac{\gamma_\pm x_1 e^{-\Phi_s} + x_{12}}{f_1 K_1^{(mic)}} + \frac{x_n}{f_n K_n^{(mic)}} \tag{6.11}$$

where x_1, x_{12} and x_n are the molar fractions of the respective amphiphilic components in monomeric form ($x_1 + x_{12} + x_n = 1$), which at the CMC (negligible micelle concentration) represent the composition of the solution. We have used the relation $c_i = x_i CMC_M$ ($i = 1$, 12, n). In many cases, the bulk molar fraction of non-ionized molecules of the ionic surfactant is very small, $x_{12} \ll 1$, so that it can be neglected in Eq. (6.11). (x_{12} can be important for carboxylate solutions.) As mentioned above, $K_n^{(mic)} = CMC_n$ is the CMC of the nonionic surfactant alone. $K_1^{(mic)}$ can be determined as explained in Section 4.5; see Table 3. Eq. (6.11) represents the generalization of Eq. (2.7) for the case of ionic–nonionic mixture.

In analogy with the derivation of Eq. (4.26), one can obtain its generalized form for the considered mixed surfactant solution:

$$\Phi_s = \ln\left(\frac{c_1\gamma_\pm}{(1-y_n)f_1 K_1^{(mic)} - K_{St} c_1 c_2 \gamma_\pm^2}\right). \tag{6.12}$$

Our aim is to calculate the dependence of CMC_M on the composition x_1, using the model based on Eqs. (6.1)–(6.10), and to compare the theoretical curve with experimental data for the CMC of mixed surfactant solutions. It is convenient to obtain the theoretical dependence $CMC_M(x_1)$ in parametric form, viz. $CMC_M(y_n)$ and $x_1(y_n)$. The principles of the used computational procedure are as follows:

(1) We give a value to y_n in the interval $0 \le y_n \le 1$.
(2) f_1, f_n, c_n and R are calculated from Eqs. (6.8), (6.1) and (6.10).
(3) To apply the bisection method for c_1, we give an initial value to c_1 and set appropriate limits for its variation; then $c_2 = I = c_1 + C_{salt}$.
(4) $\gamma_\pm$ and κ, Φ_s and y_1 are calculated from Eqs. (4.7), (4.14), (6.12) and (6.3), respectively.
(5) The obtained κ and Φ_s are substituted in Eq. (6.9) along with $\pi_{el}(\Phi_s)$ from Eq. (4.21a); Eq. (6.9) is solved numerically to determine c_1 using the bisection method; $j = 2$ for spherical micelles of radius R.
(6) Using the obtained values of c_1, c_2, y_1, Φ_s, f_1, f_n and $\gamma_\pm$, we calculate y_2 from Eq. (6.5); c_{12} from Eq. (4.3), $x_i = c_i / (c_1 + c_{12} + c_n)$ for $i = 1$, 12, n; finally, from Eq. (6.11) we calculate $CMC_M(y_n)$ and plot it vs. $x_1(y_n)$.

From the numerical results, one can plot the theoretical dependence $CMC_M = CMC_M(x_1, C_{salt}, \beta)$, which is fitted to the experimental data (see e.g., Fig. 16a) by varying the adjustable parameter β with the help of the least squares method. In the framework of the model, β is a constant parameter that characterizes a given pair of surfactants; β should be independent of x_1 and C_{salt}. If the processing of experimental data gives non-constant β values, this would be an evidence for imperfections in the used model.

In many cases, the bulk molar fraction of non-ionized monomers of the ionic surfactant, x_{12}, is very low, but it is given as an outgoing quantity by the computational procedure without making it more sophisticated. Strictly speaking, at the CMC, we have $z_n = x_n$ and $z_1 = x_1 + x_{12}$, where z_n and z_1 are the input molar fractions, respectively, of the nonionic and ionic surfactants; see Eq. (2.1). The effect of x_{12} can be material at high concentrations of added electrolyte and for carboxylate solutions.

6.3. Effect of electrolyte on the CMC of mixed solutions

Here, the theoretical model from Section 6.1 is tested against a set of experimental data from Ref. [65] for the CMC of mixed aqueous solutions of the anionic surfactant SDS and the nonionic surfactant *n*-decyl β-D-glucopyranoside ($C_{10}G$) at different concentrations of added NaCl, C_{salt}; see Fig. 16a. The parameters K_{St}, $K_1^{(mic)}$, $\gamma_{0,1}$ and R_1 for SDS were taken from Table 3. In addition, for $C_{10}G$ we have $K_n^{(mic)} = CMC_n = 2$ mM and $R_n = 2.5$ nm. We fitted all four experimental curves in Fig. 16a simultaneously using the procedure from Section 6.2, and obtained a single value $\beta = -0.8$. The small magnitude and the negative sign of β mean that the mixture of these two surfactants is slightly synergistic. The fact that β is independent of C_{salt} means that the electrostatic double-layer interactions are adequately taken into account by Eqs. (6.3) and (6.9), so that the value of β is determined only by non-double-layer interactions between the two surfactants. Note that in Ref. [65] another model is used, which gives different β for different C_{salt}.

Having determined β from the fit in Fig. 16a, we can further calculate all variables (characteristics of the system) that are predicted by

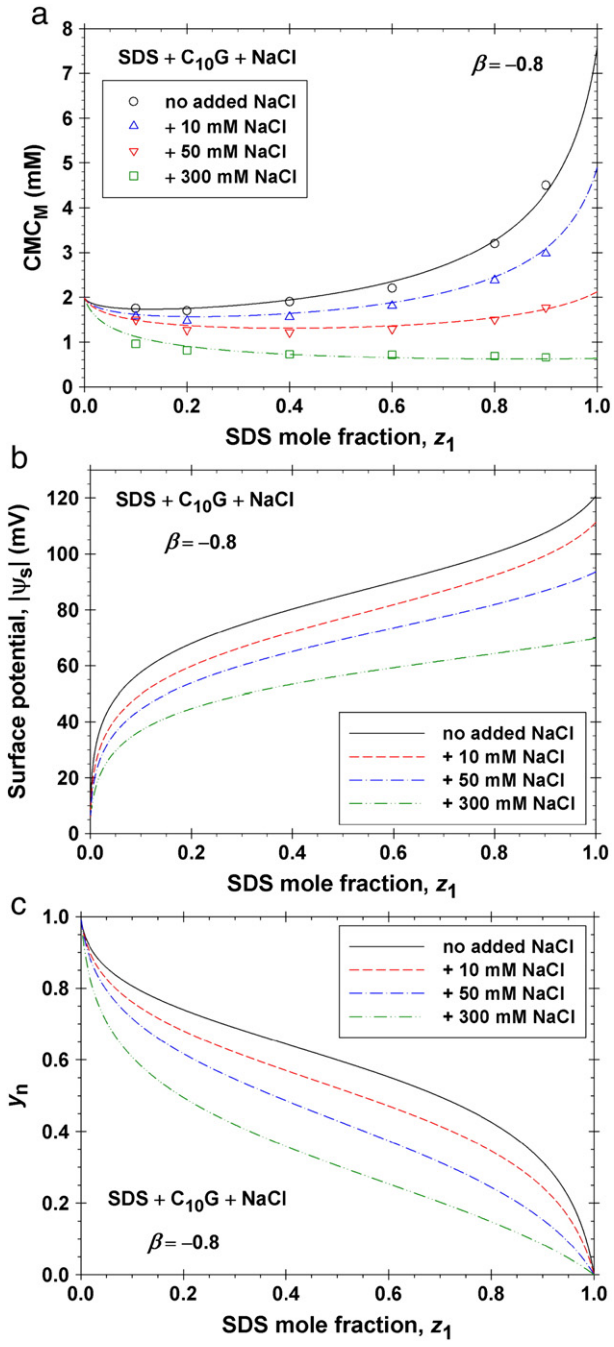

Fig. 16. Results for mixed solutions of SDS and $C_{10}G$. (a) CMC_M vs. z_1: the points are data from Ref. [65] at various fixed C_{salt} denoted in the figure; the lines are fits to the data by the model in Section 6.1; all lines correspond to the same $\beta = -0.8$ determined from the fit. (b) Dependences of $|\psi_s|$ on z_1 and (c) of the mole fraction of $C_{10}G$ in the mixed micelles, y_n, on z_1 predicted by the model at various C_{salt} at the CMC.

the model. As an example, in Fig. 16b and c we have plotted the obtained results for the magnitude of the surface potential $|\psi_s|$ and the mole fraction of $C_{10}G$ in the micelles. As expected, $|\psi_s|$ grows with the increase of the mole fraction of SDS, z_1, but decreases with the rise of C_{salt}. Moreover, $|\psi_s|$ sharply increases at small values of z_1, whereas at greater z_1 the potential increases slower. The latter can be explained with the effect of counterion binding. Indeed, at greater $|\psi_s|$ the counterion concentration near the micelle headgroups increases, which leads to a greater degree of counterion binding.

Fig. 16c shows the strong effect of ψ_s on the micelle composition. Because the micelle electrostatic potential increases the chemical potential of DS^- ions in the micelle, the nonionic surfactant is more competitive in the micelle despite of its shorter chain length (C_{10} vs. C_{12}). Thus, at $C_{salt} = 0$ we have $y_n = 0.50$ at $x_n \approx 0.30$. The addition of salt decreases ψ_s (and the electrostatic repulsion), and restores the priority of the surfactant with longer hydrocarbon chain: at $C_{salt} =$ 300 mM we already have $y_n = 0.50$ at $x_n \approx 0.81$. Note that the main factors in the competition between the two surfactants to dominate the micelle are (i) the hydrophobic effect related to the length of the surfactant paraffin chain, which is incorporated into the micellization constants $K_1^{(mic)}$ and $K_n^{(mic)}$, and (ii) the electrostatic potential Φ_s that diminishes the fraction of the ionic surfactant in the mixed micelle. In comparison with the effects of the chain length and surface potential, the effect of the interaction parameter β is related to a small correction and plays a secondary role.

It should be noted that the curves with $C_{salt} = 300$ mM in Fig. 6 represent the only case considered in Section 6, for which x_{12} (and the difference between x_1 and z_1) is not completely negligible.

6.4. Mixed solutions of anionic and zwitterionic surfactants

As another example, here the theoretical model is applied to interpret experimental data from Ref. [121] for the CMC of mixed aqueous solutions of the anionic SDS and the zwitterionic cocamidopropyl betaine (CAPB). As before, the parameters K_{St}, $K_1^{(mic)}$, $\gamma_{0,1}$ and R_1 for SDS were taken from Table 3. For CAPB, we have $K_n^{(mic)} = CMC_n =$ 0.088 mM and $R_n = 2.6$ nm [10]. (Because of a misprint, $CMC_n =$ 0.88 mM is given in Ref. [121].)

In Fig. 17a, the data are plotted as $1 / CMC_M$ vs. x_1 in view of Eq. (6.11). The solid line is the fit by means of the model from Section 6.1, which gives $\beta = 1.2$. As seen in the figure, the data are close to a linear dependence. Note, however, that in the presence of ionic surfactant the straight line does not mean $\beta = 0$ (ideal mixing) because of the multiplier $e^{-\Phi_s}$ in Eq. (6.11). The curve corresponding to $\beta = 0$ is also shown in Fig. 17a. The positive β means that the mixture of these two surfactants is weakly antagonistic.

Fig. 17b shows the calculated magnitude of the micelle surface potential $|\psi_s|$ and the electrostatic component of surface pressure, π_{el} from Eq. (4.21a), which are plotted vs. the mole fraction of SDS, x_1. As expected, $|\psi_s|$ and π_{el} both increase with the rise of x_1. The growth of π_{el} is the fastest at $x_1 \to 1$.

Fig. 17c indicated that the effect of ψ_s strongly suppresses the entry of the ionic surfactant into the micelles. Indeed, we have $y_1 = y_n = 0.44$ at $x_1 = 0.97$. The effect of counterion binding to the dodecylsulfate headgroups, described by the fraction y_2 of the neutralized headgroups, becomes essential for $x_1 > 0.95$. Thus, at $x_1 = 1$ we have $y_1 = 0.60$ and $y_2 = 0.40$, i.e., the fractions of the ionized and neutralized headgroups are comparable.

6.5. Mixed solutions of C_nTAB and $C_{12}E_m$

Here, the model from Section 6.1 is applied to interpret available experimental data for the CMC of mixed solutions from alkyltrimethylammonium bromide, C_nTAB ($n = 12$, 14 and 16), and polyoxyethylene (m) lauryl ether, $C_{12}E_m$ ($m = 4$, 8). The parameters K_{St}, $K_1^{(mic)}$, $\gamma_{0,1}$ and R_1 for C_nTAB were taken from Table 3. For the micellization constant of the nonionic surfactant we have $K_n^{(mic)} = CMC_n = 0.046$ mM for $C_{12}E_4$ [164] and 0.12 mM for $C_{12}E_8$, [165]. Because R has to be estimated at the surface of charges, we took $R_n =$ 2.4 nm for both nonionics. (The model in Section 6.1 is weakly sensitive to the value of R.)

In Fig. 18, the data are plotted as CMC_M vs. x_1. The solid lines are the best fits by means of the model. For each pair of surfactants, the CMC of the nonionic one is by orders of magnitude lower than that of the ionic surfactant. For this reason, CMC_M is plotted in log scale, except for the pair CTAB + $C_{12}E_8$ in Fig. 18c, for which the two CMCs are relatively closer. From each fit, the interaction parameter β is determined as an adjustable parameter. Its value is shown in

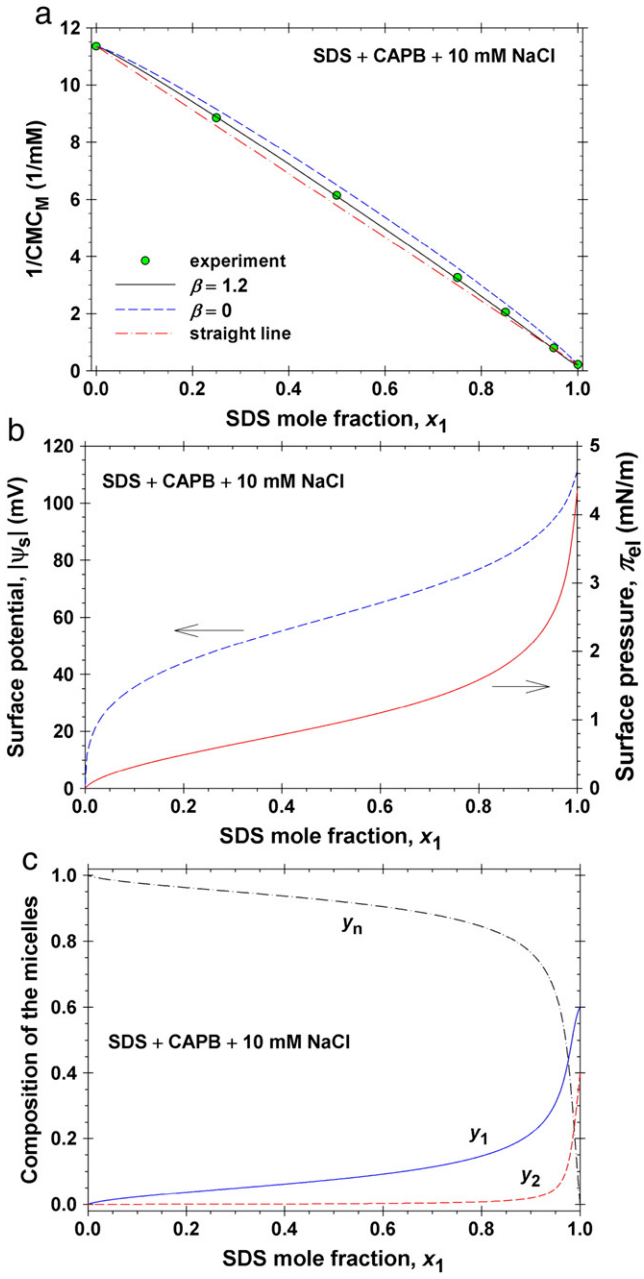

Fig. 17. Results for mixed micellar solutions of SDS and CAPB. (a) 1 / CMC_M vs. x_1: the points are data from Ref. [121]; the solid line is fit to the data by the model in Section 6.1; the interaction parameter $\beta = 1.2$ is determined from the fit. (b) Dependences of $|\psi_s|$ and π_{el} vs. x_1 and (c) of the mole fractions y_1, y_2 and y_n, respectively, of DS^-, SDS and $C_{10}G$ in the micelles vs. x_1, predicted by the model at the CMC.

the respective figure. For all pairs, β is negative, i.e., the mixing is energetically favorable (synergistic). For the pairs $C_nTAB + C_{12}E_8$, $n = 12$, 14, 16 in Fig. 18a,b,c, the value of β increases with n, which means that the mixing becomes less favorable with the rise of the mismatch between the hydrophobic chain lengths of the two surfactants. The replacement of $C_{12}E_8$ with $C_{12}E_4$ leads to a smaller β (more synergistic mixing): compare Fig. 18c and d. This could be explained with the less hydrophilic head group of $C_{12}E_4$. In other words, $C_{12}E_4$ could penetrate deeper in the micelle than $C_{12}E_8$ and, thus, to partially compensate the unfavorable mismatch with the longer hydrophobic chain of CTAB.

Fig. 19 shows the calculated micelle surface potential ψ_s and the electrostatic component of surface pressure, π_{el} from Eq. (4.21a), for the same pairs of surfactants as in Fig. 18. In addition, Fig. 20 shows the micellar composition for the same systems, which is presented as plots of the molar fractions y_1, y_2 and y_n vs. x_1. The comparison of the plots in Figs. 18 and 19 indicates that the properties of the mixed micelles are dominated by the effect of the lengths of the hydrophobic chains of the constituent surfactants, which is accounted in the theory by the constants $K_1^{(mic)}$ and $K_n^{(mic)}$. Indeed, y_n is the smallest (and y_1 is the greatest) for CTAB, which is the ionic surfactant with the longest chain length in Fig. 20. In turns, the greatest fraction of the ionic surfactant, y_1, leads to the highest surface potential, ψ_s, and greatest electrostatic component of surface pressure, π_{el}; see Fig. 19c. Note however that the higher ψ_s counteracts the effect of the longer chain length, and tends to diminish y_1. In its own turn, the effect of the highest ψ_s for CTAB is partially diminished by the greatest K_{St} (strongest counterion binding) for this surfactant; see Table 3 and the curve for y_2 in Fig. 20c. In a final reckoning, this balance of effects leads to the fact that the plots in Figs. 19 and 20 for different pairs of surfactants are not so different. A common feature for all systems in Fig. 20 is that the effect of counterion binding, described by y_2, becomes essential for $x_1 > 0.90$.

Another common feature for all investigated mixed systems is that for all of them the ranges of variation of the micelle surface potential and electrostatic surface pressure are the same: $0 < |\psi_s| < 120$ mV and $0 < \pi_{el} < 5$ mN/m; compare Figs. 16b, 17b and 19.

7. Generalization to one ionic surfactant with several different counterions

In view of potential applications, here we generalize the model from Section 4 to the case of one ionic surfactant with several different counterions, for example SDS with Li^+, Na^+ and K^+ counterions.

7.1. Stern isotherm and adsorption equations

For simplicity, we assume that all investigated surfactants and salts are 1:1 electrolytes. Component 1 is the surfactant ion; components $2 \le i \le m$ are the counterions and components $m + 1$, $m + 2$, … — the coions due to the added non-amphiphilic salts.

In the bulk solution, we have association–dissociation equilibrium of the surfactant and a given counterion, which is described by the equation:

$$c_1 c_i = Q_{1i} c_{1i}, \quad 2 \le i \le m \tag{7.1}$$

— see the comments after Eq. (3.1). Here, c_1 and c_i ($2 \le i \le m$) are the concentrations of the respective ions; c_{1i} denotes concentration of non-ionized surfactant molecules with bound counterion of kind i; Q_{1i} is the equilibrium constant of the reaction corresponding to Eq. (7.1).

As in Section 3, let us consider the binding of counterions to the headgroups of the surfactant molecules in a flat adsorption layer. The concentrations of the reagents in a surface layer of thickness δ are (Fig. 2a):

$$c_i = c_{is}; \quad c_1 = \frac{1}{\delta}\left(\Gamma_1 - \sum_{j=2}^{m} \Gamma_j\right); \quad c_{1i} = \frac{\Gamma_i}{\delta}. \tag{7.2}$$

Here, c_{is} ($2 \le i \le m$) is the subsurface concentration of the counterions of kind i; Γ_1 is the total surface concentration of component 1 (the surfactant), both ionized and non-ionized, in the adsorption layer; Γ_i is the surface concentration of bound counterions of the kind i. Substituting Eq. (7.2) into Eq. (7.1), we obtain:

$$\left(\Gamma_1 - \sum_{j=2}^{m} \Gamma_j\right) c_{is} = Q_{1i} \Gamma_i, \qquad 2 \le i \le m. \tag{7.3}$$

As in Section 3, to obtain Eq. (7.3) we used the circumstance that in a closed system, the final equilibrium state of the system is

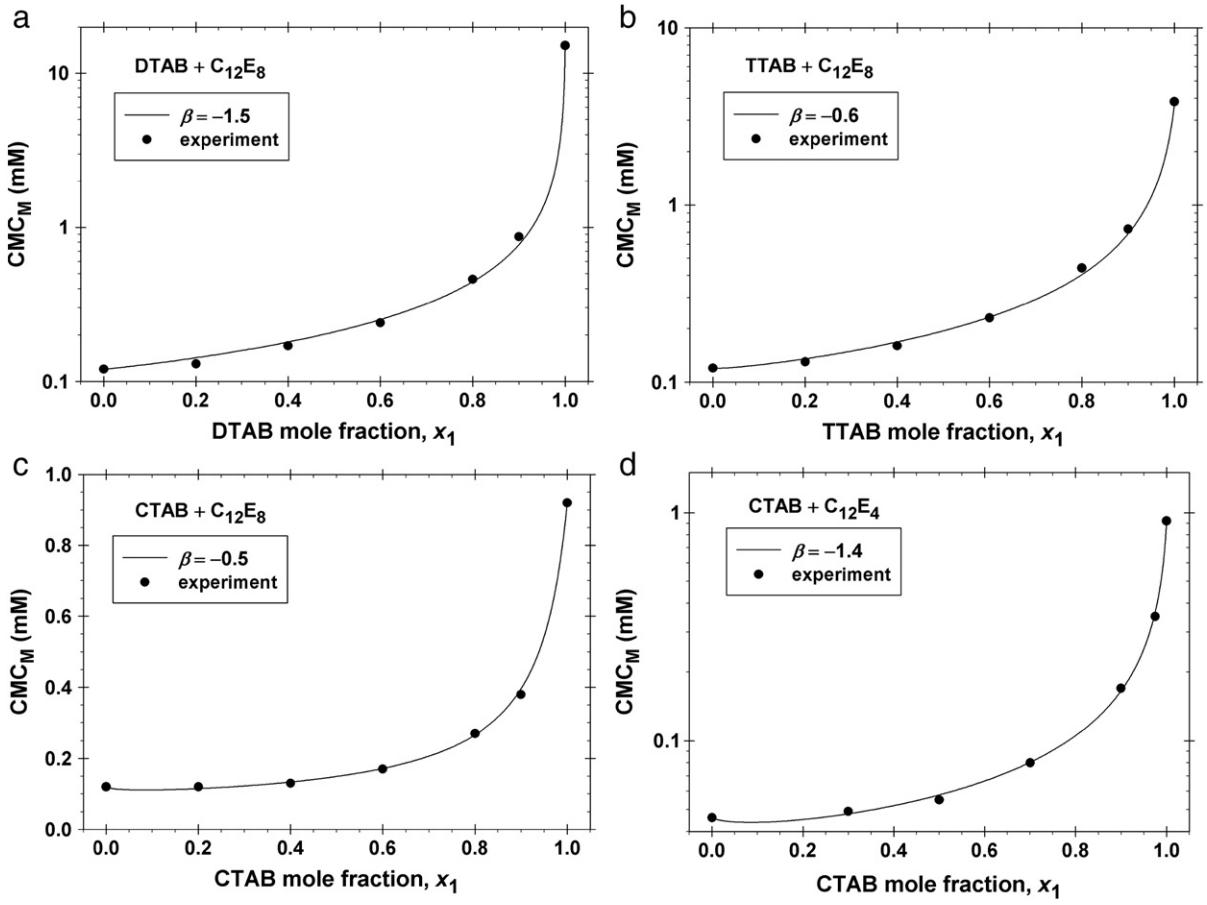

Fig. 18. Plots of CMC_M, vs. the mole fraction of the ionic surfactant, x_1. (a) DTAB + $C_{12}E_8$; (b) TTAB + $C_{12}E_8$; (c) CTAB + $C_{12}E_8$; (d) CTAB + $C_{12}E_4$. The data with $C_{12}E_8$ are from Ref. [165], and those with $C_{12}E_4$ — from Ref. [164]; the temperature is 25 °C. The solid lines are fits by the model from Section 6.1. The determined values of the single adjustable parameter, β, are given in the respective figures.

independent of the reaction path [94]. Eq. (7.3) can be rearranged in the form:

$$c_{is}/Q_{1i} = \frac{\Gamma_i}{\Gamma_1 - \sum_{j=2}^{m} \Gamma_j}, \qquad 2 \le i \le m. \tag{7.4}$$

Summing up the above equations, we derive:

$$1 + \sum_{j=1}^{m} c_{js}/Q_{1j} = \frac{\Gamma_1}{\Gamma_1 - \sum_{j=2}^{m} \Gamma_j}. \tag{7.5}$$

Substituting the denominator in Eq. (7.5) into Eq. (7.3), we obtain the most popular form of the Stern isotherm for a system with several counterions [84,99]:

$$\frac{\Gamma_i}{\Gamma_1} = \frac{K_{St,i} c_{is}}{1 + \sum_{j=1}^{m} K_{St,j} c_{js}} \quad (2 \le i \le m) \tag{7.6}$$

where $K_{St,i}$ is the Stern constant for counterion of kind i, and

$$K_{St,i} = \frac{1}{Q_{1i}} \quad (2 \le i \le m). \tag{7.7}$$

In other words, the Stern constant $K_{St,i}$ equals the reciprocal reaction constant, Q_{1i}. Eq. (7.7) is the generalization of Eq. (3.5). The adsorption isotherm of the considered ionic surfactant can be expressed in the form [84,99]:

$$K_1 \left(1 + \sum_{j=1}^{m} K_{St,j} c_{js}\right) c_{1s} = \frac{\Gamma_1}{\Gamma_\infty} f(\Gamma_1). \tag{7.8}$$

The meaning of K_1, Γ_∞ and $f(\Gamma_1)$ is the same as in Section 3.2. In view of Eq. (7.7), the substitution of Eq. (7.5) into Eq. (7.8) yields:

$$K_1 c_{1s} = \frac{\hat{\Gamma}_1}{\Gamma_\infty} f(\Gamma_1) \tag{7.9}$$

where by definition

$$\hat{\Gamma}_1 \equiv \Gamma_1 - \sum_{j=2}^{m} \Gamma_j \tag{7.10}$$

is the surface concentration (adsorption) of ionized surfactant molecules. By multiplication of Eqs. (7.4) and (7.9), in view of Eqs. (7.7) and (7.10) we obtain:

$$K_1 K_{St,i} c_{1s} c_{is} \equiv \frac{\Gamma_i}{\Gamma_\infty} f(\Gamma_1). \tag{7.11}$$

The surface concentrations c_{1s} and c_{is} are related to the respective bulk concentrations, c_1 and c_i by means of the Boltzmann equation:

$$c_{1s} = c_1 \exp(-\Phi_s), \qquad c_{is} = c_i \exp(\Phi_s) \qquad (2 \le i \le m). \tag{7.12}$$

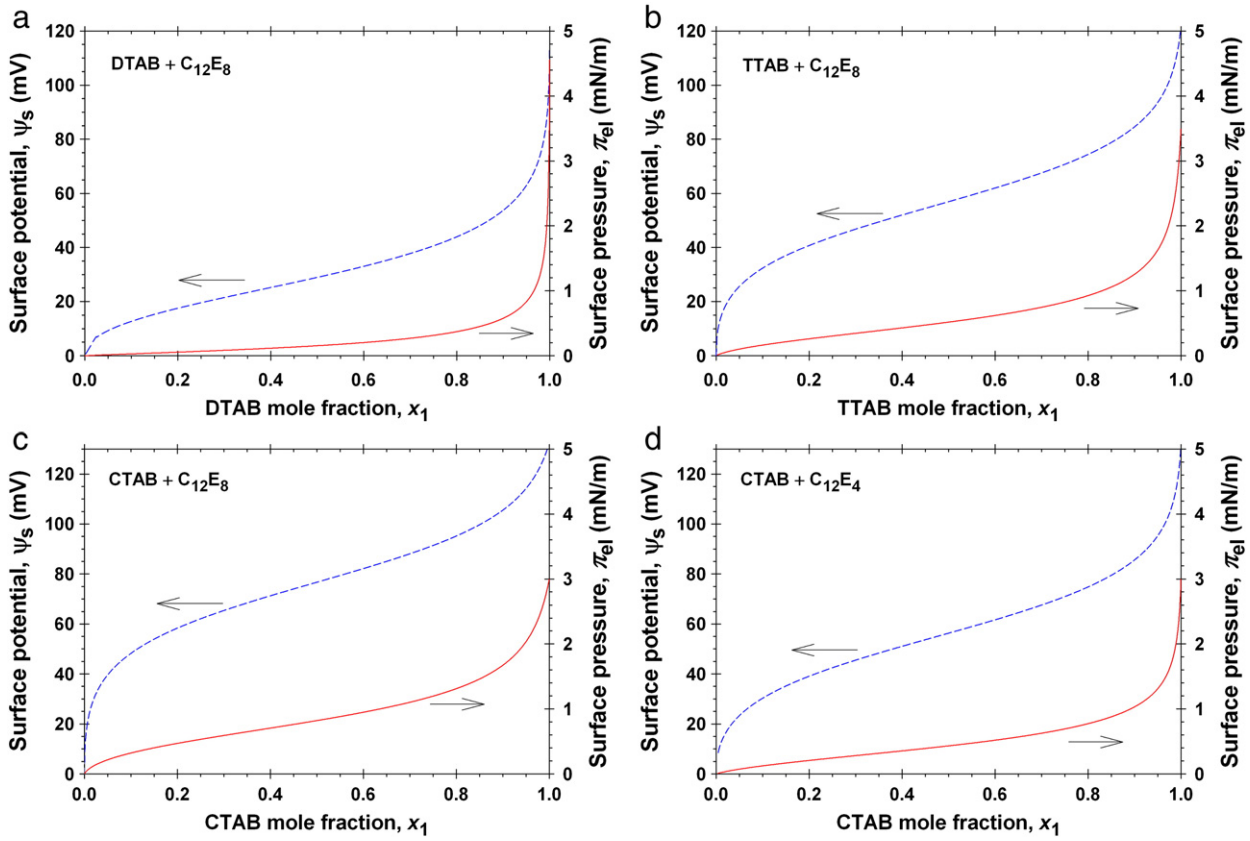

Fig. 19. Plots of the calculated micelle surface potential, ψ_s, and of the electrostatic component of micelle surface pressure, π_{el}, vs. the mole fraction of the ionic surfactant, x_1, in mixed surfactant solutions at the CMC. (a) DTAB + $C_{12}E_8$; (b) TTAB + $C_{12}E_8$; (c) CTAB + $C_{12}E_8$; (d) CTAB + $C_{12}E_4$.

Using Eqs. (7.1), (7.7) and (7.12), we can bring Eq. (7.11) in the form:

$$K_1 c_{1i} \equiv \frac{\Gamma_i}{\Gamma_\infty} f(\Gamma_1) \qquad (2 \le i \le m). \tag{7.13}$$

Eq. (7.13), which is the adsorption isotherm for the non-ionized surfactant molecules, which generalizes Eq. (3.12) for the case of many kinds of counterions.

7.2. System of equations describing the micelle–monomer equilibrium

As in Section 3.3, we consider a micelle as a gas bubble in the limiting case of infinitely small volume of the gas in the bubble. Then, the basic thermodynamic equations describing the surfactant adsorption at the bubble surface can be used in the limiting case of a micelle. In the case of micelles, we make the following replacements:

$$1/K_1 \to K_1^{(\mathrm{mic})}; \quad f(\Gamma_1) \to f_1; \quad \frac{\hat{\Gamma}_1}{\Gamma_\infty} \to y_1; \quad \frac{\Gamma_i}{\Gamma_\infty} \to y_i \quad (2 \le i \le m) \tag{7.14}$$

which are analogous to those in Section 3, with y_i being the mole fraction of non-ionized surfactant molecules of kind i in the micelle (the molar fraction of the bound counterions of kind i). Because we are dealing with a single ionic surfactant, we can set $f_1 \equiv 1$.

Thus, in the case of single ionic surfactant with several counterions ($2 \le i \le m$), the system of equations acquires the form:

$$\ln(c_1 \gamma_\pm) = \ln K_1^{(\mathrm{mic})} + \ln y_1 + \Phi_s \tag{7.15}$$

$$\ln c_{1i} = \ln K_1^{(\mathrm{mic})} + \ln y_i \quad (2 \le i \le m) \tag{7.16}$$

$$c_{1i} = K_{\mathrm{St},i} c_i c_1 \quad (2 \le i \le m) \tag{7.17}$$

$$\sum_{i=1}^{m} y_i = 1 \tag{7.18}$$

$$c_1 + \sum_{i=2}^{m} c_{1i} + c_{\mathrm{mic}} = C_1 \tag{7.19}$$

$$c_i + c_{1i} + y_i c_{\mathrm{mic}} = C_i \quad (2 \le i \le m). \tag{7.20}$$

Here, Eq. (7.15) is the analog of Eq. (7.9) and is identical to Eq. (4.1). Eq. (7.16) is the analog of Eq. (7.13) and generalizes Eq. (4.2). Furthermore, Eqs. (7.17)–(7.20) represent the generalizations of Eqs. (4.3)–(4.6). The generalized expression for the ionic strength can be expressed in two equivalent forms:

$$\begin{aligned} I &= \frac{1}{2}\left(c_1 + \sum_{i=2}^{m} c_i + \sum_{i=2}^{m} C_i\right) \\ &= c_1 + \sum_{i=2}^{m} C_i + \frac{1}{2} y_1 c_{\mathrm{mic}}. \end{aligned} \tag{7.21}$$

The two forms of Eq. (7.22) are equivalent because of the electroneutrality of the solution as a whole:

$$\sum_{i=2}^{m} c_i = \sum_{i=2}^{m} C_i + c_1 + y_1 c_{\mathrm{mic}}. \tag{7.22}$$

Thus, we arrive at a complete system of $3\,m + 3$ equations, viz. Eqs. (4.7), (4.21) and (7.5)–(7.21) for determining the following $3\,m + 3$ variables: $y_1, \ldots, y_m$; $c_1, \ldots, c_m$; $c_{12}, \ldots, c_{1m}$; c_{mic}, $\gamma_\pm$, I, and Φ_s.

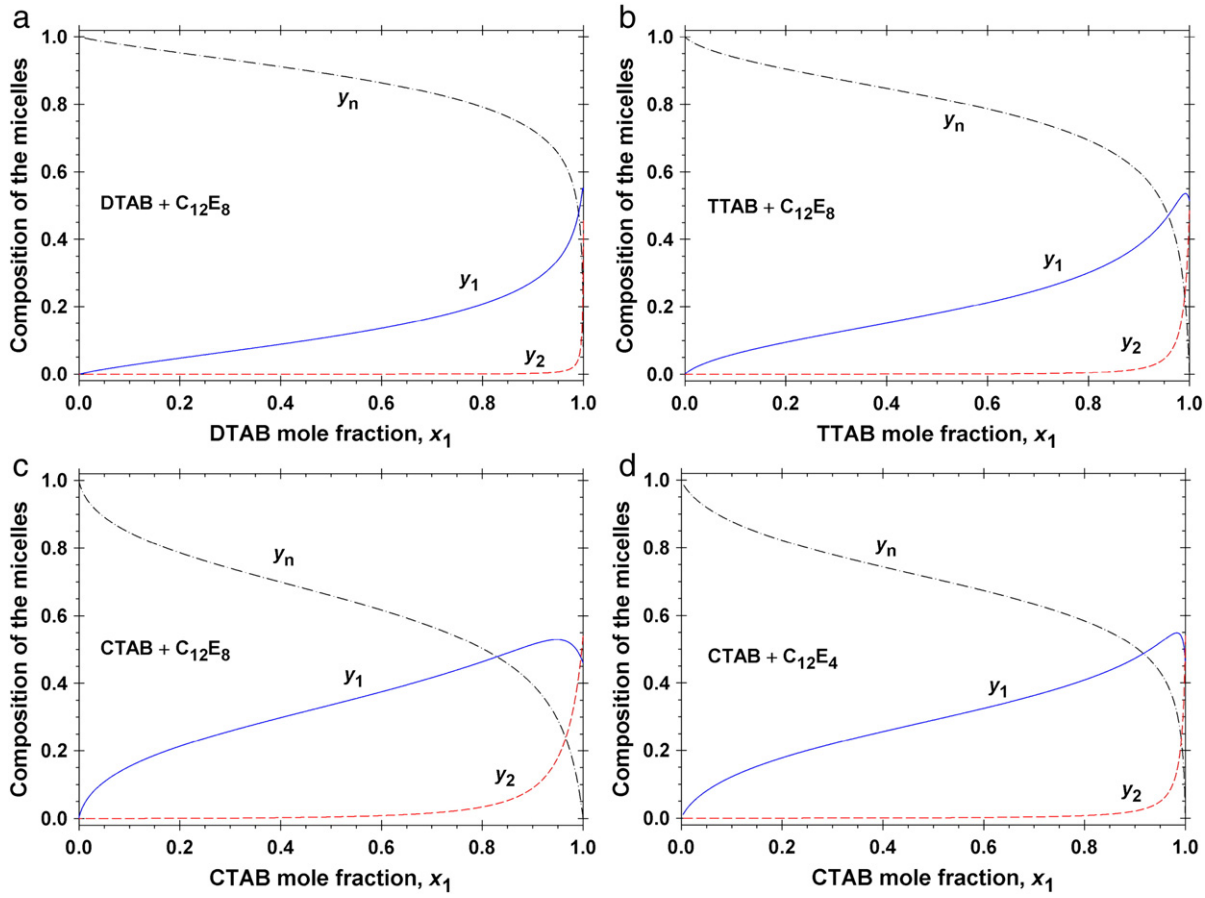

Fig. 20. Plots of the calculated molar fractions of the components in the micelles at the CMC: y_1 — of ionized molecules of the ionic surfactant; y_2 — of non-ionized molecules of the ionic surfactant (with bound counterion); y_n — of the nonionic surfactant. (a) DTAB + $C_{12}E_8$; (b) TTAB + $C_{12}E_8$; (c) CTAB + $C_{12}E_8$; (d) CTAB + $C_{12}E_4$.

8. Conclusions

Our task in the present article is to put together physically grounded equations, expressing either chemical equilibria or mass balances, in order to construct a detailed physicochemical model of the micellar solutions of ionic surfactants and their mixtures with nonionic surfactants. It turns out that the aforementioned equations are not enough — an additional equation is necessary to close the system. We demonstrate that excellent agreement with the experiment can be obtained if the Mitchell–Ninham (MN) closure [85] is used. The latter expresses a mechanical balance, which states that the electrostatic and non-electrostatic components of the micelle interfacial tension counterbalance each other, so that the micelle exists in a tension free state.

Solving the system of equations, we further predict the concentrations of all monomeric species, the micelle composition, ionization degree, surface potential and mean area per head group. Upon additional assumptions for the micelle shape, the mean aggregation number can be also estimated. It is important that the model contains a minimal number of thermodynamic parameters, which have been determined for several surfactants by comparing the theory with experimental data. Thus, each nonionic surfactant is characterized by a single thermodynamic parameter — its micellization constant, $K_n^{(mic)}$. Each ionic surfactant is characterized by three parameters: the micellization constant, $K_1^{(mic)}$, the Stern constant K_{St} that accounts for the effect of counterion binding, and the non-electrostatic component of micelle surface tension, γ_0. In the case of mixed micelles, each pair of surfactants is characterized with an interaction parameter, β, in terms of the regular solution theory.

The constructed detailed physicochemical model gives several nontrivial predictions. First, the model gives an interpretation of the slope, A_1, of the Corrin–Harkins plot [3] of the CMC vs. the ionic strength in double log scale. This slope is often interpreted as a degree of counterion binding, $y_2 = 1 - \alpha$. The present analysis shows that in general $y_2 \neq A_1$, and that y_2 can be considerably smaller than A_1 in the absence of added salt.

Second, the model predicts an increase of the micelle aggregation number, N_{agg}, with the rise of the surfactant concentration. In many studies, N_{agg} = const. has been assumed for spherical micelles. The present model predicts that the variation of N_{agg} can be considerable, in agreement with the experimental studies on this effect.

Third, the proposed detailed model allows verification of simpler models of the electrolytic conductivity of micellar solutions without added salt. Using the calculated concentrations of all monomeric ionic species, we predicted their total conductivity, which turned out to exactly coincide with the experimentally measured conductivity, κ_e, in the whole range of surfactant concentrations above the CMC. In other words, there is nothing left for the micelles, so that their equivalent conductance, λ_m, turns out to be zero (or negligible). A possible explanation is that the electrostatic repulsion between a given ionic micelle and its neighbors is so strong that it counterbalances the effect of the applied external electric field, which is unable to bring the micelles into directional motion as carriers of electric current. The result $\lambda_m = 0$ calls into question the predictions of the simplified models that completely neglect the interactions between the micelles. In the simplified models, an expression for λ_m, see Eq. (5.3), is postulated from the very beginning. Because this expression gives an a priori non-zero λ_m, the remaining part of conductivity (due to the dissociated counterions) becomes smaller, which results in systematically smaller values of the micelle ionization degree, α, determined as an adjustable parameter in the simplified models.

Fourth, the comparison of the detailed model with experimental data for various pairs of ionic and nonionic surfactants (with respect to the CMC of their mixed solutions) gives a constant interaction parameter, β. In other words, the determined β is independent of the micelle composition and of the bulk concentration of electrolyte, as it must be. The constancy of the β values obtained in the present study is an additional argument in favor of the adequacy of the proposed model.

As every model, the present one has its limitations. It works in terms of mean aggregation numbers, mean charges per micelle, etc. The micelle size distribution, polydispersity and growth are out of the scope of this model. The variation of N_{agg} with the rise of the ionic surfactant concentration can be described presuming monodisperse spherical micelles. The onset of growth of non-spherical aggregates can be detected as a deviation between the value of N_{agg} predicted by the model for spherical micelles and the experimental N_{agg}.

The proposed model can find applications for characterization of ionic surfactant micelles by aggregation number and charge; for interpreting the dependence of CMC on the mole fractions of mixed surfactants and on the electrolyte concentration; for analyzing the precipitation and pH variation in carboxylate solutions, see e.g., [91]; for determining the solubility limits of fatty acids and alcohols in micelles of conventional surfactants, see e.g., [89]; for analysis of data from the micellar electrokinetic chromatography (MEKC), where the micelles are used as a pseudo-stationary phase [159–162], etc.

Acknowledgments

We thankfully acknowledge the support from the National Science Fund of Bulgaria, grant No. DID-02-18/2009; from Unilever R&D, Trumbull, USA; from the FP7 project Beyond-Everest, and from COST Action CM1101 of the ESF. The authors are grateful to Ms. Mariana Paraskova for her assistance in the figure preparation.

Appendix A. Micelle surface charge, potential and electrostatic surface pressure

Here, our goal is to generalize (i) the Gouy equation that relates the surface charge and potential and (ii) the expression for the micelle electrostatic surface pressure, π_{el}, for the case of micellar solutions above the CMC. Note that the respective expressions available in the literature [85] are valid at the CMC, where $c_{mic} = 0$ and $\nu = 0$; see Eq. (4.15). We will use the jellium model (Section 4.2), which leads to the following form of the Poisson–Boltzmann equation:

$$\frac{d^2\Phi}{dr^2} = \kappa^2[\sinh\Phi + \nu(\cosh\Phi - 1)] - \frac{j}{r}\frac{d\Phi}{dr} \tag{A.1}$$

— see Eq. (4.13) for the notations. Let us multiply Eq. (A.1) by $d\Phi / dr$ and integrate:

$$\frac{1}{2}\left(\frac{d\Phi}{dx}\right)^2 = \cosh\Phi - 1 + \nu(\sinh\Phi - \Phi) + \int_x^\infty \frac{j}{\tilde{x}}\left(\frac{d\Phi}{d\tilde{x}}\right)^2 d\tilde{x} \tag{A.2}$$

$x = \kappa r$ is a dimensionless radial coordinate and $\tilde{x}$ is an integration variable. The integral in Eq. (A.2) can be estimated by means of the following iteration procedure. In zero order approximation, $\Phi = \Phi_0$, we neglect the integral term in Eq. (A.2) and bring this equation in the form:

$$\frac{d\Phi_0}{dx} = -2\sinh\left(\frac{\Phi_0}{2}\right)\left(1 + \nu\frac{\sinh\Phi_0 - \Phi_0}{\cosh\Phi_0 - 1}\right)^{1/2}. \tag{A.3}$$

One can check that the function $\Phi_0(x)$ determined by Eq. (A.3) decays exponentially at $x \to \infty$, i.e., $\Phi_0(x)$ decays much faster than $1 / x$. For this reason, a good estimate of the integral term in Eq. (A.2) is [85,109]:

$$\begin{aligned}\int_x^\infty \frac{j}{\tilde{x}}\left(\frac{d\Phi}{d\tilde{x}}\right)^2 d\tilde{x} &\approx \frac{j}{x}\int_x^\infty \left(\frac{d\Phi_0}{d\tilde{x}}\right)^2 d\tilde{x} \\ &= \frac{j}{x}\int_0^{\Phi_0}\left(\frac{-d\tilde{\Phi}_0}{d\tilde{x}}\right)d\tilde{\Phi}_0 \equiv \frac{2j}{x}F(\Phi_0).\end{aligned} \tag{A.4}$$

In view of Eq. (A.3), the function $F(\Phi_0)$ is defined by the expression:

$$F(y) \equiv \int_0^y \sinh\left(\frac{u}{2}\right)\left(1 + \nu\frac{\sinh u - u}{\cosh u - 1}\right)^{1/2} du \tag{A.5}$$

where u is an integration variable. Using double integration by parts in Eq. (A.5), we obtain:

$$\begin{aligned}F(y) = {} & 4\sinh^2\left(\frac{y}{4}\right)\left(1 + \nu\frac{\sinh y - y}{\cosh y - 1}\right)^{1/2} \\ & - \nu y\frac{\frac{y}{4} - \tanh\left(\frac{y}{4}\right)}{\sinh\left(\frac{y}{2}\right)}\left(1 + \nu\frac{\sinh y - y}{\cosh y - 1}\right)^{-1/2} + \ldots\end{aligned} \tag{A.6}$$

For all y and $0 < \nu < 1$, the first term in the right-hand side of Eq. (A.6) yields $F(y)$ with a maximal relative error smaller than 6%. The two terms in the right-hand side of Eq. (A.6) give $F(y)$ with a maximal relative error smaller than 2%.

Next, in Eq. (A.2) we substitute Eq. (A.4), along with Eq. (A.6). Taking square root and expanding in series, we derive:

$$\begin{aligned}-\frac{d\Phi}{dx} \approx {} & 2\sinh\left(\frac{\Phi}{2}\right)\left(1 + \nu\frac{\sinh\Phi - \Phi}{\cosh\Phi - 1}\right)^{1/2} \\ & + \frac{2j}{x}\left[\tanh\left(\frac{\Phi}{4}\right) - \nu\Phi\frac{\frac{\Phi}{4} - \tanh\left(\frac{\Phi}{4}\right)}{\cosh\Phi - 1 + \nu(\sinh\Phi - \Phi)}\right].\end{aligned} \tag{A.7}$$

Substituting Eq. (A.7) into the boundary condition Eq. (4.16) with $Z = y_1 N_{agg}$, after some transformations we obtain Eq. (4.17), where $\Phi_s = \Phi|_{r=R}$ and the definitions of Φ and κ by Eqs. (4.11) and (4.14) have been used.

The electrostatic contribution to the micelle surface pressure, π_{el}, can be calculated from the expression [112,166]:

$$\pi_{el} = \frac{\varepsilon\varepsilon_0}{j+1}\int_R^\infty \left(\frac{d\psi}{dr}\right)^2\left(j\frac{R}{r} + \frac{r^j}{R^j}\right)dr > 0. \tag{A.8}$$

Eq. (A.8) is obtained by substituting the Maxwell electrostatic stress tensor into Eq. (40) of Ref. [112], or into Eq. (3.69) of Ref. [166]. For large κR, Eq. (A.8) reduces to

$$\begin{aligned}\pi_{el} &= \varepsilon\varepsilon_0\int_R^\infty \left(\frac{d\psi}{dr}\right)^2 dr + O\left[\frac{1}{(\kappa R)^2}\right] \\ &\approx -\varepsilon\varepsilon_0\left(\frac{kT}{e}\right)^2\int_0^{\Phi_s}\frac{d\Phi}{dr}d\Phi.\end{aligned} \tag{A.9}$$

To calculate π_{el}, we substitute Eq. (A.7) into Eq. (A.9). The last term in Eq. (A.7) represents a small correction,

$$\frac{\nu\Phi}{\tanh\left(\frac{\Phi}{4}\right)}\frac{\frac{\Phi}{4} - \tanh\left(\frac{\Phi}{4}\right)}{\cosh(\Phi) - 1 + \nu(\sinh\Phi - \Phi)} < 0.04, \tag{A.10}$$

and can be neglected. The integrals of the remaining terms in Eq. (A.7) can be taken analytically, so that the integration in Eq. (A.9) yields Eq. (4.21) as a final result.

Appendix B. Expression for the slope of the Corrin–Harkins plot

Eq. (4.26) can be represented in the form:

$$\ln\left[c_1\gamma_\pm\left(e^{-\Phi_s}+K_{St}c_2\gamma_\pm\right)\right]=\ln K_1^{(mic)}. \tag{B.1}$$

The differential of Eq. (B.1) reads:

$$d\ln c_1+d\ln\gamma_\pm+d\left[\ln\left(e^{-\Phi_s}+K_{St}c_2\gamma_\pm\right)\right]=0. \tag{B.2}$$

Differentiating in the brackets and using again Eq. (B.1), we get:

$$d\ln c_1+\left(1+\frac{K_{St}c_1c_2\gamma_\pm^2}{K_1^{(mic)}}\right)d\ln\gamma_\pm+\frac{K_{St}c_1c_2\gamma_\pm^2}{K_1^{(mic)}}d\ln c_2=\frac{c_1\gamma_\pm e^{-\Phi_s}}{K_1^{(mic)}}d\Phi_s. \tag{B.3}$$

In view of Eq. (4.33), the coefficients in Eq. (B.3) can be expressed in terms of y_1 and y_2:

$$d\ln c_1+(1+y_2)d\ln\gamma_\pm+y_2d\ln c_2=y_1d\Phi_s. \tag{B.4}$$

Because $\gamma_0=$ const., the differentiation of Eq. (4.21a) yields:

$$d\left[\kappa\sinh^2\left(\frac{\Phi_s}{4}\right)\right]+\frac{j}{R}d\ln\left[\cosh\left(\frac{\Phi_s}{4}\right)\right]=0. \tag{B.5}$$

Separating the differentials of Φ_s and κ, we further obtain:

$$\left[\frac{\kappa}{4}\sinh\left(\frac{\Phi_s}{2}\right)+\frac{j}{4R}\tanh\left(\frac{\Phi_s}{4}\right)\right]d\Phi_s=-\kappa\sinh^2\left(\frac{\Phi_s}{4}\right)d\ln\kappa. \tag{B.6}$$

At the CMC, κ^2 is proportional to c_2. Then, $2d\ln\kappa=d\ln c_2$, and Eq. (B.6) acquires the form:

$$d\Phi_s=-\tanh\left(\frac{\Phi_s}{4}\right)\left[1+\frac{j}{2\kappa R\cosh^2\left(\frac{\Phi_s}{4}\right)}\right]^{-1}d\ln c_2. \tag{B.7}$$

At the CMC, we have $c_1=$ CMC and $c_2=I$, and consequently

$$A_1\equiv\frac{d\ln(CMC)}{d\ln I}=\frac{d\ln c_1}{d\ln c_2}. \tag{B.8}$$

Finally, we substitute Eq. (B.7) into Eq. (B.4), and obtain an expression for the derivative in the right-hand side of Eq. (B.8), which coincides with Eq. (4.30).

References

[1] McBain JW, Cornish ECV, Bowden RC. CCXV. — Studies of the constitution of soap in solution: sodium myristate and sodium laurate. J Chem Soc Trans 1912;101:2042–56.
[2] Hartley GS. Aqueous solutions of paraffin chain salts, a study in micelle formation. Paris: Hermann et Cie; 1936.
[3] Corrin ML, Harkins WD. The effect of salts on the critical concentration for the formation of micelles in colloidal electrolytes. J Am Chem Soc 1947;69:683–8.
[4] Corrin ML. The effect of salts and chain length on the critical concentration of colloidal electrolytes. J Colloid Sci 1948;3:333–8.
[5] Klevens HB. Structure and aggregation in dilute solution of surface active agents. J Am Oil Chem Soc 1953;30:74–80.
[6] Rosen MJ, Kunjappu JT. Surfactants and interfacial phenomena. 4th ed. New Jersey: John Wiley & Sons; 2012.
[7] Becher P. Hydrophile–lypophile balance: history and recent developments. Langmuir lecture 1983. J Dispers Sci Technol 1984;5:81–96.
[8] Ravey JC, Gherbi A, Stébé MJ. Comparative study of fluorinated and hydrogenated nonionic surfactants. I. Surface activity properties and critical concentrations. Progr Colloid Polym Sci 1988;76:234–41.
[9] Hofmann S, Rauscher A, Hoffmann H. Shear induced micellar structures. Ber Bunsenges Phys Chem Chem Phys 1991;95:153–64.
[10] Christov NC, Denkov ND, Kralchevsky PA, Ananthapadmanabhan KP, Lips A. Synergistic sphere-to-rod micelle transition in mixed solutions of sodium dodecyl sulfate and cocoamidopropyl betaine. Langmuir 2004;20:565–71.
[11] Shanks PC, Franses EI. Estimation of micellization parameters of aqueous sodium dodecyl sulfate from conductivity data. J Phys Chem 1992;96:1794–805.
[12] Shah SS, Saeed A, Sharif QM. A study of micellization parameters and electrostatic interactions in micellar solution of sodium dodecyl sulfate. Colloids Surf A 1999;155:405–12.
[13] Bhat MA, Dar AA, Amin A, Rashid PI, Rather GM. Temperature dependence of transport and equilibrium properties of alkylpyridinium surfactants in aqueous solutions. J Chem Thermodyn 2007;39:1500–7.
[14] Lah J, Pohar C, Vesnaver G. Calorimetric study of the micellization of alkylpyridinium and alkyltrimethylammonium bromides in water. J Phys Chem B 2000;104:2522–6.
[15] Kroflič A, Šarac B, Bešter-Rogač M. Influence of the alkyl chain length, temperature, and added salt on the thermodynamics of micellization: alkyltrimethylammonium chlorides in NaCl aqueous solutions. J Chem Thermodyn 2011;43:1557–63.
[16] Lianos P, Zana R. Fluorescence probe studies of the effect of concentration on the state of aggregation of surfactants in aqueous solution. J Colloid Interface Sci 1981;84:100–7.
[17] Gehlen MH, De Schryver FC. Fluorescence quenching in micelles in the presence of a probe-quencher ground-state charge-transfer complex. J Phys Chem 1993;97:11242–8.
[18] Bhattacharya SC, Das HT, Moulik SP. Quenching of fluorescence of 2-anthracenesulphonate by cetylpyridinium chloride in micellar solutions of Tweens, Triton X-100, sodium dodecylsulphate (SDS) and cetyltrimethylammoniumbromide (CTAB). J Photochem Photobiol A Chem 1993;71:257–62.
[19] Aoudia M, Al-Maamari T, Al-Salmi F. Intramolecular and intermolecular ion–dipole interactions in sodium lauryl ether sulfates (SLES) self-aggregation and mixed micellization with Triton X-100. Colloids Surf A 2009;335:55–61.
[20] Basheva ES, Kralchevsky PA, Danov KD, Ananthapadmanabhan KP, Lips A. The colloid structural forces as a tool for particle characterization and control of dispersion stability. Phys Chem Chem Phys 2007;9:5183–98.
[21] Danov KD, Basheva ES, Kralchevsky PA, Ananthapadmanabhan KP, Lips A. The metastable states of foam films containing electrically charged micelles or particles: experiment and quantitative interpretation. Adv Colloid Interface Sci 2011;168:50–70.
[22] Anachkov SE, Danov KD, Basheva ES, Kralchevsky PA, Ananthapadmanabhan KP. Determination of the aggregation number and charge of ionic surfactant micelles from the stepwise thinning of foam films. Adv Colloid Interface Sci 2012;183–184:55–67.
[23] Alargova R, Petkov J, Petsev D, Ivanov IB, Broze G, Mehreteab A. Light scattering study of sodium dodecyl polyoxyethylene-2 sulfate micelles in the presence of multivalent counterions. Langmuir 1995;11:1530–6.
[24] Shiloach A, Blankschtein D. Measurement and prediction of ionic/nonionic mixed micelle formation and growth. Langmuir 1998;14:7166–82.
[25] Reiss-Husson F, Luzzati V. The structure of the micellar solutions of some amphiphilic compounds in pure water as determined by absolute small-angle X-ray scattering techniques. J Phys Chem 1964;68:3504–11.
[26] Lang P, Glatter O. Small-angle X-ray scattering from aqueous solutions of tetra(oxyethylene)-n-octyl ether. Langmuir 1996;12:1193–8.
[27] Griffiths PC, Paul A, Heenan RK, Penfold J, Ranganathan R, Bales BL. Role of counterion concentration in determining micelle aggregation: evaluation of the combination of constraints from small-angle neutron scattering, electron paramagnetic resonance, and time-resolved fluorescence quenching. J Phys Chem B 2004;108:3810–6.
[28] Petkov JT, Tucker IM, Penfold J, Thomas RK, Petsev DN, Dong CC, Golding S, Grillo I. The impact of multivalent counterions, Al^{3+}, on the surface adsorption and self-assembly of the anionic surfactant alkyloxyethylene ulfate and anionic/nonionic surfactant mixtures. Langmuir 2010;26:16699–709.
[29] Bales BL, Messina L, Vidal A, Peric M, Nascimento OR. Precision relative aggregation number determinations of SDS micelles using a spin probe. A model of micelle surface hydration. J Phys Chem B 1998;102:10347–58.
[30] Törnblom M, Henriksson U, Ginley M. A field dependent ^{2}H nuclear magnetic relaxation study of the aggregation behavior in micellar solutions of CTAB and SDS. J Phys Chem 1994;98:7041–51.
[31] Gharibi H, Sohrabi B, Javadian S, Hashemianzadeh M. Study of the electrostatic and steric contributions to the free energy of ionic/nonionic mixed micellization. Colloids Surf A 2004;244:187–96.
[32] Colafemmina G, Recchia R, Ferrante AS, Amin S, Palazzo G. Lauric acid-induced formation of a lyotropic nematic phase of disk-shaped micelles. J Phys Chem B 2010;114:7250–60.
[33] Aniansson EAG, Wall SN, Almgren M, Hoffmann H, Kielmann I, Ulbricht W, et al. Theory of the kinetics of micellar equilibria and quantitative interpretation of chemical relaxation studies of micellar solutions of ionic surfactants. J Phys Chem 1976;80:905–22.
[34] Zana R, editor. Dynamics of surfactant self-assemblies. Boca Raton (FL): CRC Press; 2005.
[35] Tanford C. Thermodynamics of micelle formation: prediction of micelle size and size distribution. Proc Natl Acad Sci USA 1974;71:1911–5.
[36] Kamrath RF, Frances EI. Mass-action model of mixed micellization. J Phys Chem 1984;88:1642–8.
[37] Bourrel M, Schechter RS. Microemulsions and related systems. Formulation, solvency, and physical properties. New York: Marcel Dekker; 1988.
[38] Tadros TF. Applied surfactants: principles and applications. Weinheim: Wiley-VCH Verlag GmbH & Co. KGaA; 2005.

[39] Israelachvili JN, Mitchell DJ, Ninham BW. Theory of self-assembly of hydrocarbon amphiphiles into micelles and bilayers. J Chem Soc Faraday Trans 1976;72:1525–68.
[40] Tanford C. The hydrophobic effect and the organization of living matter. Science 1978;200:1012–8.
[41] Tanford C. The hydrophobic effect. New York: John Wiley & Sons; 1980.
[42] Missel PJ, Mazer NA, Benedek GB, Young CY, Carey MC. Thermodynamic analysis of the growth of sodium dodecyl sulfate micelles. J Phys Chem 1980;84: 1044–57.
[43] Gelbart WM, Ben-Shaul A. The "new" science of "complex fluids". J Phys Chem 1996;100:13169–89.
[44] Israelachvili JN. Intermolecular and surface forces. 3rd Ed. Amsterdam: Academic Press; 2011.
[45] Phillips JN. The energetics of micelle formation. Trans Faraday Soc 1955;51: 561–9.
[46] Evans DF, Ninham BW. Ion binding and the hydrophobic effect. J Phys Chem 1983;87:5025–32.
[47] Alargova RG, Ivanova VP, Kralchevsky PA, Mehreteab A, Broze G. Growth of rod-like micelles in anionic surfactant solutions in the presence of Ca^{2+} counterions. Colloids Surf A 1998;142:201–18.
[48] Alargova RG, Danov KD, Kralchevsky PA, Broze G, Mehreteab A. Growth of giant rodlike micelles of ionic surfactant in the presence of Al^{3+} counterions. Langmuir 1998;14:4036–49.
[49] Scrinivasan V, Blankstein D. Effect of counterion binding on micellar solution behavior. 1. Molecular-thermodynamic theory of micellization of ionic surfactants. Langmuir 2003;19:9932–45.
[50] Scrinivasan V, Blankstein D. Effect of counterion binding on micellar solution behavior. 2. Prediction of micellar solution properties of ionic surfactants–electrolyte systems. Langmuir 2003;19:9946–61.
[51] Lange H. Über die Mizellenbildung in Mischlösungen homologer Parrafinkettensalze. Kolloid Z Z Polym 1953;131:96–103.
[52] Shinoda K. The critical micelle concentration of soap mixtures (two component mixture). J Phys Chem 1954;58:541–4.
[53] Clint J. Micellization of mixed nonionic surface active agents. J Chem Soc Faraday Trans 1975;71:1327–34.
[54] Rubingh DN. Mixed micelle solutions. In: Mittal KL, editor. Solution. Chemistry of surfactants. New York: Plenum Press; 1979. p. 337–54.
[55] Scamehorn JF, Schechter RS, Wade WH. Micelle formation in mixtures of anionic and non-ionic surfactants. J Dispers Sci Technol 1982;3:261–78.
[56] Kamrath RF, Frances EI. Thermodynamic of mixed micellization. Pseudo-phase separation models. Ind Eng Chem Fundam 1983;22:230–9.
[57] Holland PM, Rubingh DN. Nonideal multicomponent mixed micelle model. J Phys Chem 1983;87:1984–90.
[58] Graciaa A, Ben Ghoulam M, Marion G, Lachaise J. Critical concentration and composition of mixed micelles of sodiumdodecylbenzenesulfonate, tetradecyltrimethylammonium bromide and polyoxyethylene octylphenols. J Phys Chem 1989;93:4167–73.
[59] Bergström M, Eriksson JC. A theoretical analysis of synergistic effect in mixed surfactant systems. Langmuir 2000;16:7173–81.
[60] Jönsson B, Wennerström H. Thermodynamics of ionic amphiphile–water systems. J Colloid Interface Sci 1981;80:482–96.
[61] Rathman JF, Scamehorn JF. Counterion binding on mixed micelles. J Phys Chem 1984;88:5807–16.
[62] Stellner KL, Scamehorn JF. Hardness tolerance of anionic surfactant solutions: 1. Anionic surfactant with added monovalent electrolyte. Langmuir 1989;5:70–7.
[63] Amante JC, Scamehorn JF, Harwell JH. Precipitation of mixtures of anionic and cationic surfactants. II. Effect of surfactant structure, temperature, and pH. J Colloid Interface Sci 1991;144:243–53.
[64] Eriksson JC, Bergström M, Persson M. Solution thermodynamics of mixed nonionic/ionic and ionic/ionic surfactant micelles. Rus J Phys Chem 2003;77: S87–94.
[65] Bergström M, Jonsson P, Persson M, Eriksson JC. A model-independent evaluation of experimental data, and comparison with theory, of synergistic effects in mixtures of an ionic and a nonionic surfactant. Langmuir 2003;19:10719–25.
[66] Maeda H. Phenomenological approaches in the thermodynamics of mixed micelles with electric charge. Adv Colloid Interface Sci 2010;156:70–82.
[67] Bergström LM, Aratono M. Synergistic effect in mixtures of two identically charged ionic surfactants with different critical micelle concentrations. Soft Matter 2011;7:8870–9.
[68] Nagarajan R. Molecular theory for mixed micelles. Langmuir 1985;1:331–41.
[69] Nagarajan R. Micellization, mixed micelles and solubilization: the role of interfacial interactions. Adv Colloid Interface Sci 1986;26:205–64.
[70] Nagarajan R, Ruckenstein E. Theory of surfactant self-assembly: a predictive molecular thermodynamic approach. Langmuir 1991;7:2934–69.
[71] Ben-Shaul A, Szleifer I, Gelbart WM. Chain organization and thermodynamics in micelles and bilayers. I. Theory. J Chem Phys 1985;83:3597–611.
[72] Szleifer I, Ben-Shaul A, Gelbart WM. Chain statistics in micelles and bilayers: effects of surface roughness and internal energy. J Chem Phys 1986;85:5345–58.
[73] May S, Ben-Shaul A. Molecular theory of the sphere-to-rod transition and the second CMC in aqueous micellar solutions. J Phys Chem B 2001;105:630–40.
[74] Puvvada S, Blankstein D. Molecular-thermodynamic approach to predict micellization, phase behavior and phase separation of micellar solutions. I. Application to nonionic surfactants. J Chem Phys 1990;92:3710–24.
[75] Zoeller NJ, Blankschtein D. Development of user-friendly computer programs to predict solution properties of single and mixed surfactant systems. Ind Eng Chem Res 1995;34:4150–60.
[76] Reif I, Mulqueen M, Blankschtein D. Molecular-thermodynamic prediction of critical micelle concentrations of commercial surfactants. Langmuir 2001;17: 5801–12.
[77] Huibers PDT, Lobanov VS, Katritzky AR, Shah DO, Karelson M. Prediction of critical micelle concentration using a quantitative structure–property relationship approach. 1. Nonionic surfactants. Langmuir 1996;12:1462–70.
[78] Huibers PDT. Quantum-chemical calculations of the charge distribution in ionic surfactants. Langmuir 1999;15:7546–50.
[79] Jalali-Heravi M, Konouz E. Prediction of critical micelle concentration of some anionic surfactants using multiple regression techniques: a quantitative structure–activity relationship study. J Surfactant Deterg 2000;3:47–52.
[80] Wang Z, Li G, Zhang X, Wang R, Lou A. A quantitative structure–property relationship study for the prediction of critical micelle concentration of nonionic surfactants. Colloids Surf A 2002;197:37–45.
[81] Katritzky AR, Pacureanu LM, Slavov SH, Dobchev DA, Karelson M. QSPR study of critical micelle concentration of nonionic surfactants. Ind Eng Chem Res 2008;47: 9687–95.
[82] Mozrzymas A, Rycka-Roszak B. Prediction of critical micelle concentration of nonionic surfactants by a quantitative structure–property relationship. Comb Chem High Throughput Screen 2010;13:39–44.
[83] Hu J, Zhang X, Wang Z. A review of progress in QSPR studies for surfactants. Int J Mol Sci 2010;11:1020–47.
[84] Kralchevsky PA, Danov KD, Broze G, Mehreteab A. Thermodynamics of ionic surfactant adsorption with account for the counterion binding: effect of salts of various valency. Langmuir 1999;15:2351–65.
[85] Mitchell DJ, Ninham BW. Electrostatic curvature contributions to interfacial tension of micellar and microemulsion phases. J Phys Chem 1983;87:2996–8.
[86] Evans EA, Skalak R. Mechanics and thermodynamics of biomembranes: part 1. CRC Crit Rev Bioeng 1979;3:181–330.
[87] Beresford-Smith B, Chan DYC. Electrical double-layer interactions in concentrated colloidal systems. Faraday Discuss Chem Soc 1983;76:65–75.
[88] Beresford-Smith B, Chan DYC, Mitchell DJ. The electrostatic interaction in colloidal systems with low added electrolyte. J Colloid Interface Sci 1985;105:216–34.
[89] Tzocheva SS, Kralchevsky PA, Danov KD, Georgieva GS, Post AJ, Ananthapadmanabhan KP. Solubility limits and phase diagrams for fatty acids in anionic (SLES) and zwitterionic (CPAB) micellar surfactant solutions. J Colloid Interface Sci 2012;369:274–86.
[90] Hill TL. An introduction to statistical thermodynamics. New York: Dover; 1987.
[91] Kralchevsky PA, Danov KD, Pishmanova CI, Kralchevska SD, Christov NC, Ananthapadmanabhan KP, Lips A. Effect of the precipitation of neutral-soap, acid-soap and alkanoic-acid crystallites on the bulk pH and surface tension of soap solutions. Langmuir 2007;23:3538–53.
[92] Winstein S, Clippinger E, Fainberg AH, Heck R, Robinson GC. Salt effects and ion pairs in solvolysis and related reactions. III. Common ion rate depression and exchange of anions during acetolysis. J Am Chem Soc 1956;78:328–35.
[93] Stern O. Zur Theorie der elektrolytischen Doppelschicht.Z Elektrochem 1924;30: 508–16 [http://electrochem.cwru.edu/estir/hist/hist-81-OStern.pdf].
[94] Prigogine I, Defay R. Chemical thermodynamics. London: Longmans, Green and Co.; 1954.
[95] Vlachy N, Jagoda-Cwiklik B, Vacha R, Touraud D, Jungwirth P, Kunz W. Hofmeister series and specific interactions of charged headgroups with aqueous ions. Adv Colloid Interface Sci 2009;146:42–7.
[96] Christov NC, Danov KD, Kralchevsky PA, Ananthapadmanabhan KP, Lips A. The maximum bubble pressure method: universal surface age and transport mechanisms in surfactant solutions. Langmuir 2006;22:7528–42.
[97] Kalinin VV, Radke CJ. An ion-binding model for ionic surfactant adsorption at aqueous-fluid interfaces. Colloids Surf A 1996;114:337–50.
[98] Warszynski P, Barzyk W, Lunkenheimer K, Fruhner H. Surface tension and surface potential of Na n-dodecyl sulfate at the air–solution interface: model and experiment. J Phys Chem B 1998;102:10948–57.
[99] Danov KD, Kralchevska SD, Kralchevsky PA, Broze G, Mehreteab A. Effect of nonionic admixtures on the adsorption of ionic surfactants at fluid interfaces. 2. Sodium dodecylbenzene sulfonate and dodecylbenzene. Langmuir 2003;19:5019–30.
[100] Overbeek JTG. The role of energy and entropy in the electrical double layer. Colloids Surf 1990;51:61–75.
[101] Robinson RA, Stokes RH. Electrolyte solutions. London: Butterworths; 1959.
[102] Hughes RIG. Theoretical practice: the Bohm–Pines quartet. Perspect Sci 2006;14: 457–524. http://dx.doi.org/10.1162/posc.2006.14.4.457.
[103] Pashley RM, Ninham BW. Double-layer forces in ionic micellar solutions. J Phys Chem 1987;91:2902–4.
[104] Nikolov AD, Kralchevsky PA, Ivanov IB, Wasan DT. Ordered micelle structuring in thin films from anionic surfactant solutions: II. Model development. J Colloid Interface Sci 1989;133:13–22.
[105] Richetti P, Kékicheff P. Direct measurements of depletion and structural forces of a micellar system. Phys Rev Lett 1992;68:1951–4.
[106] Klapp SHL, Qu D, von Klitzing R. Long-range interactions between soft colloidal particles in slit–pore geometries. J Phys Chem B 2007;111:1296–303.
[107] Gouy LG. Sur la constitution de la charge électrique à la surface d'un électrolyte.J Phys 1910;9:457–68 [http://electrochem.cwru.edu/estir/hist/hist-21-Gouy-1.pdf].
[108] Davies JT, Rideal EK. Interfacial phenomena. 2nd Ed.London: Academic Press; 1963.
[109] Ohshima H, Healy TW, White LR. Accurate analytic expressions for the surface charge density/surface potential relationship and double-layer potential distribution for a spherical colloidal particle. J Colloid Interface Sci 1982;90:17–26.
[110] Bales BL, Almgren M. Fluorescence quenching of pyrene by copper(II) in sodium dodecyl sulfate micelles. Effect of micelle size as controlled by surfactant concentration. J Phys Chem 1995;99:15153–62.

[111] Eriksson JC, Ljunggren S, Henriksson U. A novel approach to the mechanics and thermodynamics of spherical micelles. J Chem Soc Faraday Trans 1985;81: 833–68.
[112] Gurkov TD, Kralchevsky PA. Surface tension and surface energy of curved interfaces and membranes. Colloids Surf 1990;47:45–68.
[113] Kralchevsky PA, Eriksson JC, Ljunggren S. Theory of curved interfaces and membranes: mechanical and thermodynamical approaches. Adv Colloid Interface Sci 1994;48:19–59.
[114] Kolev VL, Danov KD, Kralchevsky PA, Broze G, Mehreteab A. Comparison of the van der Waals and Frumkin adsorption isotherms for sodium dodecyl sulfate at various salt concentrations. Langmuir 2002;18:9106–9.
[115] Kralchevsky PA, Danov KD, Kolev VL, Broze G, Mehreteab A. Effect of nonionic admixtures on the adsorption of ionic surfactants at fluid interfaces. 1. Sodium dodecyl sulfate and dodecanol. Langmuir 2003;19:5004–18.
[116] Valkovska DS, Shearman GC, Bain CD, Darton RC, Eastoe J. Adsorption of ionic surfactants at an expanding air–water interface. Langmuir 2004;20:4436–45.
[117] Tanaka A, Ikeda S. Adsorption of dodecyltrimethylammonium bromide on aqueous surface of sodium bromide solutions. Colloid Surf 1991;56:217–28.
[118] Asakawa T, Mochizuki S, Ohta A. Aqueous solution behavior of cationic surfactants containing sulfide linked alkyl chain. J Oleo Sci 2011;60:165–70.
[119] Pérez-Rodríguez M, Prieto G, Rega C, Varela LM, Sarmietno F, Mosquera V. A comparative study of the determination of the critical micelle concentration by conductivity and dielectric constant measurements. Langmuir 1998;14:4422–6.
[120] Mukerjee P, Mysels KJ. Critical micelle concentrations of aqueous surfactant systems. Washington DC: US Department of Commerce, National Bureau of Standards; 1971.
[121] Danov KD, Kralchevska SD, Kralchevsky PA, Ananthapadmanabhan KP, Lips A. Mixed solutions of anionic and zwitterionic surfactant (betaine): surface-tension isotherms, adsorption, and relaxation kinetics. Langmuir 2004;20:5445–53.
[122] Danov KD, Kralchevsky PA, Ananthapadmanabhan KP, Lips A. Interpretation of surface-tension isotherms of n-alkanoic (fatty) acids by means of the van der Waals model. J Colloid Interface Sci 2006;300:809–13.
[123] Jalšenjak N, Težak Đ. A new method for simultaneous estimation of micellization parameters from conductometric data. Chem Eur J 2004;10:5000–7.
[124] Pérez-Rodríguez M, Varela LM, García M, Mosquera V, Sarmietno F. Conductivity and relative permittivity of sodium n-dodecyl sulfate and n-decyl trimethylammonium bromide. J Chem Eng Data 1999;44:944–7.
[125] Harned HS, Owen BB. The physical chemistry of electrolytic solutions. 2nd Ed. New York: Reinhold Publishing Corp; 1950.
[126] Kralchevsky PA, Boneva MP, Danov KD, Ananthapadmanabhan KP, Lips A. Method for analysis of the composition of acid soaps by electrolytic conductivity measurements. J Colloid Interface Sci 2008;327:169–79.
[127] Ravdel AA, Ponomareva AM, editors. Concise handbook of physicochemical quantities. 8th ed. Leningrad: Khimiya; 1983 [in Russian].
[128] Lide DR, editor. CRC handbook of chemistry and physics. 89th ed. Boca Raton (FL): CRC Press; 2008.
[129] Taylor CD, Valkovska DS, Bain CD. A simple and rapid method for the determination of the surface equations of state and adsorption isotherms for efficient surfactants. Phys Chem Chem Phys 2003;5:4885–91.
[130] Imae T, Abe A, Taguchi Y, Ikeda S. Solubilization of a water–insoluble dye in aqueous solutions of dodecyltrimethylammonium halides, and its relation to micelle size and shape. J Colloid Interface Sci 1986;109:567–75.
[131] Mahajan RK, Vohra KK, Aswal VK. Small angle neutron scattering measurements of aggregation behaviour of mixed micelles of conventional surfactants with triblock polymer L64. Colloids Surf A 2008;326:48–52.
[132] Lainez A, del Burgo P, Junquera E, Aicart E. Mixed micelles formed by n-octyl-β-D-glucopyranoside and tetradecyltrimethylammonium bromide in aqueous media. Langmuir 2004;20:5745–52.
[133] Barry BW, Morrison JC, Russell GFJ. Prediction of critical micelle concentration of mixtures of alkyltrimethylammonium salts. J Colloid Interface Sci 1970;33: 554–61.
[134] Muñoz-Pérez M, Rodríguez A, Graciani MM, Mozo JD, Moyá ML. Dehydrochlorination of 1,1,1-trichloro-2,2-bis(*p*-chlorophenyl)ethane in cationic micellar systems. Langmuir 1998;14:3524–30.
[135] Attwood D, Patel HK. Mixed micelles of alkyltrimethylammonium bromides and chlorhexidine digluconate in aqueous solution. J Colloid Interface Sci 1989;129: 222–30.
[136] Zana R, Yiv S, Strazielle C, Lianos P. Effect of alcohol on the properties of micellar systems: I. Critical micellization concentration, micelle molecular weight and ionization degree, and solubility of alcohols in micellar solutions. J Colloid Interface Sci 1981;80:208–23.
[137] Sehgal P, Doe H, Bakshi MS. Aggregated assemblies of hexadecyltrimethylammonium bromide and phospholipids at the interface and in the bulk solution. J Surf Detergents 2002;5:123–30.
[138] Sepūlveda L, Cortes J. Ionization degrees and critical micelle concentrations of hexadecyltrimethylammonium and tetradecyltrimethylammonium micelles with different counterions. J Phys Chem 1985;89:5322–4.
[139] Zana R, Lévy H. Mixed micellization of cetyltrimethylammonium bromide and an anionic dimeric (Gemini) surfactant in aqueous solution. Langmuir 1997;13: 402–8.
[140] Adamson AW, Gast AP. Physical chemistry of surfaces. 6th Ed.New York: Wiley-Interscience; 1997.
[141] Danov KD, Kralchevsky PA. The standard free energy of surfactant adsorption at air/water and oil/water interfaces: theoretical vs. empirical approaches. Colloid J 2012;74:172–85.
[142] Mukhim T, Ismail K. Micellization of cetylpyridinium chloride in aqueous lithium chloride, sodium chloride and potassium chloride media. J Surf Sci Technol 2005;21:113–27.
[143] Umlong IM, Ismail K. Micellization behaviour of sodium dodecyl sulfate in different electrolyte media. Colloids Surf A 2007;299:5–14.
[144] Dutkiewicz E, Jakubowska A. Effect of electrolytes on the physicochemical behaviour of sodium dodecyl sulphate micelles. Colloid Polym Sci 2002;280: 1009–14.
[145] Tajima K, Muramatsu M, Sasaki T. Radiotracer studies on adsorption of surface active substance at aqueous surface: I. Accurate measurement of adsorption of tritiated sodium dodecylsulfate. Bull Chem Soc Jpn 1970;43:1991–8.
[146] Tajima K. Radiotracer studies on adsorption of surface active substance at aqueous surface: II. The effect of excess salt on the adsorption of sodium dodecylsulfate. Bull Chem Soc Jpn 1970;43:3063–6.
[147] Tajima K. Radiotracer studies on adsorption of surface active substance at aqueous surface: III. The effect of salt on the adsorption of sodium dodecylsulfate. Bull Chem Soc Jpn 1971;44:1767–71.
[148] Williams RJ, Phillips JN, Mysels JK. The critical micelle concentration of sodium lauryl sulphate at 25 °C. Trans Faraday Soc 1955;51:728–37.
[149] Moroi Y, Yoshida N. A new approach to micellization parameters: its application to sodium dodecyl sulfate micelle. Langmuir 1997;13:3909–12.
[150] Carrique F, Arroyo FJ, Delgado AV. Electrokinetics of concentrated suspensions of spherical colloidal particles: effect of a dynamic Stern layer on electrophoresis and DC conductivity. J Colloid Interface Sci 2001;243:351–61.
[151] Hiemenz PC, Rajagopalan R. Principles of colloid and surface chemistry. 3rd ed.New York: Marcel Dekker; 1997.
[152] Dukhin SS, Derjaguin BV. Electrokinetic phenomena. In: Matijevič E, editor. Surface and colloid science, vol. 7. New York: Wiley; 1974. p. 1–48.
[153] Nikolov AD, Wasan DT, Kralchevsky PA, Ivanov IB. Ordered structures in thinning micellar foam and latex films. In: Ise N, Sogami I, editors. Ordering and organisation in ionic solutions. Singapore: World Scientific; 1988. p. 302–14.
[154] Nikolov AD, Wasan DT. Ordered micelle structuring in thin films from anionic surfactant solutions: I. Experimental. J Colloid Interface Sci 1989;133:1–12.
[155] Tulpar A, Van Tassel PR, Walz JY. Structuring of macroions confined between like-charged surfaces. Langmuir 2006;22:2876–83.
[156] Zeng Y, Grandner S, Oliveira CLP, Thünemann AF, Paris O, Pedersen JS, Klapp SHL, von Klitzing R. Effect of particle size and Debye length on order parameters of colloidal silica suspensions under confinement. Soft Matter 2011;7:10899–909.
[157] Klapp SHL, Grandner S, Zeng Y, von Klitzing R. Asymptotic structure of charged colloids between two and three dimensions: the influence of salt. J Phys Condens Matter 2008;20:494232.
[158] Terabe S, Otsuka K, Ichihara K, Tsuchiya A, Ando T. Electrokinetic separations with micellar solutions and open-tubular capillaries. Anal Chem 1984;56:111–3.
[159] Muijselaar PG, Otsuka K, Terabe S. Micelles as pseudo-stationary phases in micellar electrokinetic chromatography. J Chromatogr A 1997;780:41–61.
[160] Fujimoto C, Fujise Y, Kawaguchi S. Macromolecular surfactant as a pseudostationary phase in micellar electrokinetic capillary chromatography. J Chromatogr A 2000;871:415–25.
[161] Giordano BC, Newman CID, Federowicz PM, Collins GE, Burg DS. Micelle stacking in micellar electrokinetic chromatography. Anal Chem 2007;79:6287–94.
[162] Akbay C, Ahmed HH, Arslan H, Graham B, Guzel M. Characterization and application of molecular binary mixed molecular micelles of sodium 10-undecenyl sulfate and sodium N-undecenyl leucinate as pseudostationary phases in micellar electrokinetic chromatography. Talanta 2012;99:441–9.
[163] Yoon H, Oostrom M, Werth CJ. Estimation of interfacial tension between organic liquid mixtures and water. Environ Sci Technol 2009;43:7754–61.
[164] Rodenas E, Valiente M, del Sol Villafruela M. Different theoretical approaches for the study of the mixed tetraethylene glycol mono-*n*-dodecyl ether/hexadecyltrimethylammonium bromide micelles. J Phys Chem B 1999;103:4549–54.
[165] Carnero Ruiz C, Aguiar J. Mixed micellization of octaoxyethylene monodecyl ether and n-alkyltrimethylammonium bromides. Colloids Surf A 2003;224:221–30.
[166] Kralchevsky PA, Nagayama K. Particles at fluid interfaces and membranes. Amsterdam: Elsevier; 2001.